Title

EXCITATION ENERGIES IN AN ELECTRICALLY PULSED LIGHT-EMISSION SOURCE APPLIED TO THE SEPARATION OP HIGHER IONIZED ATOMIC STATES: SPECTRA AND ENERGY LEVELS OF SCANDIUM 2+ AND VANADIUM 4+

Author

Deurzen, Cornelius H.H. Van

Publication Date

1973-05-01

Thesis/dissertation

LBL-1657

EXCITATION ENERGIES IN AN ELECTRICALLY PULSED LIGHT-EMISSION SOURCE APPLIED TO THE SEPARATION OF HIGHER IONIZED ATOMIC STATES: SPECTRA AND ENERGY LEVELS OF SCANDIUM 2+ AND VANADIUM 4+

Cornelius H. H. Van Deurzen
(Ph. D. Thesis)

May 1973

Prepared for the U. S. Atomic Energy Commission
under Contract W-7405-ENG-48

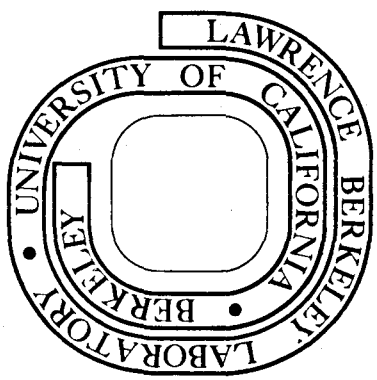

LBL-1657

DISCLAIMER

EXCITATION ENERGIES IN AN ELECTRICALLY PULSED LIGHT-EMISSION SOURCE APPLIED TO THE SEPARATION OF HIGHER IONIZED ATOMIC STATES: SPECTRA AND ENERGY LEVELS OF SCANDIUM 2+ AND VANADIUM 4+

Cornelius H. H. Van Deurzen

Lawrence Berkeley Laboratory
University of California
Berkeley, California 94720

May 1973

ABSTRACT

Spectra of vanadium have been produced in a vacuum sliding spark and their relative line intensities measured as parameters of the electrical circuit were varied. Intensity maxima of the spectral lines are interpreted as representing excitation energies and have been found to depend in a definitive manner on the power delivered to the source and on the duration of the discharge. The differential equation of the circuit is solved for the charge and energy transfer rates from the capacitor to the source, and two functions of the continuous circuit parameter $\gamma \equiv \frac{C}{L}(\frac{R}{2})^2$ are defined which greatly assist in interpreting the effect of the circuit parameters on the excitation in the source. With these solutions, the relationship between the excitation in the source and the electrical circuit parameters may be expressed in terms of the inductance, capacitance, the initial voltage on the capacitor, the two known functions one of which is directly associated with

the power delivered to the source during a current pulse and the other with the discharge duration, and two constants which in general depend on the source geometry and the electrode sample material.

The circuit parameters were varied to excite and separate spectra of scandium (Sc II and Sc III) by observing total light pulses and spectra of vanadium (V II - V V) by observing both total and time-resolved light pulses. For Sc III, 93 lines are reported in the region 550Å-9400Å which give rise to 23 new levels with an accuracy of about 0.03 cm^{-1} and the ionization energy is revised to 199677.37 ± 0.1 cm^{-1}. The results for Sc III have been published in J. Opt. Soc. Am. 63, 158 (1973). For V V, 61 lines in the region 480Å-8500Å give rise to 18 new levels and the ionization energy is revised to 526524 ± 5 cm^{-1}. The ionization energies have been calculated with a method presented here that allows the use of all the known levels in a series simultaneously. Series formulae are presented which are used to predict some of the newly found levels to within 0.25 cm^{-1}. An isoelectronic comparison confirms the inversion of the $3p^6 4f\ ^2F^o_{5/2,7/2}$ levels in V V as being caused by the interaction of these levels with those of the $^2F^o$ term in the $3p^5 3d^2$ configuration.

TABLE OF CONTENTS

LIST OF TABLES

LIST OF FIGURES

The universe *in toto* may not be equal to the sum of its dissociative parts.

1-1. INTRODUCTION

Perhaps the most widely used method of generating the spectra of higher ionized atomic species is the discharge of a capacitor across a gap between electrodes of the material to be studied. The degree of atomic ionization in such a discharge depends to some extent on the capacitance, inductance and resistance in the discharge circuit and a method of separating the spectra of the various stages of ionization entails the study and exploitation of this dependence. It is desired to establish a definitive relationship between the excitation observed in a spark discharge and the parameters involved in its production.

A long practiced method of obtaining the spectra of higher ionized atomic states is to use a high voltage spark generator consisting of a rather small capacitor (< 0.1 μf) charged to a high voltage ($\gtrsim 10$ kV), an inductor, and usually an auxiliary gap to trigger the discharge synchronously with the charging cycle. No external resistance is employed in the discharge circuit because for small capacitors the resistance necessary to change appreciably the character of the discharge dissipates a good amount of energy; less energy is delivered to the light source itself causing a reduction in the intensity of the spectra. The discharge is thus oscillatory and although the degree of excitation is affected to some extent by the variation of inductance, it is not possible to obtain the spectrum of one stage of ionization free of its neighboring stages.

Since 1943 three major developments in this type of spectroscopic unit have arisen in attempts to achieve greater control over the discharge through external parameters. In 1943 Hasler and Dietert[1] developed the idea that by separating the charge and discharge cycles of the capacitor making each independently controllable, breakdown of the gap can be achieved with a low-power high voltage ignitor circuit and a low-voltage high power capacitor discharged through the gap once it has broken down. Several advantages over the previous sparks are: (1) the amount of energy discharge in each cycle is more reproducible, (2) higher capacitances ($\sim$ 10 μf) can be used with the lower voltages ($\sim$ 1 kV) for a given amount of energy allowing variation from underdamped through critically damped and overdamped discharges, (3) termination of the discharge depends only on the circuit and gap constants, it is no longer affected by the synchronous rotating gap and (4) lower voltages reduces the broadening and shifting of atomic spectral lines caused by the Stark effect which is particularly important for radiation involving levels with large azimuthal quantum number. In 1950 Vodar and Astoin[2] suggested the sliding spark which was further developed by Bockasten[3] who introduced a porcelain or quartz spacer with a small bore along its axis through which the spark passes and with a radial channel viewport. The chief advantages are: (1) the voltage necessary for the breakdown of the spark gap is reduced, (2) confining the discharge enhances the spectral line intensity, and (3) it operates with large

inductances ($\sim$ 1000 μh) which is not possible with vacuum sparks. Spacer impurity spectral lines such as carbon, silicon and oxygen are also produced. The third development in the spark was the introduction of an electronic switching circuit consisting essentially of an ignitron triggered by a mercury thyratron to initiate the discharge.[4] This allowed still better control over the reproducibility of the current discharge and is essential for synchronization in the time resolution of spectral line intensities within the current pulse.

The present investigation consists of two chief parts: (1) to determine the excitation of different stages of atomic ionization and investigate the circuit conditions that optimize the variation between these stages when observing the total discharge pulses, and (2) the investigation of the behaviour of the ionization stages within a given discharge pulse via the time resolution of its light pulse. The intent is to discuss the basic equations governing the discharge of a capacitor in order to obtain a knowledge of the characteristic times involved as well as of the current and power-per-pulse relations in terms of the circuit parameters, the voltage and the discharge repetition rate. The results will then be correlated with the experimentally observed intensity variations in a discharge incorporating all three of the above developments.

1-2. MATHEMATICS OF TRANSIENT DISCHARGES OF CAPACITORS

The general mathematics of transient discharges of capacitors has been developed in many texts and with particular application to the study of spectrochemical sources[5] but the characteristic times involved and the rate of charge and energy delivery to the source in terms of the circuit parameters are not usually discussed. When a capacitor (C), which at the time (t = 0) when the current (i) starts, is triggered to discharge through an inductor (L) and resistance (R), the voltages in the LCR circuit sum to give the differential equation

$$L\frac{di}{dt} + Ri + \frac{q}{C} = 0 \qquad (1\text{-}1)$$

where q(t) is the charge on the capacitor. The solution of this equation for the current in the circuit as a function of time, i(t), is

$$i(t) = \frac{V_o}{R}\left\{\frac{e^{-\frac{R}{2L}\left(1-\sqrt{1-\frac{1}{\gamma}}\right)t} - e^{-\frac{R}{2L}\left(1+\sqrt{1-\frac{1}{\gamma}}\right)t}}{\sqrt{1-\frac{1}{\gamma}}}\right\} \qquad (1\text{-}2)$$

where V_o is the negative initial voltage on the capacitor and $\gamma \equiv \frac{C}{L}\left(\frac{R}{2}\right)^2 \geqslant 0$ is an appropriate circuit parameter, continuous over the region of possible behaviour of the discharge ($0 \leqslant \gamma \leqslant \infty$). Three quite different current flows are possible depending on the value of γ: $\gamma < 1$ underdamped, $\gamma = 1$ critically damped, and $\gamma > 1$ overdamped.

A characteristic discharge time is the time (t_p) at which the discharge current reaches its peak value i.e. where the charge transfer from the capacitor through the circuit for a given interval of time is a maximum. The time t_p may be obtained by putting the time derivative of the current equal to zero and solving for t_p; the peak current $i_p \equiv i(t_p)$ is then obtained by substituting the value of t_p in Eq. (1-2).

$$\frac{di}{dt} = \frac{V_o}{2L}\left\{\frac{e^{-\frac{R}{2L}\left(1-\sqrt{1-\frac{1}{\gamma}}\right)t}\left(1-\sqrt{1-\frac{1}{\gamma}}\right) - e^{-\frac{R}{2L}\left(1+\sqrt{1-\frac{1}{\gamma}}\right)t}\left(1+\sqrt{1-\frac{1}{\gamma}}\right)}{\sqrt{1-\frac{1}{\gamma}}}\right\} = 0$$

$$\frac{R}{2L}\,t_p = \frac{\frac{1}{2}\,\ell n\left(\frac{1+\sqrt{1-\frac{1}{\gamma}}}{1-\sqrt{1-\frac{1}{\gamma}}}\right)}{\sqrt{1-\frac{1}{\gamma}}} = \frac{\tanh^{-1}\sqrt{1-\frac{1}{\gamma}}}{\sqrt{1-\frac{1}{\gamma}}}$$

or

$$t_p = \sqrt{LC}\; g(\gamma) \qquad (1\text{-}3)$$

where

$$g(\gamma) \equiv \frac{1}{\sqrt{\gamma}}\,\frac{\tanh^{-1}\sqrt{1-\frac{1}{\gamma}}}{\sqrt{1-\frac{1}{\gamma}}}$$

$$i_p = \frac{V_o}{R}\left\{\frac{e^{-\left(1-\sqrt{1-\frac{1}{\gamma}}\right)\frac{\tanh^{-1}\sqrt{1-\frac{1}{\gamma}}}{\sqrt{1-\frac{1}{\gamma}}}} - e^{-\left(1+\sqrt{1-\frac{1}{\gamma}}\right)\frac{\tanh^{-1}\sqrt{1-\frac{1}{\gamma}}}{\sqrt{1-\frac{1}{\gamma}}}}}{\sqrt{1-\frac{1}{\gamma}}}\right\}$$

or

$$i_p = \sqrt{\frac{C}{L}}\, V_o\, h(\gamma) \qquad (1\text{-}4)$$

where

$$h(\gamma) \equiv \frac{1}{2\sqrt{\gamma}}\left\{\frac{e^{-\left(1-\sqrt{1-\frac{1}{\gamma}}\right)\frac{\tanh^{-1}\sqrt{1-\frac{1}{\gamma}}}{\sqrt{1-\frac{1}{\gamma}}}} - e^{-\left(1+\sqrt{1-\frac{1}{\gamma}}\right)\frac{\tanh^{-1}\sqrt{1-\frac{1}{\gamma}}}{\sqrt{1-\frac{1}{\gamma}}}}}{\sqrt{1-\frac{1}{\gamma}}}\right\}.$$

The charge and energy transfer rates may be determined as follows. The maximum amount of charge transported through the circuit per unit time (i_p) occurs at the time t_p and may be expressed in terms of t_p, γ, C and V_o using Eqs. (1-3) and (1-4)

$$i_p t_p = CV_o\, h(\gamma)\, g(\gamma) \qquad (1\text{-}5)$$

A measure of the rate of energy transfer from the capacitor to the circuit containing the spark gap i.e. a measure of the power in a current pulse can be obtained by considering the time interval τ_f

between the times ($t_{\pm}$) that the current is a given fraction (f) of its peak value. From Eqs. (1-2) and (1-4)

$$f \equiv \frac{i(t)}{i(t_p)} = \frac{e^{-\frac{R}{2L}t}\left\{e^{\frac{R}{2L}\sqrt{1-\frac{1}{\gamma}}\,t} - e^{-\frac{R}{2L}\sqrt{1-\frac{1}{\gamma}}\,t}\right\}}{e^{-\frac{R}{2L}t_p}\left\{e^{\frac{R}{2L}\sqrt{1-\frac{1}{\gamma}}\,t_p} - e^{-\frac{R}{2L}\sqrt{1-\frac{1}{\gamma}}\,t_p}\right\}}$$

or
$$e^{\sqrt{\frac{\gamma}{LC}}\,t_p(1-r)}\,(e^{\theta r} - e^{-\theta r}) = f\,(e^{\theta} - e^{-\theta}) \qquad (1\text{-}6)$$

where

$$\theta \equiv \frac{R}{2L}\,t_p\sqrt{1-\frac{1}{\gamma}} = \sqrt{\frac{\gamma-1}{LC}}\,t_p = \tanh^{-1}\sqrt{1-\frac{1}{\gamma}} = \sqrt{\gamma-1}\;g(\gamma)$$

and r is the double-valued ratio $\frac{t_{\pm}}{t_p}$ for a given current pulse. Given the circuit parameter γ and the fraction f, Eq. (1-6) may be solved for the ratios $\frac{t_{\pm}}{t_p}$, and the time interval τ_f formed in terms of t_p i.e. $\frac{\tau_f}{t_p} \equiv \frac{t_+ - t_-}{t_p} \geqslant 0$. The power in any current pulse may thus be expressed as

$$i_p V_o = \frac{CV_o^2}{\sqrt{LC}}\,h(\gamma) = \frac{CV_o^2}{\tau_f}\,h(\gamma)\;g(\gamma)\,\frac{\tau_f}{t_p} \qquad (1\text{-}7)$$

where in the expression on the right, $\frac{\tau_f}{t_p}$ is the solution obtained from Eq. (1-6).

Note that for a fixed LC, $g(\gamma)$ determines t_p and together with f it determines the chosen time interval τ_f i.e. $g(\gamma)$ is the discharge duration function. The function $h(\gamma)$ is the power function in the sense that given $\frac{C}{L}$ and V_o it determines i_p and therefore the power per current pulse, $i_p V_o$. Equations (1-3) to (1-7) will be useful in discussing charge and energy transfer rates in terms of t_p, i_p, V_o and the associated functions $g(\gamma)$ and $h(\gamma)$; for given L, C, γ, and the initial voltage V_o on the capacitor. The above equations were solved for the range $10^{-4} \leqslant \gamma \leqslant 10^{3}$ and the results for $f = \frac{1}{2}$ and principal values of the trigonometric functions are presented in Figs. 1.1 and 1.2. In the case of $\gamma < 1$, calculations were made for the first current pulse in the oscillatory train; the calculations for following pulses in the train are straight forward. Note that the functions plotted are monotonic in γ $(0 \leqslant \gamma \leqslant \infty)$, and that both the peak current and the product $i_p t_p$ are maximum as $\gamma \to 0$ for fixed (CV_o, L) and (CV_o), respectively. Of course, L, C, R (or γ for fixed $\frac{C}{L}$), and V_o uniquely determine the discharge pulse. In addition Table 1.1 shows the limits of Eqs. (1-3) and (1-4) to first order in the significant variable as γ ranges from zero, through unity to infinity. The limits were obtained by proper expansions[6] or by differentiation. When γ is outside the range plotted in the figures or $\gamma \simeq 1$, the expressions in Table 1.1 are applicable. It should be noted that in the limit when the resistance added to the circuit approaches zero, the resistance of the spark gap and the resistance corresponding to

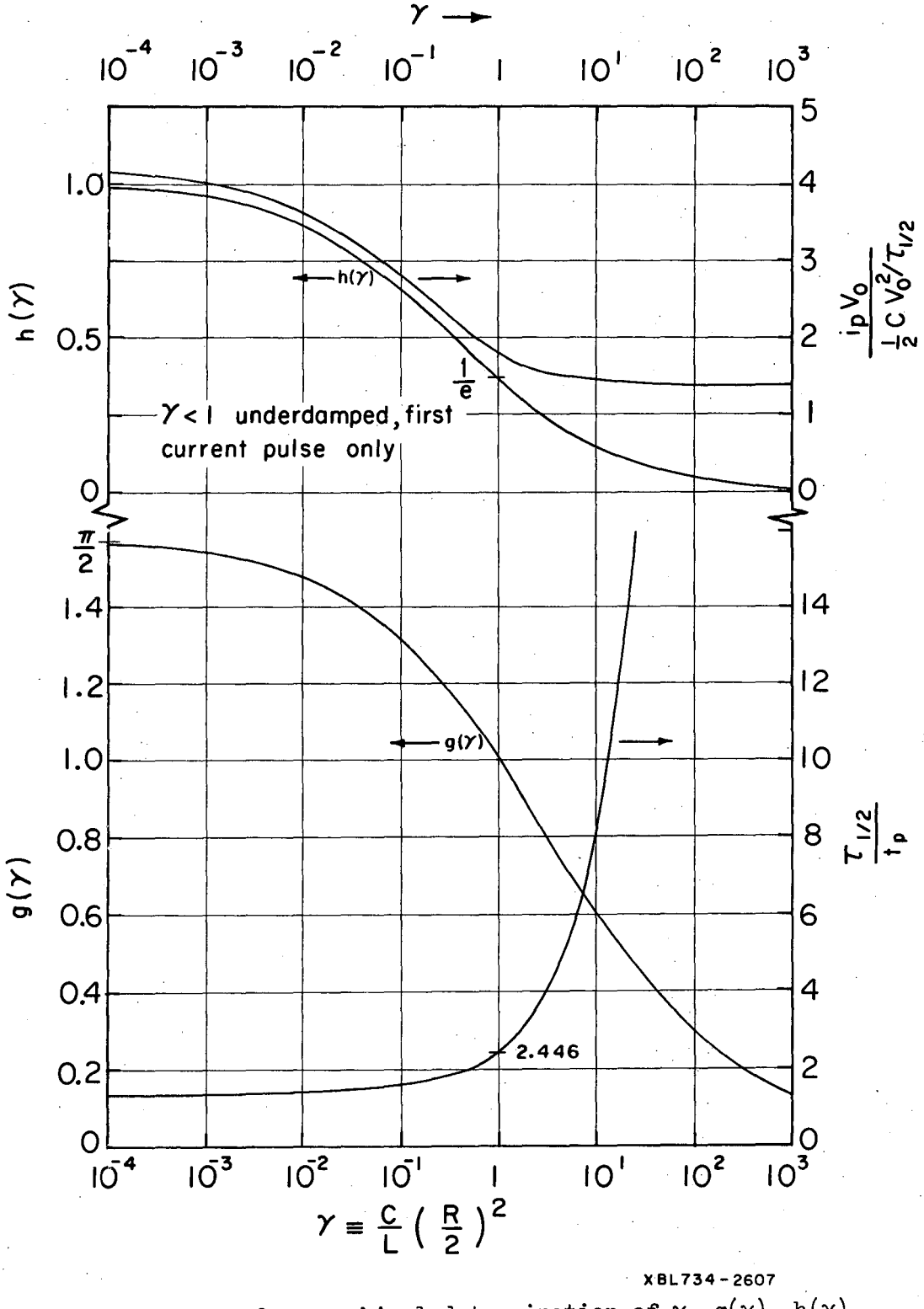

FIG. 1.1. Curves for graphical determination of γ, $g(\gamma)$, $h(\gamma)$, and $i_p V_o$ from given values of t_p, $\tau_{1/2}$, C, and V_o.

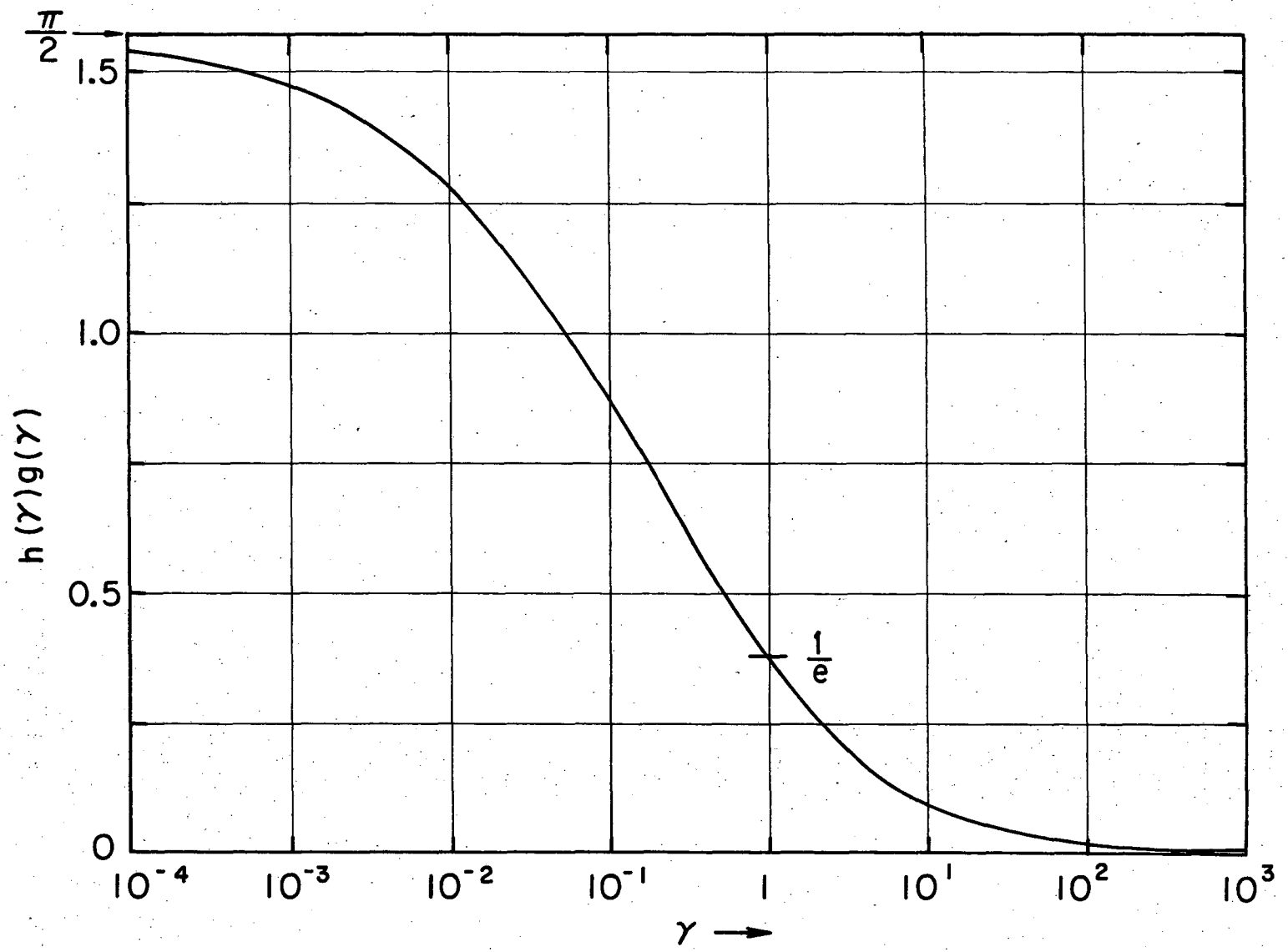

FIG. 1.2. Curve for graphical determination of charge transfer, $h(\gamma)g(\gamma) = i_p t_p / CV_o$.

TABLE 1.1. Limits of t_p and $\frac{Ri_p}{V_o}$ in Capacitor Discharges.

	$\gamma < 1$ Underdamped	$\gamma = 1$ Critical	$\gamma > 1$ Overdamped			
	$0 \leftarrow \gamma$		$\gamma \rightarrow \infty$			$\gamma \rightarrow 1$
	$L \rightarrow \infty \quad C \rightarrow 0 \quad R \rightarrow 0$		$L \rightarrow 0$	$C \rightarrow \infty$	$R \rightarrow \infty$	
$t_p =$	$\frac{\pi}{2}\sqrt{LC}\left(1 - \frac{2}{\pi}\sqrt{\gamma} + \cdots\right)^a$	$\sqrt{LC}$	$\sqrt{\frac{LC}{\gamma}}\left(\frac{1}{2 - \frac{1}{\gamma}}\right) \rightarrow 0$	$\sqrt{\gamma LC} = \frac{RC}{2} \rightarrow \infty^b$	$\sqrt{\frac{LC}{\gamma}} = \frac{2L}{R} \rightarrow 0^c$	$\sqrt{\frac{LC}{\gamma}}\left[1 - \frac{1}{3}\left(\frac{1}{\gamma} - 1\right) + \cdots\right]$
$\frac{Ri_p}{V_0} =$	$R\sqrt{\frac{C}{L}}\left(1 - \frac{\pi}{2}\sqrt{\gamma} + \cdots\right)^d$	$\frac{2}{e}$	$\frac{e^{-\frac{1 - \sqrt{1 - \frac{1}{\gamma}}}{1 + \sqrt{1 - \frac{1}{\gamma}}}}}{\sqrt{1 - \frac{1}{\gamma}}} \rightarrow 1^f$			$\frac{2}{e}\sqrt{\gamma}\left[1 + \frac{1}{3}\left(\frac{1}{\gamma} - 1\right) + \cdots\right]$

XBL 734-441

[a] Sinusoidal as $R \rightarrow 0$.

[b] Current never peaks as $C \rightarrow \infty$ implies infinite energy available.

[c] Open circuit never starts.

[d] $\frac{i_p}{V_o}$ independent of R.

[f] Ohms Law.

r.f. radiation losses are no longer negligible and must be taken into account. For a discussion in the underdamped case see Ref. 5. Consider now the three various current discharges possible.

A. Underdamped Discharge ($\gamma < 1$)

In this case $\sqrt{1-\frac{1}{\gamma}}$ is imaginary and the equations are more appropriately written

$$i(t) = \frac{V_o}{\sqrt{1-\gamma}} \sqrt{\frac{C}{L}}\, e^{-\sqrt{\frac{\gamma}{LC}}\, t} \sin\left(\sqrt{\frac{1-\gamma}{LC}}\, t\right) \qquad (1\text{-}2a)$$

$$\sqrt{\frac{\gamma}{LC}}\, t_p = \frac{\tan^{-1}\sqrt{\frac{1}{\gamma}-1}}{\sqrt{\frac{1}{\gamma}-1}} \quad ; \qquad g(\gamma) = \frac{\tan^{-1}\sqrt{\frac{1}{\gamma}-1}}{\sqrt{1-\gamma}} \qquad (1\text{-}3a)$$

$$i_p = V_o \sqrt{\frac{C}{L}}\, e^{-\frac{\tan^{-1}\sqrt{\frac{1}{\gamma}-1}}{\sqrt{\frac{1}{\gamma}-1}}} \quad ; \qquad h(\gamma) = e^{-\sqrt{\gamma}\, g(\gamma)} \qquad (1\text{-}4a)$$

$$e^{\sqrt{\frac{\gamma}{LC}}\, t_p(1-r)} \sin(\theta' r) = f\sqrt{1-\gamma} \qquad (1\text{-}6a)$$

where

$$\theta' \equiv \frac{R}{2L}\, t_p \sqrt{\frac{1}{\gamma}-1} = \sqrt{\frac{1-\gamma}{LC}}\, t_p = \tan^{-1}\sqrt{\frac{1}{\gamma}-1} = \sqrt{1-\gamma}\, g(\gamma)$$

and the identities $\tanh(ix) = i \tan(x)$, $\sin[\tan^{-1}(x)] = \frac{x}{\sqrt{1+x^2}}$ have been used. It is of interest to note that as γ decreases from unity both t_p and $2\sqrt{\frac{L}{C}}\frac{i_p}{V_o}$ increase; and when γ approaches zero, t_p approaches one quarter of the period $(2\pi\sqrt{LC})$ of pure sinusoidal oscillations ($R \equiv 0$ for all LC) while i_p becomes independent of R (Table 1.1). It is in this region that the earlier sparks ($\gamma \to 0$ through $C \to 0$) previously discussed were operated and it may now be seen why no external resistance is employed in the high-voltage, small-capacitor spark. In short, when employing a small capacitor, higher energy-dissipating resistances of low inductance are necessary to change appreciably the character of the discharge pulse from oscillatory behaviour ($\gamma < 1$) to critical damping ($\gamma = 1$).

B. Critically Damped Discharge ($\gamma = 1$)

When $\gamma = 1$ Eqs. (1-2) to (1-5) are indeterminate. However, by taking appropriate limits ($\sqrt{1-\frac{1}{\gamma}} \to 0$) or by differentiation the equations can be written

$$i(t) = \frac{V_o}{L} e^{-\frac{t}{\sqrt{LC}}} t \qquad (1\text{-}2b)$$

$$\frac{t_p}{\sqrt{LC}} = 1 \quad ; \quad g(\gamma) = 1 \qquad (1\text{-}3b)$$

$$i_p = \sqrt{\frac{C}{L}}\ \frac{V_o}{e} \qquad ; \qquad h(\gamma) = \frac{1}{e} \tag{1-4b}$$

$$e^{(1-r)}r = f \tag{1-6b}$$

Note that the equations in this case depend on but two of the three circuit parameters (L, C, and R) e.g. $t_p = \frac{2L}{R} = \frac{RC}{2} = \sqrt{LC}$ and that $\tau_{1/2} = 2.446\ t_p$.

C. Overdamped Discharge ($\gamma > 1$)

The equations are perhaps most appropriately written in the form (1-2) to (1-6). From Table 1.1 note that as γ increases from unity to large values, the time at which the peak current is a maximum decreases and approaches zero (except when $\gamma \to \infty$ through $C \to \infty$ in which case t_p increases linearly with C, as expected because $C \to \infty$ implies large energies available and the current never reaches its peak value). In this limit of γ, $\frac{Ri_p}{V_o}$ increases from $\frac{2}{e}$ at $\gamma = 1$, to unity (Ohm's Law) as $\gamma \to \infty$; while the rate of energy transfer approaches a constant value (Fig. 1.1). This is the case that approaches the continuous d.c. arc type of source across which a nearly constant voltage is maintained and pulse discharge duration is sufficiently long for the discharge to achieve thermal equilibrium. In the case of electrode contact the voltage may be varied for the conducting metal and Ohm's Law is obeyed.

1-3. EXPERIMENTAL DETAILS

To excite and separate the spectra of higher ionized atomic states, the light source used was a vacuum sliding spark connected in a series LCR circuit with a trigger unit.

A. Light Source

As originally used by Vodar and Astoin,[2] their arrangement in vacuum consisted of a carbon rod, along which the produced spark slides, provided with two ring electrodes connected to a (0.03-0.1 μf) capacitor charged to 30 kV. They reported spectra similar to ordinary sparks but with additional carbon lines present. The idea was further developed by Bockasten[3] who used cylindrical electrodes of the material studied and replaced the carbon rod with an axially-bored porcelain disk provided with a small (1 mm) radial viewing slit towards the spectrograph. In this manner a great gain in intensity was obtained since all the sparks occured in the bore hole rather than along the outside of a cylinder. To trigger the discharge Bockasten inserted in series an auxiliary spark gap in air, consisting of two brass spheres whose distance apart determined the desired voltage. The spark voltage was between 6-15 kV with a capacitor of 0.3 μf, triggered 6-8 times per second. The inductance was varied to obtain different degrees of oscillatory discharges.

The light source used in this experiment is similar to the one used at the Johns Hopkins University[4,7] and the National Bureau

of Standards[8,9] which is a somewhat modified version of the one used by Bockasten. The vacuum chamber consists of a glass envelope in the shape of two cylindrical glass tubings crossed at their centre (Fig. 1.3). The two vertical ends are kovar-to-metal seals through which the water-cooled electrodes are inserted and O-ring sealed. The right end of the horizontal tubing fits, through a ball-joint connection, to a pump outlet and an O-ring sealed window holder; the left end is a glass window for alignment and visual observation. The pump system consists of a rotary roughing pump and an oil diffusion pump with which operating pressures of about 5×10^{-6} mm of Hg are maintained. The quartz spacer between the electrodes, instead of being a flat disk which necessitates smooth fitting of the electrodes to the disk to prevent part of the discharge occuring outside the disk, has a recessed bore hole through which the spark passes. It is provided with a horizontal viewport, centered between the electrodes. The spacing between the electrodes is a quarter of an inch. At pressures above about 10^{-4} mm of Hg occasional electrical flash-over occurred between the electrodes and the brass window holder, some five inches apart. The horizontal windows should not be closer to the central electrodes than about five inches to prevent excessive sputter deposition from the sparking which decreases their light transmission.

B. Electrical Circuit

The circuit is basically a series LCR circuit (heavy lines Fig. 1.4) with the light source and a trigger unit connected in

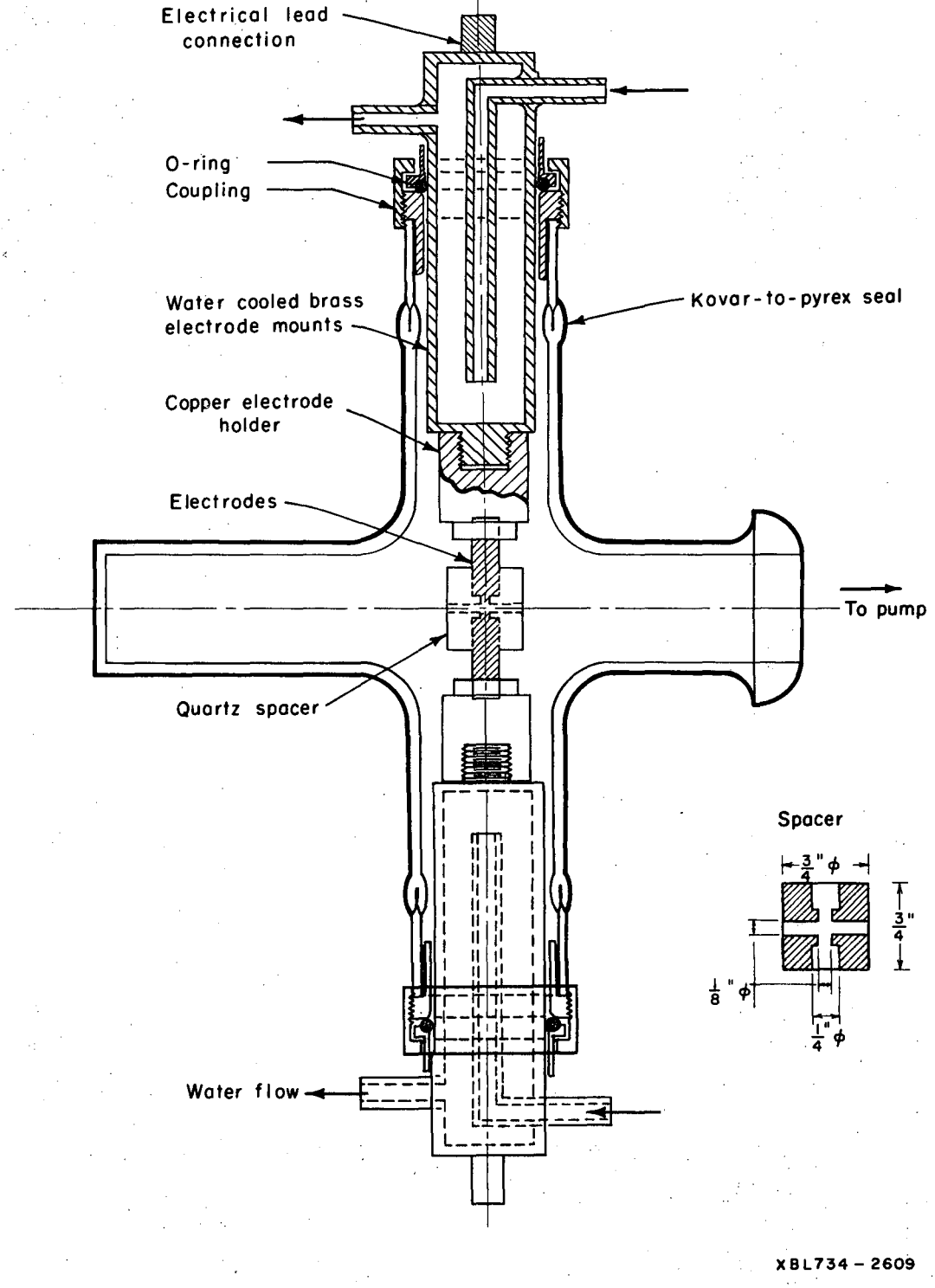

FIG. 1.3. Sliding spark light source.

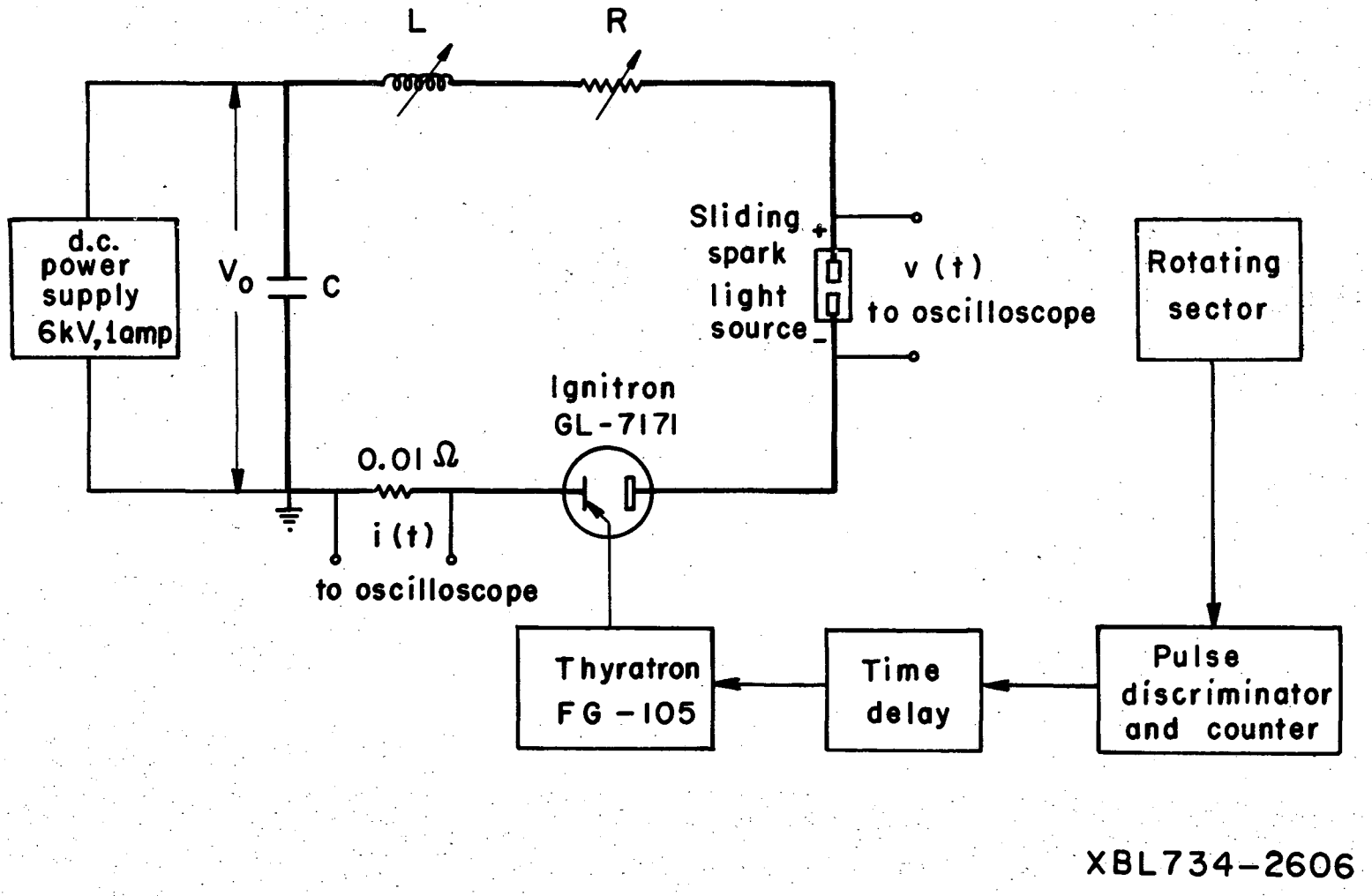

FIG. 1.4. Schematic of electrical circuit.

series. Inductance coils were made from copper wire (1.02-2.05 mm dia.) coated with an insulating varnish and consist of the values 13, 36, 133, 312, 592 and 860 μh. Two capacitor values were used, 4 μf and 24 μf, though most of the results were obtained with the latter. Two types of negligible-inductance (< 0.5 μh) resistance were used: for high peak currents several carbon pile compression rheostats were coupled in series as needed, while for the lower currents (< 100 amp) two doubly-wound wire rheostats of up to 100 ohms each were added. With this arrangement the external resistance in the circuit could be varied from a fraction of an ohm to 240 ohms. The trigger unit used originally was a rotating spark gap of variable frequency (typically operated at 5-30 times/sec) but this was soon abandoned in favour of an electronic switching unit which gave better stability and improved the suppression of undesirable current ends.

The electronic switching unit is similar to the one used at Johns Hopkins University[4] and consists of an ignitron (GL-7171) used as a switching tube which in turn is triggered by a mercury vapour thyratron (FG-105). A modification is that the thyratron is not controlled by the voltage on the capacitor but is itself triggered by a rotating sector wheel which at the same time may serve as a time-selection window when observing the light intensity versus time within a current pulse. The rotating sector wheel consists of an aluminum disk (20 cm dia.) into which have been cut, at a radius of 7.5 cm and at 90° from each other, four slits 3/4

inches in length radially and 0.005, 0.010, 0.020, and 0.050 inches wide azimuthally. When rotated on the axis of a synchronous motor (115 volts a.c., 60 cycle, 0.59 amp, 1 h.p., by Bodine Electric Company) at 3600 revolutions per minute, the result is four time windows i.e. when placed in front of the spectrograph slit, the sector slits will pass light into the spectrograph for 4.5, 9, 18 and 45 μsec.

The trigger and synchronization units were obtained from this rotating sector wheel as follows. At 60° before a given sector slit reaches the top vertical position of its cycle, it passes between a small light and a photo-diode. The resulting signal is amplified to diode-transitor-logic level (0-5 volts) and transmitted (1) to a pulse width discriminator (2) to a counter and (3) through a fixed ($\frac{1}{6}\frac{60}{3600} \simeq 2.8$ msec) delay plus a variable (± 300 μsec) delay. The pulse width discriminator selects the desired slit while the scalar demands a coincidence between the number of times the selected slit has passed the photo-diode and the externally preassigned discharge repetition rate ($\frac{60}{\text{integer}}$ per second). When the coincidence occurs the signal, appropriately delayed and once more amplified to 50 volts, is transmitted to trigger the thyratron which fires the ignitron, thereby discharging the capacitor and firing the light source at the time (within the variable delay) that the chosen sector slit is passing in front of the spectrograph slit.

In the time resolution of the light pulse the time location of the window in relation to the current pulse was determined as follows. A fiber optics light guide, of $\frac{1}{4}$" diameter and 12" long which transmits wavelengths between 400 and 2000 nm, was placed inside the spectrograph at 1 m from the entrance slit. The light guide intercepts approximately 4% of the light entering the spectrograph which is tranmitted to a photomultiplier (1P28) and the resulting signal displayed on the dual beam oscilloscope, synchronously triggered with the spark discharge (Fig. 1.5). With the built-in variable time delay between the time at which the sector slit is passing in front of the spectrograph slit and the firing of the discharge, the light pulse could be translated across the coincident slits in intervals of the window duration.

C. Mode of Operation

Electrical isolation of the power supply and the LCR circuit was ensured by placing an LR filter (200 mh, 750 ohm power resistor) between the two. This may easily be checked by means of the relation $\tau_{1/2} = 2.446\ t_p$ at critical damping. For a given LCR circuit and source, a lower limit on the initial voltage on the capacitor is set by the minimum voltage necessary to operate the source, while the upper limit is set by the power supply delivery and the discharge repetition rate. The discharge repetition rate of firing the source is itself limited; the lower limit ($\sim$40/sec) being determined by the desire to prevent spacer heat and glow, and the

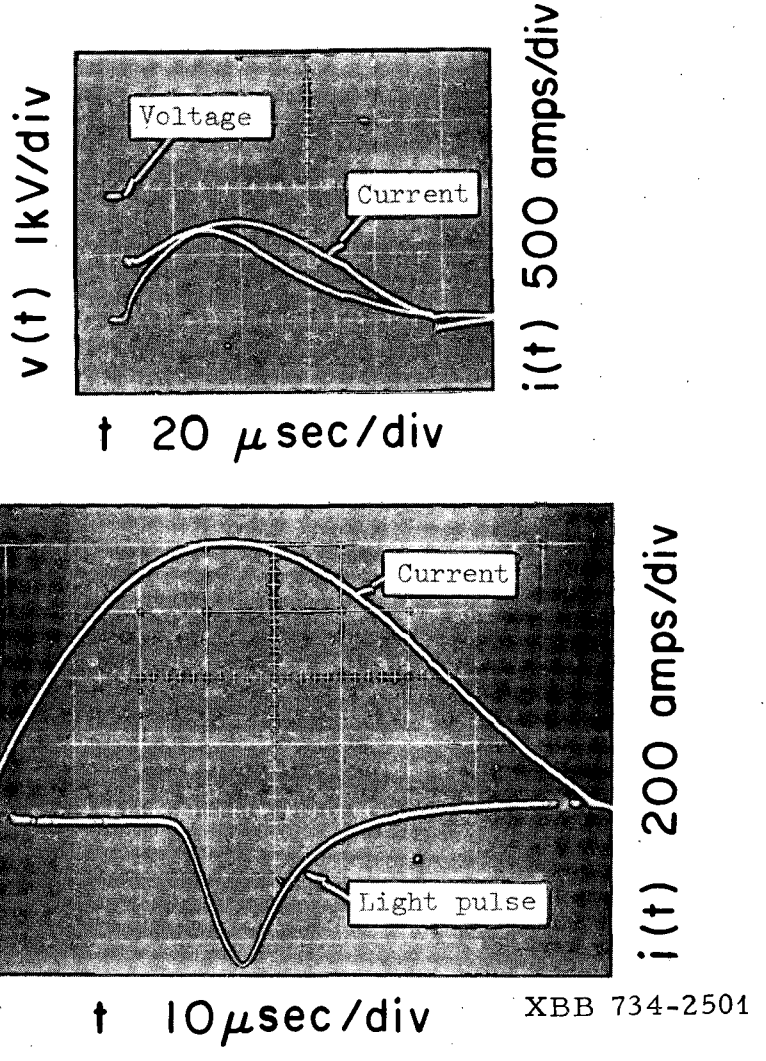

FIG. 1.5. Typical voltage, current, and light pulse (9 μsec window). L = 13 μh, C = 24 μf, $R_{added} < 1\Omega$, V_o = 980 volts.

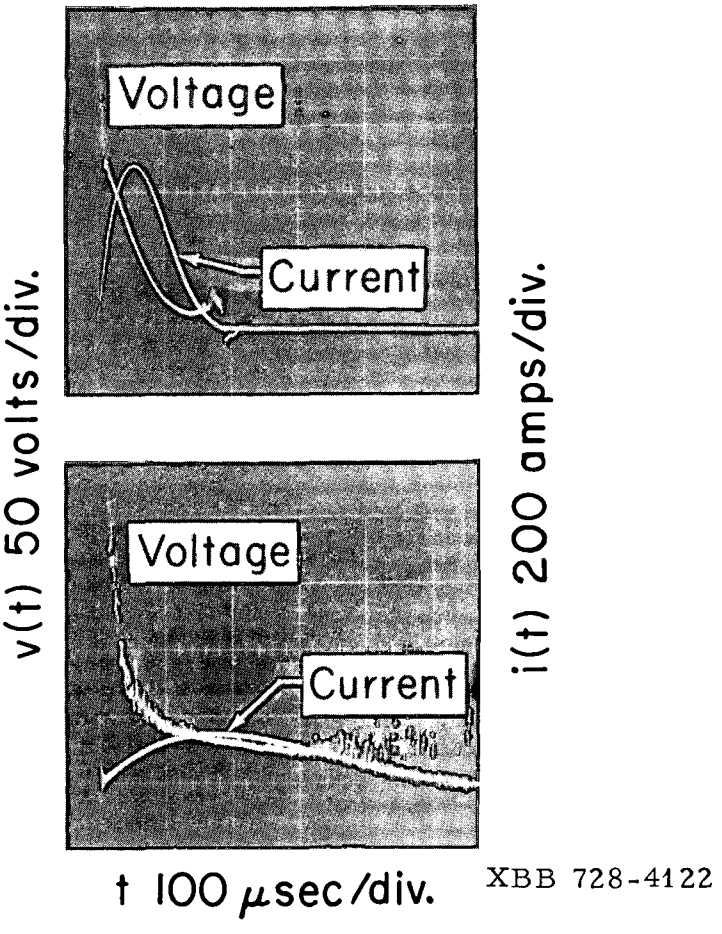

FIG. 1.6. Typical oscillographs of the voltage across and current through the light source.

Top: L = 68 μh, C = 24 μf, $R_{added} \simeq 3\Omega$.
Excites mainly Sc III and spacer impurities.

Bottom: L = 860 μh, C = 24 μf, $R_{added} \simeq 14\Omega$.
Excites mainly Sc I and II, and only the strongest lines of Sc III.

upper limit being decided by the power supply. Of course there exists a direct trade off between the repetition rate and the total elapsed time required for proper spectrographic plate exposure times. The current through and the voltage across the light source were monitored on a dual-beam oscilloscope by means of which i_p, t_p, $\tau_{1/2}$, and the total pulse length were readily reproducible for a given combination of L, C, R, V_o, and the discharge repetition rate. Typical oscillographs of the voltage and current versus time for some widely separated LCR settings are presented in Fig. 1.6. Note in Fig. 1.5 that the start of the current pulse is delayed 4 μsec. Critical damping could be achieved by adjusting the resistance while the source was in operation until the ends of the voltage and current pulses on the oscilloscope appeared sharp resulting in $\tau_{1/2}/t_p = 2.45$. Because there exists a lower limit on V_o, below which the spark gap will not operate, it is necessary to operate the source in the overdamped case in order to achieve lower peak current ($\leqslant$ 125 amperes). Peak currents as low as 20 amperes may be achieved without difficulty, but for still lower currents the source fires intermittently unless L is made smaller and R correspondingly larger. No attempt was made to overcome this intermittent firing by introducing a carrier gas as this would probably result in electrical flash-over between the electrodes and the metallic parts of the present source. Furthermore, since it was found that in this source there is no great difference in stage excitation between 10 and 20 amperes and

because the first and second stages of ionization are produced with better line quality (smaller Stark effect, etc.) in other sources, no advantage was to be gained by investigating these lower currents with respect to the separation of higher ionized atomic states.

The oscillatory case was not examined as it is known[4] that critically damped discharges are superior for the separation of ionization states when observing total pulses. This is evident from the results obtained by Strasheim and Blum[10] who reported that the radiated spectra of neutral aluminum and Al^{1+} follow the frequency of the discharge and that the intensity of the ionized line decays faster in the consecutive pulses of the oscillatory train. The fact that the ignitron in the circuit prevents oscillation was utilized to achieve higher peak currents for a given power; the external resistance was decreased to obtain underdamping while the ignitron prevented undershoot. Thus, the first current pulse of an underdamped discharge was investigated. It was found that the experimentally determined value of $\frac{t_p}{\sqrt{LC}}$ does not represent the value of the effective γ very well, probably because of breakdown effects and residual inductances. A more reliable and more sensitive measure of γ is obtained from the ratio $\frac{\tau_{1/2}}{t_p}$ which involves that part of the current pulse which more closely obeys the energy and charge transfer rates as determined by the values of the circuit parameters.

In an effort to maintain source conditions as constant as possible, the electrode surfaces were machined flat and the spacer bore hole cleaned every time a spectrographic plate was exposed. To start the spark a pencil line was made along the bore of the quartz spacer. For wear on the electrodes as a function of the inductance and capacitance see Ref. 10.

D. Observations

In the light of the foregoing discussion and previous experience gained from separating the spectrum of Sc III from lower ionization stages,[11,12] observations were made on vanadium spectra in an effort to correlate the excitation observed in the discharge of a vacuum sliding spark and the parameters involved in its production. The scandium spectra were separated by varying the inductance and resistance at constant voltage and capacitance; observations were made for two values of the capacitance, C = 4 μf and 24 μf. Observations on vanadium spectra were made of both total time-integrated and time-resolved light pulses with constant capacitance and various values of the voltage at different values of L and R.

The light emission of the spark, using vanadium metal electrodes (99.7% pure), was observed by means of a 3.4 m focal length, Ebert-mount spectrograph from 2300-4800Å in air (grating: 600 lines/mm, 5.2Å/mm dispersion, 5000Å blaze). The capacitance of 24 μf was discharged 15 times per second. Observations on the

total pulses were made with inductances of 13, 36, 133, 312, and 593 μh and resistances adjusted to obtain $\frac{\tau_{1/2}}{t_p} = 1.60 \pm 0.01$ ($\gamma = 0.08$) and overdamping. At each of the five inductances the voltage was varied over its range. The constant-time exposures (400 pulses) were made on one photographic plate. Table 1.2 lists the parameter values of the discharge pulses investigated, which have been numbered for easy reference. The quantities γ, $g(\gamma)$, and $h(\gamma)$ in Table 1.2 were obtained from Fig. 1.1 using the observed ratios $\frac{\tau_{1/2}}{t_p}$. Confidence in the value of γ thus obtained is demonstrated as follows. First, the current pulses with the same value of $\frac{\tau_{1/2}}{t_p}$ were observed on the oscilloscope to have the same damping character. Second, plotting the observed values of t_p^2 versus the inductance added to the circuit at constant C and constant damping character, results in a straight line with ordinate intercept 0.6 μh, presumably the residual inductance of the circuit and source, Eq. (1-3). Third, Eq. (1-4) is approximately obeyed for the pulses listed in Table 1.2. In general, the source will operate if $\sqrt{\frac{C}{L}}\, V_o = \frac{i_p}{h(\gamma)} \geqslant K$ where K is approximately 200 amperes for the present source as determined from pulses 18 and 22 which were obtained with V_o near the minimum voltage at which the source barely operates stably. This confirms the well known phenomenon that for a given electrical circuit the voltage across a source gap is nearly independent of current, i.e. the voltage at which the source barely operates is nearly constant for fixed circuit parameters, source geometry and electrode material. For constant

γ ($\simeq$ 0.5) with various values of L, C, and R, and for the minimum voltage at which the source barely operates, it was found that $\frac{CV_o}{i_p \tau_{1/2}}$ is approximately constant, Eq. (1-7).

To investigate the behaviour of the ionization stages versus time within a given discharge pulse, light pulses were time resolved by use of the rotating sector wheel. With the 9-μsec window, observations were made at 10 μsec intervals on the pulses marked tr (time resolved) in Table 1.2. Photographic plate exposure times were constant at 4000 pulses. Three plates sufficed to obtain the results of the seven pulses, each plate representing a fixed value of L, C, and R. Each plate was also exposed to a Tungsten-Halogen lamp, reproducible through constant voltage and photomultiplier monitoring, for appropriately stepped times from $\frac{1}{9}$ to $\frac{20}{9}$ minutes, in order to monitor plate variations and determine plate emulsion calibration curves. Measurements were made on the intensities of representative and convenient lines listed in Table 1.3, and the relative intensities read from each plate's calibration curve. The observations using the 24 μf capacitor are presented in graphical form in Figs. 1.7 to 1.10. In fig. 1.7 the relative intensities of the lines listed in Table 1.3 are plotted versus peak current for the five different inductance values. Figures 1.8, 1.9, and 1.10 show the relative intensities of the lines of different ionization stages versus time within the time resolved current pulses.

TABLE 1.2. Circuit Parameter Values of Discharge Pulses Investigated.

Pulse No.	Observed							From FIG. 1.1.		
	Circuit Parameters (C = 24 μf)			Current Pulse						
	L (μh)	V_o (volts)	R[a] (Ω)	i_p (amp)	t_p	$\tau_{1/2}$ (μsec)	d[b]	γ	g(γ)	h(γ)
1	13	300	<1	150	35	56	96	0.08	1.34	0.68
2	13	450	<1	300	35	56	96	0.08	1.34	0.68
3	13	560	<1	400	35	56	96	0.08	1.34	0.68
4	13	690	<1	500	35	56	96	0.08	1.34	0.68
5(tr)[c]	13	750	<1	600	35	56	96	0.08	1.34	0.68
6	13	850	<1	700	35	56	96	0.08	1.34	0.68
7(tr)	13	980	<1	800	35	56	96	0.08	1.34	0.68
8	13	1050	<1	900	35	56	96	0.08	1.34	0.68
9(tr)	13	1160	<1	1000	35	56	96	0.08	1.34	0.68
10	36	300	1	150	48	77	115	0.08	1.34	0.68
11	36	480	1	300	48	77	115	0.08	1.34	0.68
12(tr)	36	580	1	400	48	77	115	0.08	1.34	0.68
13	36	700	1	500	48	77	115	0.08	1.34	0.68
14(tr)	36	780	1	600	48	77	115	0.08	1.34	0.68
15	36	890	1	700	48	77	115	0.08	1.34	0.68
16(tr)	36	1000	1	800	48	77	115	0.08	1.34	0.68
17	133	860	20*	50	35	300	750	10.0	0.595	0.15
18	133	350	1.5	150	83	133	190	0.08	1.34	0.68
19	133	550	1.5	300	83	133	190	0.08	1.34	0.68
20(tr)	133	700	1.5	400	83	133	190	0.08	1.34	0.68
21	312	1350	30*	50	65	380	700	6.30	0.68	0.18
22	312	600	2	150	125	200	300	0.08	1.34	0.68
23	312	1050	2	300	125	200	300	0.08	1.34	0.68
24	593	1400	30*	50	65	380	1100	6.30	0.68	0.18
25	593	1400	15*	100	110	330	600	1.06	0.915	0.32
26	593	1010	3	200	160	255	400	0.08	1.34	0.68

[a]Added resistance values are approximate only; * = overdamped.

[b]Total time duration of current pulse.

[c]Pulses marked (tr) were time resolved.

TABLE 1.3. Vanadium Lines Selected for Intensity Measurements.

	Wavelengths (Å)	Transition	Reference	Excitation energy[a] (electron volts)
V II	2924.017	$a^5F_5-z^5F^\circ_5$	13	11.4
V II	3257.893	$c^3P_1-y^3D^\circ_2$	14	13.0
V II	3263.33	$b^3G_4-z^3H^\circ_4$	14	12.6
V II	3271.124	$a^3F_3-z^3G^\circ_4$	14	11.6
V III	3107.817	$c^2D_{5/2}-z^2F^\circ_{7/2}$	15	32.4
V III	3350.211		16	$\geqslant$ 25.1
V III	3351.56		16	$\geqslant$ 25.1
V IV	3294.259	$3d(4d^3P_2-5p^3P^\circ_2)$	17	82.7
V IV	3295.501	$3d(5p^3F^\circ_2-5d^3F_2)$	17	86.2
V IV	3328.527	$3d(5p^3F^\circ_4-5d^3F_4)$	17	86.3
V IV	3333.986	$3d(4d^3P_2-5p^3P^\circ_1)$	17	82.6
V IV	3334.79	$3d(4d^1G_4-5p^1F^\circ_3)$	17	82.7
V V	2774.998	$5p^2P^\circ_{3/2}-5d^2D_{5/2}$	12	145.6
V V	3363.517		12	$\geqslant$ 101.2

[a]The excitation energy is defined as the total energy necessary to excite a neutral atom in its ground state to the upper state of the transition emitting the radiation.

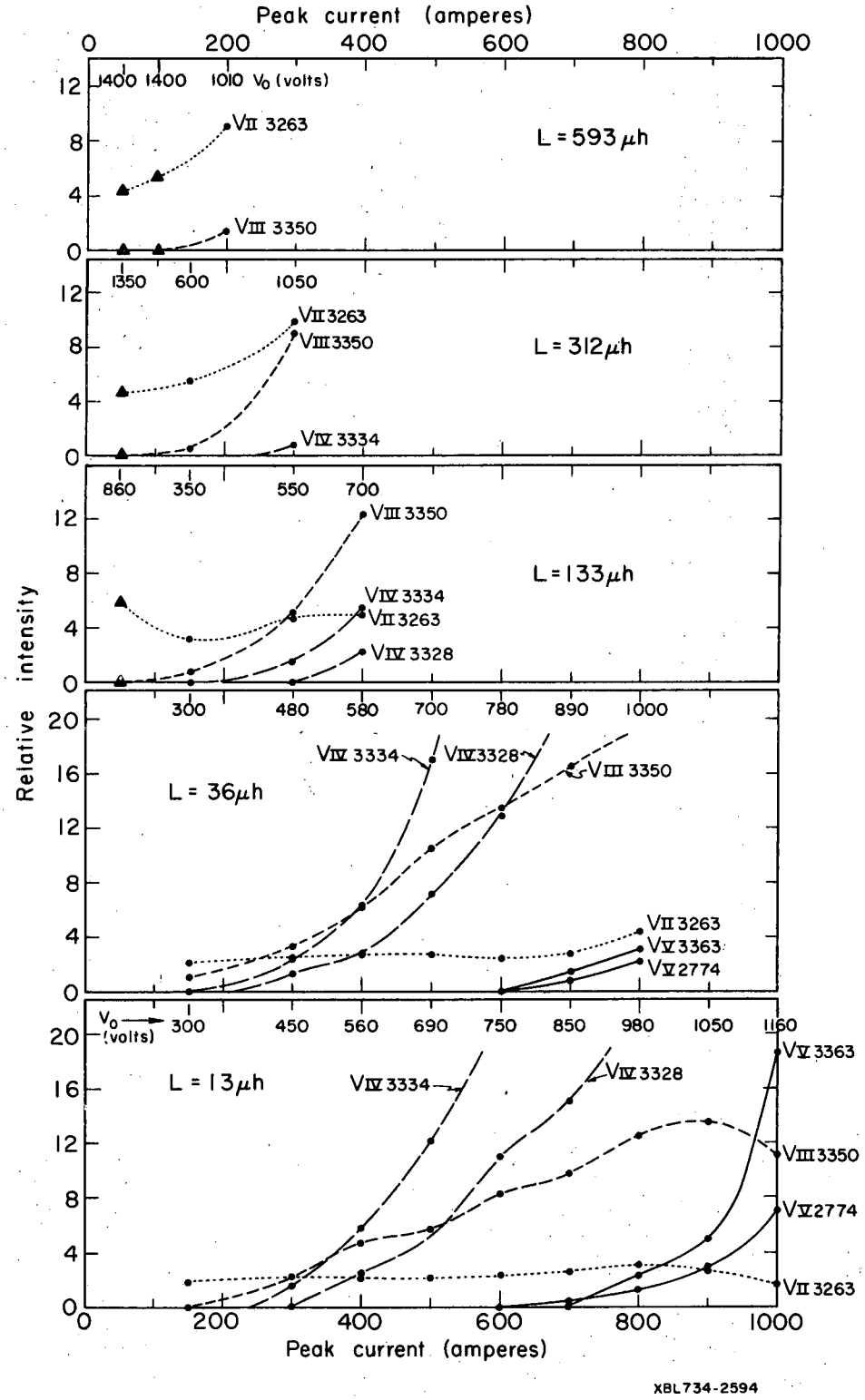

FIG. 1.7. Relative line intensities versus peak current.
C=24μf, γ=0.08 except ▲ = overdamped.
For additional circuit parameter values see Table 1.2.

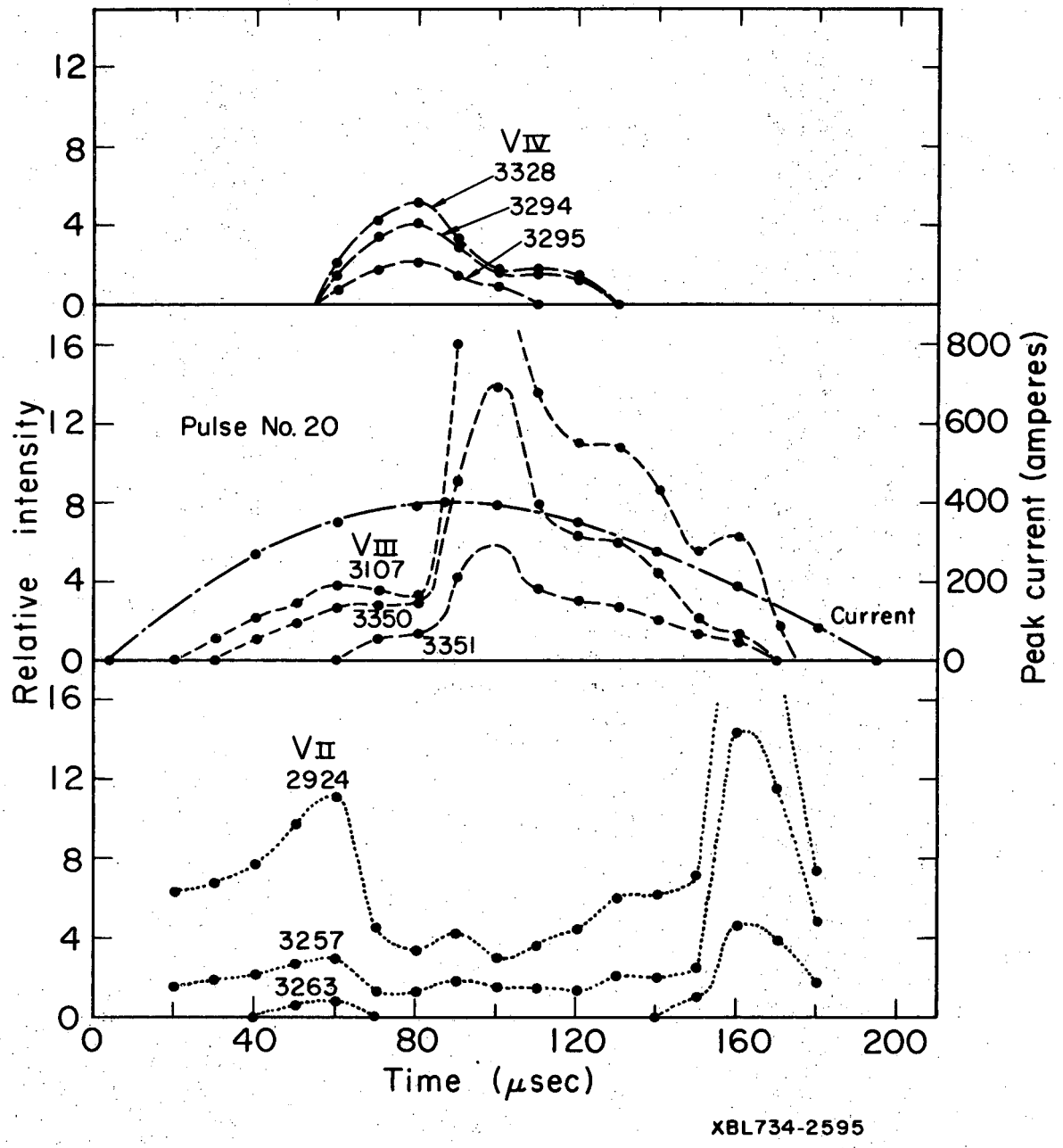

FIG. 1.8. Relative line intensities versus time. L=133 μh; pulse 20, Table 1.2.

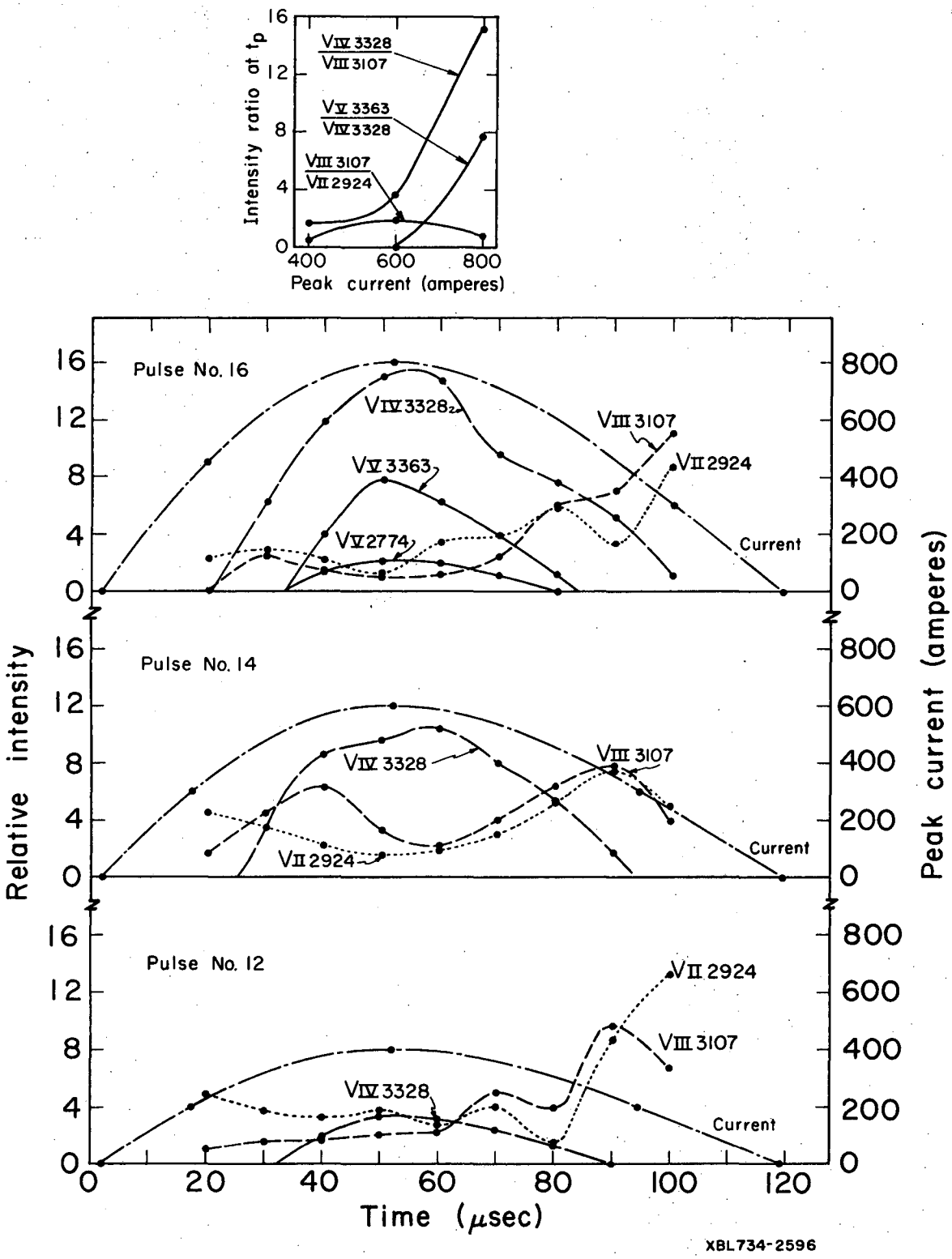

FIG. 1.9. Relative line intensities versus time.
L = 36 μh; pulses 12, 14, and 16, Table 1.2.

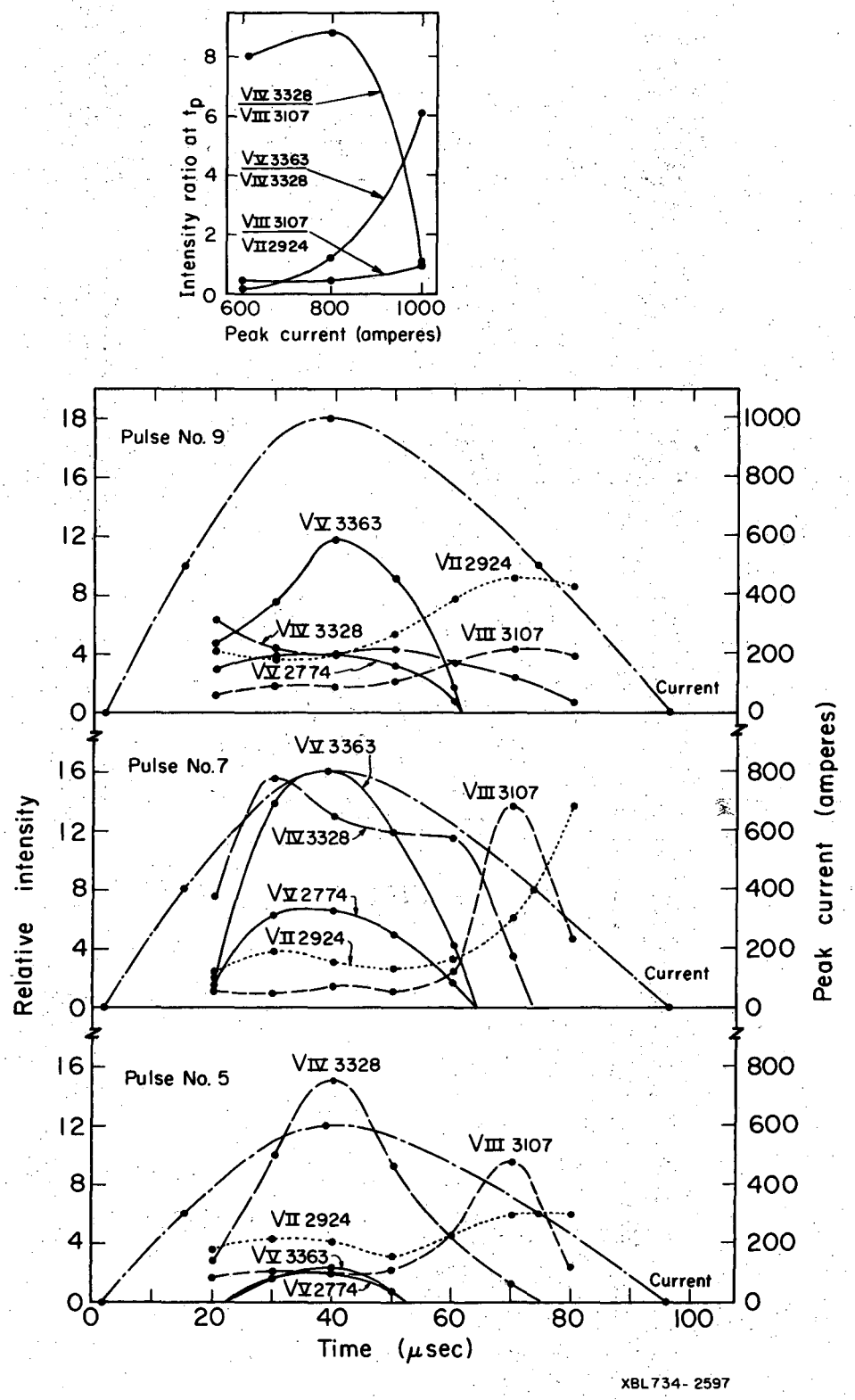

FIG. 1.10. Relative line intensities versus time. L = 13 μh; pulses 5, 7, and 9, Table 1.2.

The light emission of scandium electrodes in the region 500Å to 9500Å was observed for three different peak currents (100, 250, and 500 amperes) with two capacitor values, 4 μf and 24 μf. The circuit parameter values were V_o = 2800 and 1400 volts respectively, with constant $\frac{\tau_{1/2}}{t_p}$ = 1.9 (γ = 0.35) and constant discharge repetition rate. Exposure times were constant. On visual comparison of the spectra three facts could be observed: (1) the intensities of the spectra obtained with the 4 μf capacitor were reduced by about a factor of four from those obtained with the 24 μf capacitor, (2) the Sc II spectrum showed a much sharper decrease in intensity with current increase (lower L values) in the 4 μf spectra than in the 24 μf spectra, and (3) the intensity of the Sc III spectrum obtained with the 4 μf capacitor showed a much slower rise with current increase than the spectrum obtained with the 24 μf capacitor.

1-4. RESULTS

A. Total Pulses

Figure 1.7 displays several interesting phenomena. As the peak current (or V_o) is increased for fixed values of L, C, and R, higher stages of ionization ($\geqslant V^{2+}$) are excited at some definite peak current and their line intensities increase with peak current. Sufficiently strong lines of the doubly ionized stage may be present at lower peak currents, e.g. the strongest lines of Sc III were observed in a 10-ampere peak current discharge. The singly ionized stage is more favourably excited in the overdamped discharge but remains present at the higher peak currents. Separation of stage ionizations by increasing the peak current for fixed values of L, C, and R, appears difficult as no useful intensity reversal of a given ionization stage is obtained within the limits of the present power supply.

In general the relationship between the line intensity and the excitation energy is complicated by the fact that the line intensity depends on the number of atoms excited to the particular upper state involved in the transition i.e. on the number of atoms released from the electrodes and their distribution over the ionizations stages present during a discharge pulse. The time resolution observations (Figs. 1.8 to 1.10) indicate that during a given time interval within the current pulse the line intensities of the higher stages of ionization stages increase at the expense of the

lower stages when the peak current (or the power) is increased. Thus, the number of atoms per unit time contributing to the rate of charge transfer through the source is approximately constant for fixed L, C, and γ (fixed t_p). This is further supported by photographs[10] of electrode wear as a function of L and C with constant γ, which show the highest degree of similarity when the product LC is constant.

From the relative line intensities in Fig. 1.7 at high peak currents, two conclusions may be drawn. For a given stage of ionization the relative line intensities (1) increase as i_p is increased for fixed L, C, and γ (fixed t_p) and (2) increase when the inductance is increased (increasing t_p) at constant C, γ and i_p. Thus, the line intensities of a given ionization stage increase as either i_p or t_p is increased at constant C and γ. A simple picture of line intensity and excitation energy as a function of the circuit parameters presents itself. Let $i_{min,s}$ be the minimum rate of charge transfer necessary to produce the highest ionization stage, (s) observed in a discharge pulse. With sample vapour leaving the electrode surface at a constant rate for fixed L and C, the longer pulse duration results in a higher intensity of a time-integrated line exposure i.e. $\tau i_{min,s}$ increases where τ is the time interval during which $i(t) \geqslant i_{min,s}$. From Eq. (1-5) $i_p t_p = CV_o h(\gamma)\, g(\gamma)$, hence for a fixed C the product $i_p t_p$ is governed by both $V_o h(\gamma)$ and the discharge duration function $g(\gamma)$, increasing with higher voltages or lower values of γ. The

departure from this generalized simple picture at low peak currents may be due to the following phenomena. Walters[18] reports that at any fixed electrode displacement the intensity-time profile contains an initial high amplitude spike, whose duration (< 15 μsec for the present source) depends on the electrode gap distance but not on the form of the discharge pulse. This would explain the irregular intensity behaviour at constant-voltage, low peak currents: (1) for sufficiently short pulses the initial intensity spike becomes a significant fraction of the total time-integrated intensities and (2) for long pulses obtained with large L values the initial intensity spike is also dominant for the highest ionization stage present because in the later part of the current pulse after breakdown effects cease to play a major role, the circuit-parameter controlled charge transfer rate is less effective in exciting the higher ionization stages as will be seen later.

To excite higher ionization stages increase the maximum rate of charge transfer; to obtain stronger line intensities increase the discharge duration for fixed peak current. In both cases this means deliver more energy ($\frac{1}{2} CV_o^2$) to the source. For a fixed energy there exists a trade-off between the highest ionization stage gained and the strength of its line intensity. For ionization stages lower than the highest ionization stage present, increasing the rate of charge transfer depletes the number of atoms excited to those stages during a given time interval for a nearly constant electrode vapourization rate. This will be

discussed in conjunction with the time resolution results. Generally then, the relationship between relative intensities and circuit parameters is complicated by the distribution of the atoms among the different ionization stages and in certain cases by breakdown effects. Caution is necessary when trying to relate relative intensities and especially intensity ratios of different ionization stages to the circuit parameters.

Intensity peaks, however, considered as the most favourable excitation of the upper state involved in the emitting transition, may be interpreted as representing excitation energies attained and are directly associated with the circuit parameters. Perhaps the most convenient intensity peaks to be considered first are those obtained when three of the four circuit parameters are held fixed. Relative intensities of the different lines may be read from Fig. 1.7 as a function of L at constant C, γ, and V_o. Results are presented in Fig. 1.11 for C = 24 μf, γ = 0.08 and V_o = 700 volts. Intensity peaks are clearly defined and good separation of ionization stages may be obtained from the spectra at constant C by varying L, adjusting R to achieve constant γ, and maintaining constant V_o (see Fig. 1.14). In this manner the spectra of Sc III and V V in the region 500Å to 9500Å were successfully separated from their lower stages of ionization.[11,12] In the top graph of Fig. 1.11 excitation energies (Table 1.3) are plotted, at the corresponding intensity peaks, versus $\frac{1}{L}$. For voltages less than

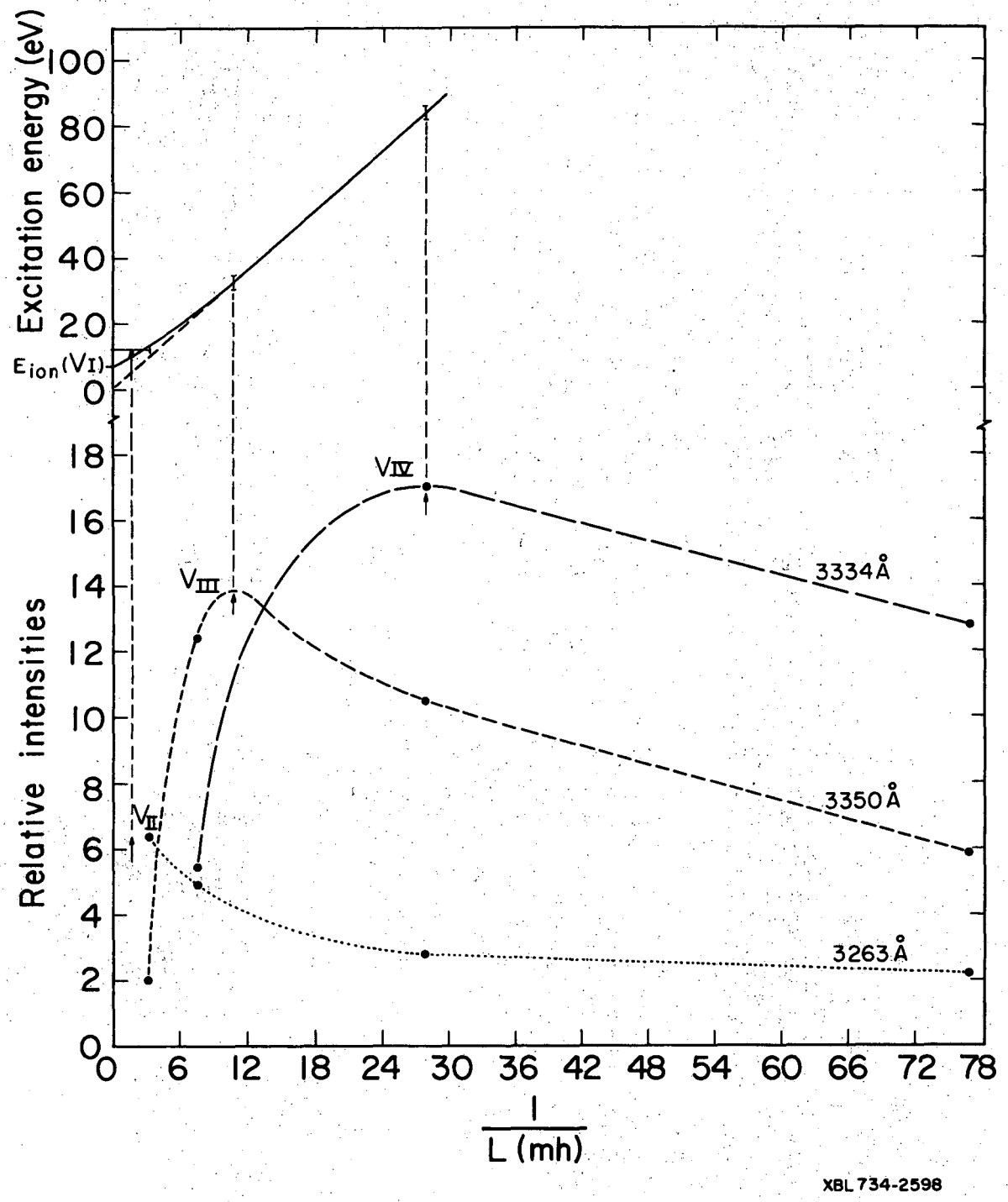

FIG. 1.11. Relative line intensities and excitation energies versus 1/L at V_o = 700 volts. C = 24 μf, γ = 0.08.

700 volts, the intensity peaks occur at lower L values and are spread further apart. Similar plots at different voltages, although further observations at different L values are necessary to determine the intensity peaks more closely, indicate that sufficiently high excitation energies are proportional to $\frac{(V_o)^\delta}{L}$ where $\delta \simeq 2$, for constant C and γ. The departure from $\frac{V_o^2}{L}$ at low voltages is attributed to breakdown effects, i.e. a certain minimum current is necessary to operate the source, which will be discussed later.

The power delivered to the source is a quantity more generally applicable to a variety of sources and it is appropriate to investigate its influence on the excitation energy attained in the source. A useful relation between the power in a pulse and $i_p V_o$ may be obtained from Eq. (1-7) which indicates that the proportionality factor between $i_p V_o$ and $CV_o^2/\sqrt{LC}$ is what has been called the power function $h(\gamma)$ for a given $\frac{C}{L}$ and V_o. For the cases of present interest in Fig. 1.7, γ is constant and $i_p V_o$ will serve as a measure of the power per pulse, the proportionality factor between $i_p V_o$ and $\frac{1}{2} CV_o^2/\tau_{1/2}$ being about three for $\gamma = 0.08$ (Fig. 1.1). Relative intensities of the different lines may be read from Fig. 1.7 as a function of L at constant C, γ and $i_p V_o$ with curves of $i_p V_o$ obtained from Table 1.2. This was done for two values of $i_p V_o$ (165 kVA and 280 kVA) and the results are presented in Fig. 1.12, plotted versus $\frac{1}{L}$. Intensity peaks of the different ionization stages occur, though there appears to be

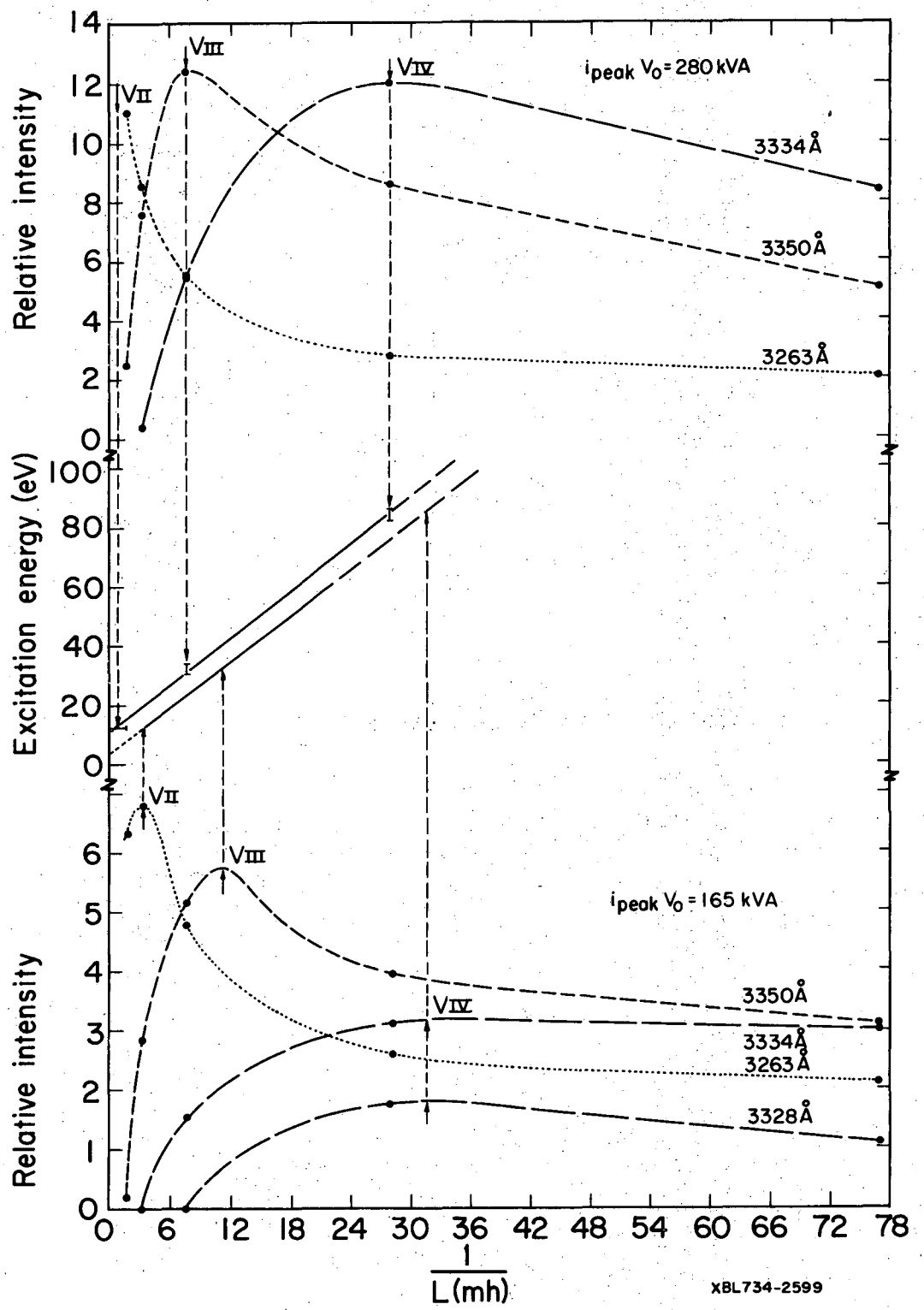

FIG. 1.12. Relative line intensities and excitation energies versus 1/L at constant $i_p V_o$. C = 24 μf, γ = 0.08.

greater mixing of ionization stages at higher L values than the plot at constant voltage (Fig. 1.11). In the central graph of Fig. 1.12 excitation energies are plotted, at the corresponding intensity peaks, versus $\frac{1}{L}$. With exception of the V IV intensity peak at 165 kVA, all points are rather well defined resulting in two linear, parallel lines of excitation energy versus $\frac{1}{L}$; the curve obtained with the higher value of $i_p V_o$ is shifted to higher excitation energies. Figure 1.7 further indicates that the intensity peaks (including that of V V) at a higher power would result in a line shifted further to the left. The graphs were obtained at constant C and γ. With breakdown effects appropriately reflected in the product $i_p V_o$, one obtains from the intercept and slope of the two linear curves

$$E_e = (1.16 \times 10^{-2}\, i_p V_o)^2 + 2.61 \times 10^3 \frac{1}{L} \qquad \text{constant } C,\gamma \qquad (1\text{-}8)$$

where the excitation energy, E_e, is in electron volts when $i_p V_o$ is expressed in kVA and L in μh. Equation (1-8) reproduces both excitation energy versus $\frac{1}{L}$ curves with an error of less than 3%, and may be useful in future investigations of other elements.

Consider now the C dependence of Eq. (1-8). From the observations using the scandium electrodes, by varying C at constant γ, the C dependence may be determined. From Eq. (1-4), $i_p V_o = \sqrt{\frac{C}{L}}\, V_o^2\, h(\gamma)$, thus forming ratios of the power associated with the 4 μf and 24 μf capacitors at constant γ obtains

$$\frac{(i_p V_o)_4}{(i_p V_o)_{24}} = \left(\frac{V_{o4}}{V_{o24}}\right)^2 \left(\frac{L_{24} C_4}{L_4 C_{24}}\right)^{1/2} \simeq 2.5 \quad .$$

Despite this increase in power per pulse used with the 4 μf capacitor, the intensities drastically decreased and the intensity peaks of Sc II and Sc III are spread further apart on an intensity versus $\frac{1}{L}$ plot. With the assumption that an increase in C is equivalent to a decrease in L, these facts indicate a linear dependence on C in the excitation energy versus $\frac{1}{L}$ plot at constant γ, so that Eq. (1-8) becomes

$$E_e = a' (i_p V_o)^2 + b' \frac{C}{L} \qquad \text{constant } \gamma \qquad (1\text{-}9)$$

where a' and b' are constants depending on the source geometry, the electrode element, and possibly γ.

Consider next the γ dependence of Eq. (1-9). First it will be established that the slope of the E_e versus $\frac{1}{L}$ plot is a decreasing function of γ. The relative intensities of V II for the pulses numbered 24, 21, and 17 in Table 1.2 are 4.1, 4.3, and 5.9, respectively. The corresponding values of L are 593, 312, and 133 μh, and of γ are 6.3, 6.3, and 10.0. From the topmost graph in Fig. 1.7 note that the V II line intensity increases with a decrease in γ and a corresponding increase in $i_p V_o$, at fixed L and C. Therefore, the relative intensity (5.9) observed from pulse 17 (L = 133 μh, γ = 10.0) would increase for a decrease in γ and a

corresponding increase in $i_p V_o$, at the given L and C. Hence, the intensity peak of the V II lines for $\gamma = 6.3$ and $i_p V_o = 69$ kVA occurs at $L < 133$ μh, resulting in a single data point on the E_e versus $\frac{1}{L}$ plot in Fig. 1.12 with ordinate 12.2 eV and abscissa not less than $\frac{1}{L} = \frac{1}{0.133} = 7.52\ \text{mh}^{-1}$. Because no negative excitation energies exist by definition the intercept of the E_e versus $\frac{1}{L}$ plot is positive and the slope at constant C is less for $\gamma = 6.3$ than for $\gamma = 0.08$ (compare Fig. 1.12), i.e. b' in Eq. (1-9) is a decreasing function of γ.

The exact γ dependence in Eq. (1-9) may be determined from the topmost graph in Fig. 1.7 (pulses 24, 25, and 26, Table 1.2) where the relative intensity of the spectra from ionization stages higher than V II is comparatively weak or nonexistent. Consider the special case when only the spectra of the neutral atom and the singly ionized stage are present in the emission of the discharge. This condition occurs for a certain minimum charge transfer per unit time through the source, sufficient to operate the source stably. For a nearly constant sample vapourization rate (fixed L and C), the number of singly ionized atoms at any given time during the discharge is chiefly determined by the rate of charge transfer through the source, i(t). At the time t_p the abundance of singly ionized atoms and hence the maximum intensity is determined by $i_p \propto V_o h(\gamma)$. In addition, when one observes time-integrated light pulses the discharge duration function $g(\gamma)$ enters in the line intensity; it determines the length of time during

which atoms are being excited to the upper level of the emitting transition. For the total-pulse observations under consideration, the time-integrated relative intensity of the V II lines thus depends on $V_o h(\gamma)$ and $g(\gamma)$, and in this special case is in principle a direct measure of the excitation energy achieved and maintained during some time interval of the discharge duration. To compare this with the controlled excitation of the neutral atom in a low-current source with constant γ and varying voltage see Ref. 19. The relative intensity of the V II lines for pulses 24, 25 and 26 are plotted versus $[V_o h(\gamma)]^2$ and versus $g^2(\gamma)$ in Fig. 1.13, where $\frac{i_p}{h(\gamma)} = 300$ amperes ($\pm$ 6%) has been used (Table 1.2). The V II line intensities have been drawn to approach zero for some minimum value of the peak current, $|(i_p)_{min}| \geq 0$; the departure from the straight line at low peak currents is interpreted as being caused chiefly by thermal equilibrium effects in the light source at high value of γ (long discharge duration). Recall that the extreme limit $\gamma \to \infty$ ($g(\gamma) \propto t_p \to 0$, long discharge duration) with voltages which barely operate the source ($\frac{i_p}{h(\gamma)}$ = constant) is the d.c. arc limit in which thermal equilibrium prevails in the light source and much lower power values suffice to operate the source. With a nearly linear relationship between $h(\gamma)$ and $g(\gamma)$ near $\gamma = 1$, the results of Fig. 1.13 indicate that the relative intensity of V II lines, I_{rel}, for sufficiently high intensities and at constant L and C, obeys

$$I_{rel} = \alpha (i_p V_o)^2 + \beta\, g^2(\gamma) = \alpha' [V_o h(\gamma)]^2 + \beta\, g^2(\gamma) \qquad (1\text{-}10)$$

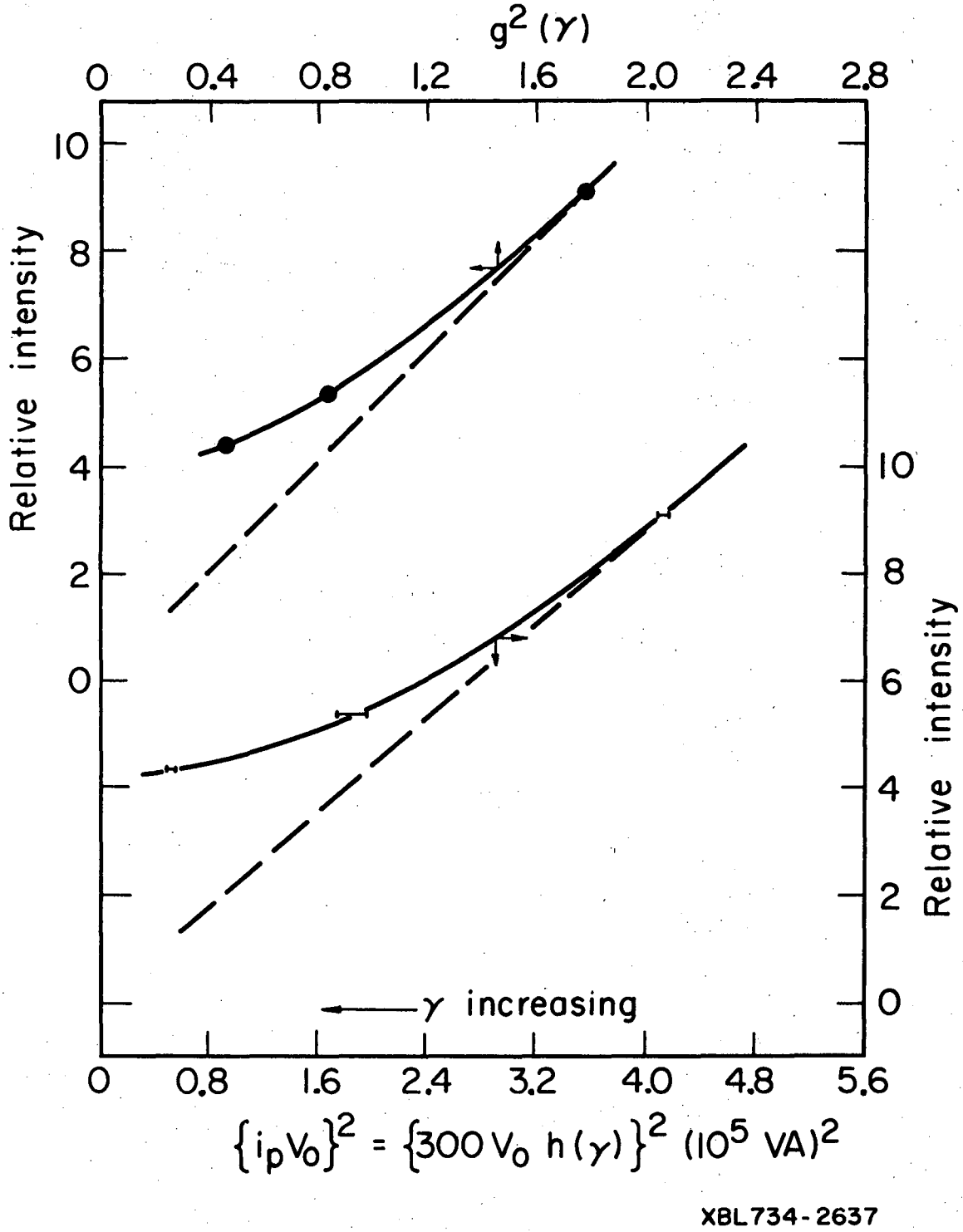

FIG. 1.13. Relative intensity of V III near critical damping and the minimum operating voltage of the source.

where α, β, and α' are independent of the circuit parameter γ. Correlating Eqs. (1-9) and (1-10), and recalling that the excitation energy is approximately proportional to $\frac{V_o^2}{L}$ for constant C and γ, results in

$$E_e = \frac{C}{L}\left\{a[V_o h(\gamma)]^2 + b\, g^2(\gamma)\right\} = a\, i_p^{\,2} + b\left(\frac{t_p}{L}\right)^2 \qquad (1\text{-}11)$$

where a and b are positive constants of the source geometry and the electrode material and the assumption has been made that an increase in C is equivalent to a decrease in L. The right hand side of Eq. (1-11) is obtained by substituting Eqs. (1-3) and (1-4) where t_p is to be reckoned from the start of a given current pulse. The correlation of Eqs. (1-9) and (1-10) implies that $\frac{Ri_p}{2\sqrt{\gamma}\, h(\gamma)} = V_o$ is constant for high values of γ and at voltages which barely suffice to operate the source stably. In the present investigation the latter condition occurs for pulses 18 and 22 (Table 1.2). In the limit $\gamma \to \infty$, $\frac{Ri_p}{V_o} = 2\sqrt{\gamma}\, h(\gamma) \to 1$ (Table 1.1) and V_o is the operating voltage of the d.c. arc. Substituting in Eq. (1-8) the appropriate values (Table 1.2) of the necessary quantities in accordance with their dependence indicated by Eq. (1-11), one obtains that the peak intensity of V II lines for the case discussed previously (C = 24 μf, γ = 6.3, $i_p V_o$ = 69 kVA) occurs at L ≃ 50 μh, consistent with the observations which indicate L < 133 μh.

The functions $h(\gamma)$ and $g(\gamma)$ in Eq. (1-11) are known, monotonically decreasing of γ ($0 \leqslant \gamma \leqslant \infty$), Eqs. (1-3) and (1-4).

The function $g(\gamma)$ is the discharge duration function and $h(\gamma)$ is the power function relating the peak current and voltage, for a given L and C. The excitation energy gained in the source depends on the power delivered to the source and the pulse duration. The $\frac{C}{L}$ dependence in Eq. (1-11) is consistent with the data reported by Schreiber and Fry[20] for an underdamped discharge at constant voltage.

B. Time Resolved Pulses

The time resolution observations are displayed in Figs. 1.8, 1.9, and 1.10. The first of these figures shows the relative intensities of the lines versus time within the current envelope of pulse 20. Three lines of each ionization stage present are shown to display their common behaviour. In Figs. (1.9) and (1.10) relative intensities are plotted versus time within three different current envelopes at constant L, C, and R; pulses 12, 14, 16 and pulses 5, 7, and 9, respectively. The intensity of the highest ionization stage present is a maximum at t_p, in accord with the results reported for the case of underdamping by Strasheim and Blum.[10] The intensity-time profiles of the lower ionization stages generally consist of two peaks separated by an intensity-minimum valley, the duration of which depends on the current pulse length[18] and the stage of ionization. Both the intensity profile of the higher ionization stages and the intensity valley of the lower stages broaden as the power is increased. It appears that as the

peak current is increased for fixed L, C, and R the intensities of the higher ionization stages is increased at the expense of the lower stage excitations. The topmost graphs in Figs. 1.9 and 1.10 show the variation of intensity ratios at t_p versus peak current at constant L, C, and R. Evidently much greater intensity variations occur within the current pulse than can be observed from the time-integrated pulses. Using a time resolution rotating sector with a window of appropriate duration, a rather sudden change in the intensity ratio of two consecutive ionization stages may be observed between two spectra, for example the $\frac{V\ V}{V\ IV}$ intensity ratio in Fig. 1.10 between 600 and 1000 amperes peak current. The spectra are shown in Fig. 1.14. Comparing relative intensities or intensity ratios between Figs. 1.9 and 1.10 it is clear that for fixed γ higher peak currents gain higher excitation energies i.e. higher charge transport through the source within a time interval results in the excitation of higher ionized atomic states during that time interval.

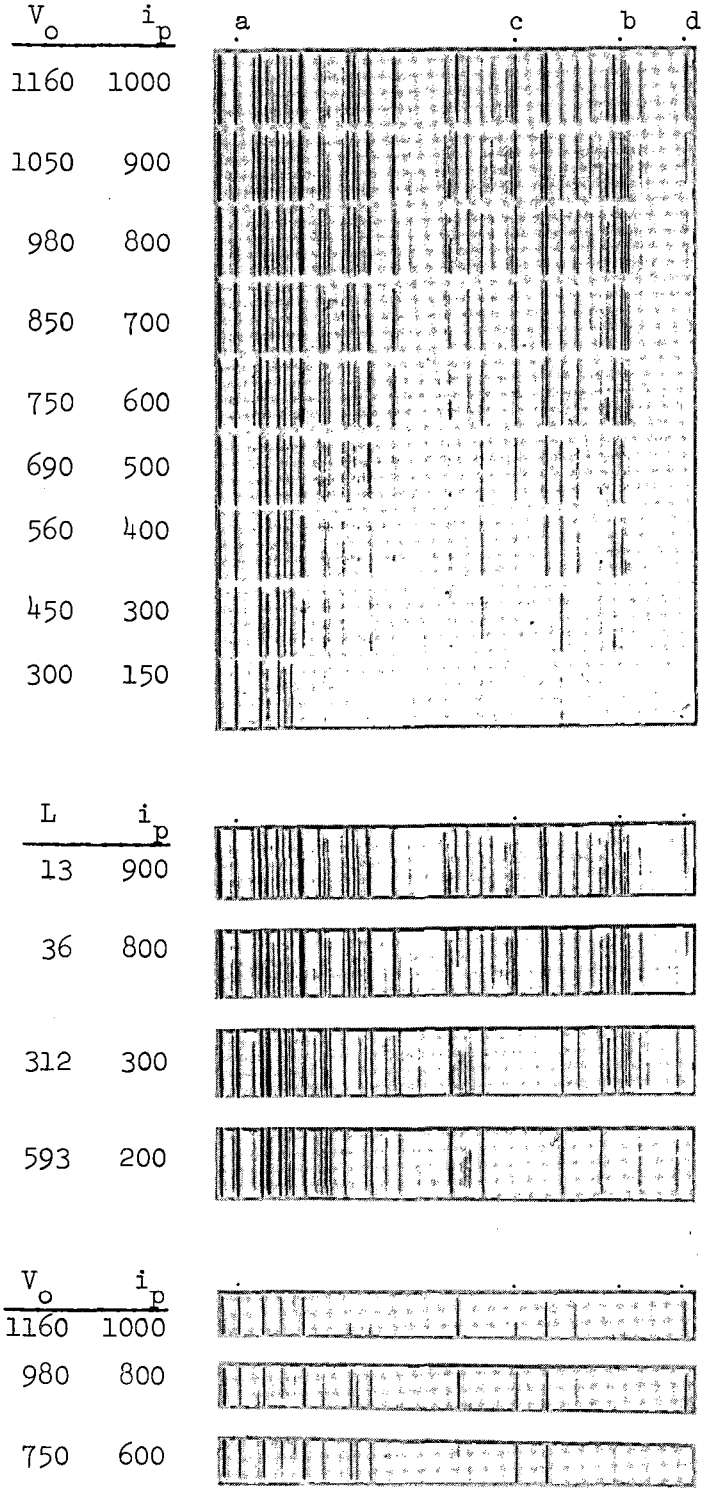

XBB 734-2500

FIG. 1.14. Ionization stages of vanadium obtained with different values of the circuit parameters at constant C = 24 μf and γ = 0.08. a=V II 3271.1, b=V III 3350.2, c=V IV 3328.5, d=V V 3363.5Å.
Top: total-pulse observation, L = 13 μh, varying V_o.
Center: total-pulse observation, $V_o \simeq 1000$ v, varying L and R.
Bottom: time-resolved at t_p, L = 13 μh, varying V_o.

1-5. DISCUSSION

Both total-pulse and time-resolution analysis indicate that higher excitation energies are gained with increased power delivered to the source. For a fixed γ, increasing the voltage increases the highest excitation energy gained in a current pulse, while for a fixed voltage increasing the discharge duration increases the time-integrated intensity. Separation of stages when observing total-pulse, time-integrated intensities may best be effected by varying the discharge duration function $g(\gamma)$ and/or $\frac{C}{L}$ while maintaining constant voltage. Time-resolution of the discharge pulse with a constant time window allows separation of ionization stages by varying the current through voltage variation with constant L, C, and R.

When observing total pulses, in addition to C and L the discharge duration may be exploited to improve separation of higher ionized atomic states. The discharge duration function $g(\gamma)$ is a monotonically decreasing function of γ $(0 \leqslant \gamma \leqslant \infty)$. Thus, the intensity peaks in the $\frac{1}{L}$ plot may be spread further apart ($\gamma \to \infty$, improved separation) or brought closer together ($\gamma \to 0$, worse separation) for fixed C and power. However, at fixed power the former means a decrease in the maximum excitation attained in the discharge, while the latter gains higher excitation. Thus, there exists a trade off between stage of excitation attainable and the

ability to separate them. Without time resolving underdamped discharges, indeed the optimum exists at critical damping ($\gamma = 1$) where high stages are best separable. For fixed CV_o, overdamping reduces the stage attainable while underdamping introduces an unduly amount of lower stages of ionization in the consecutive pulses of the oscillatory train.

Consider first low excitation energies. It is well known that spectroscopic sources will not operate below a certain minimum current i.e. a sufficient number of electrons must be present to give rise to a current, and that no electrical source will excite only the neutral atom. This may be interpreted as saying that there exists a minimum excitation energy below which a source will not operate, e.g. of the order of the first ionization energy of the neutral atom. Thus, there exists a lower threshold $E_e \geqslant E_{min} > 0$, the last inequality because no negative ionization energies exist by definition, which represents a horizontal line in the E_e versus $\frac{1}{L}$ plot. This then explains the intermittent firing of the vacuum sliding spark at low currents achieved by overdamping with large values of L, i.e. Eq. (1-11) approaches zero as γ and/or L approach large values such that E_e is below E_{min} for the electrode element and the source geometry. Similarly it explains why a vacuum spark (low C and γ) will not operate at some fixed voltage for sufficiently large L value.

In the limit $\gamma \to \infty$ and voltages such that the source barely operates the d.c. arc results. In this limit $g(\gamma) \to 0$ and the slope

of the E_e versus $\frac{1}{L}$ plot approaches zero; for powers just sufficient to operate the source stably only the radiation of the neutral atom and the single ionized stage is observable. In addition, the intensity peak of the singly ionized stage broadens and moves off to $\frac{1}{L} \to \infty$, making its detection difficult. In the opposite limit ($\gamma \to 0$), e.g. the highly underdamped discharge of a vacuum spark, the slope increases which allows the excitation of much higher stages of ionization but the intensity peaks of neighbouring stages crowd closer together and the lower stages are unduly excited in the consecutive pulses of the oscillatory train, both making stage separation difficult when observing all the light from such a train of pulses.

For total discharge observations, it is also clear now why stage separation by means of intensity peaks is difficult by just increasing the peak current (increasing V_o) at fixed L, C, and R (fixed γ). The separation dimension - second term in Eq. (1-11) - is not utilized, all that occurs is a vertical traversal in the E_e versus $\frac{1}{L}$ plot, exciting more and higher stages of ionization as the power is increased. At best, broad intensity peaks may be obtained by exciting higher stages of ionization at the expense of the lower stages for a constant sample vapourization rate. (see bottom of Fig. 1.7, V III at i_p = 900 amperes).

Time resolving the first current pulse of an underdamped discharge achieves the two-fold optimum of exciting higher stages of ionization while at the same time presenting an excellent

opportunity to separate them. It has been noted that the highest stage of ionization occurs at t_p. This is as expected since the amount of charge transported through the source within a fixed time interval is a maximum at t_p, i.e. the highest stages of ionization enter the discharge at this time. In addition to sample vapour leaving the electrode surface during the discharge, it was found that the sputtered sample material on the surface of the spacer borehole contributes significantly to the material being excited. As the current is less on either side of t_p, lower ionization stages enter the discharge at times different from t_p. This would explain the observed twin-peaked intensities of the lower stages on both sides of t_p. When either $\sqrt{\frac{C}{L}}\, V_o$ is increased or γ is decreased the maximum rate of charge transfer increases. The necessary charge transfer rate to gain a given stage of ionization is achieved before t_p and lasts after t_p; the intensity-time profile of the highest stage present broadens as does the intensity-minimum valley of the lower stages. When the peak current is increased still further, higher stages of ionization begin to appear at the time t_p at the expense of the lower stages. With a time resolution window, a proper fraction of the discharge duration wide, this appearance and disappearance of the ionization stages has been observed (Figs. 1.9 and 1.10). Necessary plate exposure times in terms of total number of pulses required remain reasonable.

To gain very high excitation energies in an electrically pulsed light source it is necessary to increase $\frac{C}{L}$ and V_o, i.e.

increase the peak current and/or $\frac{t_p}{L}$ (Eq. 1-11). Both these quantities, $i_p = \sqrt{\frac{C}{L}}\ V_o\ h(\gamma)$ and $\frac{t_p}{L} = \sqrt{\frac{C}{L}}\ g(\gamma)$, are a maximum for a given $\frac{C}{L}$ and V_o as $\gamma \propto R^2 \to 0$ ($\lim_{\gamma \to 0} h(\gamma) = 1$, $\lim_{\gamma \to 0} g(\gamma) = \frac{\pi}{2}$). Consider then the limit $R \to 0$ for given V_o and $\frac{C}{L}$ with small values of L in which case the discharge approaches a pure sinusoidal wave ($R \to 0$) with pulses of high peak current and short duration ($t_p \to \frac{\text{period}}{4} \to \frac{\pi}{2}\sqrt{LC} \to$ small). In practice, R and L (and therefore γ) remain finite and the peak current decays in the consecutive pulses of the oscillatory train. Thus, lower neighbouring stages of ionization are excited in the consecutive current pulses of an oscillatory train making stage separation difficult in total discharge observations. Separation of these high ionization stages may be attained when the following is considered. For sufficiently short current pulses the intensities of the highest ionization stages present tend to dominate (Figs. 1.10 and 1.12), so that pulses with high peak current and with t_p not larger than a few microseconds excite but a few high ionization stages. These few high ionization stages present in a single current pulse may be observed by transmitting into the spectrograph only light arising from pulses with nearly the same peak current, for example, by use of a rotating sector window of appropriate duration. Alternatively, the spectrum of the highest stage of ionization present in any one of the current pulses may be observed with a time-window of sufficiently short duration and appropriately synchronized with the

discharge. Thus, for high values of V_o and fixed $\frac{C}{L}$ with sufficiently small values of L and γ, high stages of ionization are excited which may be separated by varying the peak current through voltage variation.

This research has confirmed that the excitation energy and the emission line intensities in a vacuum sliding spark depend on the power delivered to the source and on the duration of the discharge pulse in a definitive manner. A relationship was found between the excitation in the source and the electrical circuit parameters that may be simple expressed in terms of the capacitance, the inductance, the initial voltage on the capacitor, two known functions of the continuous circuit parameter γ one of which is directly associated with the discharge duration and the other directly to the peak current through the source, and two constants which in general depend on the source geometry and the electrode sample material. No such direct relationship could be ascertained between the intensities of the spectral lines and the electrical circuit parameters. In general the line intensity depends on the distribution of the sample-vapour atoms among the different stages of ionization present in the light source.

Excellent separation of the spectra of higher ionized atomic states was obtained by two different methods. The first method consisted of analyzing the total light pulse while varying the inductance and resistance, with constant capacitance, γ, and

constant initial voltage on the capacitor. The second method, superior to the first in separating higher ionization stages, consisted of time-resolving the light pulse while varying the initial voltage on the capacitor with constant inductance, capacitance, and resistance. Other variations of the circuit parameters may be employed to attain different degrees of excitation and separation of ionization stages.

The equations developed and found have here been applied to the excitation and separation of spectra of higher ionized atomic states. In addition, these equations should be of use in spectrochemical analysis where quantitative application of the specification of spark source parameters and their correlation with spectral character is of basic importance. With the improved understanding and control of the excitation in the source as a function of the circuit parameters, it is feasible to investigate Zeeman studies of higher ionized atomic states by placing the light source in a magnetic field.

Further work is in progress especially to place the C and γ dependence of Eq. (1-11) on a more secure basis, to extend the source analysis to higher stages of ionization, and to investigate Zeeman analysis of higher ionized atomic states.

2-1. INTRODUCTION

The Sc^{2+} and V^{4+} ions have a ground state [Ar] $3d^1\ 3^2D_{3/2}$ and are isoelectronic with neutral potassium. Previous investigations of Sc III have been conducted by Gibbs and White[21] and revised by Smith,[22] who identified the seven lowest levels. Russell and Lang[23] predicted seven new levels from an analysis of the quantum defect variation and isoelectronic data. The known data for V V are scanty, consisting of 15 classified lines in the region between 286Å and 1811Å, eleven of which were observed by Gibbs and White[24] and four by Iglesias,[17] from which a total of seven levels were deduced. The objectives for renewing the investigations of the spectra from these two ions are two-fold. Firstly, it was desired to improve and extend the knowledge about these ions, thereby extending the isoelectronic data of the neutral potassium series for further analysis of other members of the series, for example Fe^{7+} the spectral lines of which are expected to be observable in the spectrum of the solar corona. Secondly, with the improved analysis of these ions, it was desired to investigate the excitation and separation of higher ionized atomic states as a function of the circuit parameters in an electrically pulsed light source, in particular a vacuum sliding spark. This chapter concerns the first objective of improving and extending the analysis of Sc III and V V.

2-2. THEORY

A. Energy Levels

The study of regularities in atomic spectra is considerably facilitated by the concept of energy levels. When an atom is unperturbed by external fields, an energy level is designated by the total angular momentum of the electron occupying the level, the principal quantum number n, and other quantum numbers. The Hamiltonian of the atom establishes (in principle) the energy of the level in terms of the quantum numbers. An experimentally observed wavelength can be expressed as the energy difference between two levels of a system of energy levels characteristic of the atom. Consider an energy level series in which only the principal quantum number varies. If E_n is the energy of the n^{th} level relative to the ground level (n = 1) and E_{ion}, the ionization energy, is the energy required to remove an electron from the ground level to a free position, then the binding energy (E_b) of an electron in the n^{th} level may be expressed as $-\frac{E_b}{hc} = \frac{E_{ion}-E_n}{hc} \equiv T_n$, where h is Planck's quantum constant and c is the velocity of light. T_n, referred to as the term value, is a convenient quantity for describing experimental regularities, especially of atomic systems whose energy-level series are nearly hydrogen-like.

If the atom is pictured as consisting of a core with charge $Z_c e$ and a single electron, interacting chiefly according to the Coulomb law, the deviation from pure Coulomb behaviour may be accounted for by introducing a penetration parameter p or a quantum

defect δ. The experimental regularities are then conveniently discussed in terms of this deviation from a central Coulomb field behaviour by defining p and δ_n by

$$T_n = R\left(\frac{Z_c+p}{n}\right)^2 = R\left(\frac{Z_c}{n-\delta_n}\right)^2 \qquad (2\text{-}1)$$

where n is the principal quantum number of the hydrogen-like Coulomb system ($p = \delta_n = 0$); $Z_c \equiv Z - N'$, N' being the total number of electrons in the system less one; and R is the Rydberg constant for the atom in question. The penetration parameter p serves most appropriately when considering for a given n, the variation of T_n versus Z_c in isoelectronic atomic systems - systems with identical electronic structure and differing only in the nuclear charge Z. The quantum defect is useful in describing for a fixed core charge Z_c, the variation of T_n versus n in a term series. The penetration parameter p and the quantum defect δ_n are related by $p(n - \delta_n) = \delta_n Z_c$.

Consider first an isoelectronic comparison. Assuming that Z_c is the main charge dependence in Eq. (2-1) a plot of $\frac{T_n}{Z_c+p_o}$ versus Z_c, where p_o is a suitably chosen constant, is nearly a linear function of Z_c. With a free choice of zero level, one may also plot $\frac{E_n-E_{ref}}{Z_c+p_o}$ versus Z_c, where E_{ref} is a convenient reference level.[25] A relation which is more sensitive to the slow variation of the penetration parameter p as a function of Z_c may be obtained by considering the difference

$$T_n - T_n^H = \frac{R}{n^2}\left[(Z_c+p)^2 - Z_c^2\right]$$

or

$$T_n - T_n^H + aZ_c = \frac{R}{n^2}p^2 \qquad (2\text{-}2)$$

where $T_n^H \equiv R\left(\frac{Z_c}{n}\right)^2$ is the term value of the equivalent hydrogen-like level and a is nearly constant for fixed n. Equation (2-2) is of practical importance when checking the analysis of spectra of highly ionized atoms for suspected interactions whenever unperturbed positions of suitable pairs of terms approach closely. Such interaction takes the form of a mixing of wave functions, resulting in a mutual repulsion of the term energies.

For a given electronic structure, consider the quantum defect variation. It has been found empirically[26] that δ_n expressed in a power series of $t_n \equiv \frac{T_n}{S}$ (where S is a scaling factor) reproduces observed unperturbed series of levels to within the experimental error. This power series expansion of δ_n was later deduced quantum-mechanically by Hartree[27] and it is known that in the limit $n \to \infty$ the quantum defect δ_n approaches in general a constant value.[28] The experimentally observed energy differences of unperturbed levels may be utilized to determine the ionization energy E_{ion} and the constants in the power series expansion of δ_n. Series formulae can thus be obtained to represent the energy level series which may then be used to predict unobserved levels of the series.

B. Ionization Energies and Series Formulae

The ionization energy of a particular atomic configuration may be calculated from an unperturbed level series that obeys a power series expansion of δ_n by considering the observed energy differences. Prior methods of calculating ionization energies[29] generally made use of four or less observed levels of a series at a time. In extended atomic analysis often more than four levels in a series are determined and calculating ionization energies by taking the known levels four at a time frequently results in disagreement between the ionization energies of a given series obtained in this manner. Furthermore, ionization energies determined from different level series in a configuration seldom agree. It is therefore desirable to calculate ionization energies using all the known levels of an unperturbed series simultaneously and compare ionization energies obtained from different series within the configuration.

Let N be the total number of levels observed in an unperturbed series and $\delta_n = \sum_{i=0}^{N-1} a_i t_n^{\,i}$, where the constants a_i are to be determined. In order to determine the correct ionization energy, E_{ion} (cm^{-1}), assume initially an approximate value $E_{ion}^{(o)}$ from which the initial values $t_n^{(o)}$ and $\delta_n^{(o)}$ may be determined by means of

$$t_n^{(o)} = (E_{ion}^{(o)} - E_n)/S$$

$$\delta_n^{(o)} = n - \left(\frac{RZ_c^2}{E_{ion}^{(o)} - E_n} \right)^{1/2} .$$

For convenience in writing the following equations the superscripts on $t_n^{(o)}$ and $\delta_n^{(o)}$ will be omitted; in what follows various ionization energies, $E_{ion}^{(o)}$, are to be investigated by means of an incremental procedure. Forming first differences of the initial quantum defects obtains

$$\delta_n - \delta_{n+1} = \sum_{i=0}^{N-1} a_i (t_n^i - t_{n+1}^i) = \sum_{i=1}^{N-1} a_i \sum_{j=0}^{i-1} (t_n - t_{n+1}) t_n^{i-1-j} t_{n+1}^j \quad (2\text{-}3)$$

or $$Q(n,n+1) \equiv \frac{\delta_n - \delta_{n+1}}{t_n - t_{n+1}} = \sum_{i=1}^{N-1} \sum_{j=0}^{i-1} a_i t_n^{i-1-j} t_{n+1}^j .$$

Similarly

$$Q(n+1,n+2) \equiv \frac{\delta_{n+1} - \delta_{n+2}}{t_{n+1} - t_{n+2}} = \sum_{i=1}^{N-1} \sum_{j=0}^{i-1} a_i t_{n+1}^{i-1-j} t_{n+2}^j .$$

Forming differences of the quantities Q one obtains

$$Q(n,n+2) \equiv \frac{Q(n,n+1)-Q(n,n+2)}{t_n - t_{n+2}} = \sum_{i=2}^{N-1} \sum_{j=1}^{i-1} \sum_{k=0}^{j-1} a_i \, t_{n+1}^{i-1-j} \, t_n^{j-1-k} \, t_{n+2}^{k}$$

and in general, to determine the constants ($1 \leqslant m \leqslant N-1$):

$$Q(n,n+m) \equiv \frac{Q(n,n+m-1)-Q(n+1,n+m)}{t_n - t_{n+m}} = \sum_{i_m=m}^{N-1} a_{i_m} \, C(i_m,n,n+m) \qquad (2\text{-}4)$$

where

$$C(i_m,n,n+m) \equiv \sum_{i_{m-1}=m-1}^{i_m-1} \sum_{i_{m-2}=m-2}^{i_{m-1}-1} \cdots \sum_{i_2=2}^{i_3-1} \sum_{i_1=1}^{i_2-1} \sum_{i_0=0}^{i_1-1} t_{n+m-1}^{i_m-1-i_{m-1}} \qquad (2\text{-}5)$$

$$\times \; t_{n+m-2}^{i_{m-1}-1-i_{m-2}} \cdots t_{n+1}^{i_2-1-i_1} \; t_n^{i_1-1-i_o} \; t_{n+m}^{i_o}$$

is a combinational expression involving $t_n, t_{n+1}, \ldots, t_{n+m}$. The quantities $C(i_m,n,n+m)$ may be constructed by means of the expression

$$C(i_m,n,k+m) = \sum_{\nu=k}^{n+m} t_\nu \, C(i_m-1,n,\nu+m) \qquad \begin{matrix} m+1 \leqslant i_m \leqslant N-1 \\ n \leqslant k \leqslant n+m \end{matrix} \qquad (2\text{-}6)$$

Designate by n_f and n_ℓ the first and last observed levels, respectively. Then for m = N-1 from Eq. (2-4)

$$Q(n_f, n_\ell) \equiv \frac{Q(n_f, n_\ell - 1) - Q(n_f + 1, n_\ell)}{t_{n_f} - t_{n_\ell}} = a_{N-1} \qquad (2\text{-}7)$$

where C(m,n,n+m) = 1 has been used. To determine the correct ionization energy and the N-1 constants a_o, a_1, a_2, . . .,a_{N-2}, set $a_{N-1} \equiv 0$ which obtains

$$Q(n_f, n_\ell - 1) = Q(n_f + 1, n_\ell)$$

or from Eq. (2-4)

$$\frac{Q(n_f, n_\ell - 2) - Q(n_f + 1, n_\ell - 1)}{Q(n_f + 1, n_\ell - 1) - Q(n_f + 2, n_\ell)} = \frac{t_{n_f} - t_{n_\ell - 1}}{t_{n_f + 1} - t_{n_\ell}} = \frac{E_{n_\ell - 1} - E_{n_f}}{E_{n_\ell} - E_{n_f + 1}} \qquad (2\text{-}8)$$

The right-hand side of Eq. (2-8) depends only on the observed energy differences, while the left-hand side depends on the chosen trial ionization energy. Varying the trial ionization energy, $E_{ion}^{(o)}$, until Eq. (2-8) is satisfied yields the correct ionization energy and the corresponding constants may then be determined from Eq. (2-4) i.e.,

$$a_m = Q(n, n+m) - \sum_{i_m = m+1}^{N-1} a_{i_m} C(i_m, n, n+m) \qquad (0 \leqslant m \leqslant N-1) \qquad (2\text{-}9)$$

where $Q(n,n) \equiv \delta_n$. The method developed here allows calculation of

the ionization energy using any number ($N \geq 2$) of observed levels in a series of which the quantum defect obeys a power series expansion in the t_n. For four observed levels with S = 1 the equations reduce to those used by Shenstone.[29] It was found as expected that the right hand side of Eq. (2-8) is nearly constant for an unperturbed series in an isoelectronic sequence and that the deviation in neighbouring elements decreases as the orbital angular momentum of the series increases. For example, the values of the right hand side of Eq. (2-8) obtained from the ng series (n = 5,6,7) in Sc III and V V agreed to better than 0.05%. This may be utilized to calculate ionization energies when only two levels of an unperturbed series have been observed. Alternatively, for the case N = 2, an estimate of the constant a_1 for the series of a particular ion under consideration may be obtained from the ion's isoelectronic sequence, the calculation then follows through in the same manner.

When the ionization energy for the configuration has been derived, one more constant ($a_{N-1} \neq 0$) may be included in the power series expansion of δ_n, thereby possibly reproducing the observed members of a series more exactly and improving the prediction of other, unobserved numbers of the series. The calculation of the constants is the same as in Eq. (2-9) starting with the derived ionization energy of the configuration under consideration and $a_{N-1} \neq 0$.

A computer program (IENEXT) has been written that (1) calculates the ionization energy and N-1 constants for a given level

series and (2) calculates N constants for a given ionization energy usually determined from a consideration of all the ionization energies obtained from the different level series in a configuration. The number of constants necessary to represent a series is the minimum number of constants that represents the observed levels of the series to within the experimental error. The computer program is included in the appendix. In general, more than one value of E_{ion} satisfies the equality of Eq. (2-8) because the left hand side may contain a singularity in E_{ion}, so that a range of E_{ion} values should be examined around any one obtained value with the ionization increment (DELTA) as small as necessary. For values of E_{ion} which satisfy Eq. (2-8) and which are close together, an independent verification of the true value of the ionization energy is necessary - for example from at least one other series in the configuration.

C. Fine-Structure Intervals

The interaction of the intrinsic spin magnetic moment of the electron with the magnetic field due to its orbital motion causes a splitting of each energy term (except when the orbital angular momentum is zero) into two levels, the level with the smaller total angular momentum having the lower energy. The experimentally observed energy splittings can be represented by the Landé formula[30]

$$\Delta E_{n\ell} = \frac{R\alpha^2 Z_c^2 (Z_c+p')^2}{(n^*)^3 \ell(\ell + 1/2)(\ell + 1)} \qquad (2\text{-}10)$$

where $\alpha \equiv 2\pi e^2/hc$ is the fine-structure constant, p' is an average

penetration parameter for the core-penetrating part of the orbit, $n^* \equiv n - \delta_n$ is the effective principal quantum number, and ℓ is the quantum number associated with the orbital angular momentum of the electron. For orbits which do not penetrate the core ($p' \to 0$) Eq. (2-10) approaches the splitting factor of a pure Coulomb field due to a charge Z_c for which quantum mechanics predicts the value[31]

$$\Delta E_{n\ell} = \frac{R\alpha^2 Z_c^4}{n^3 \ell(\ell + 1/2)(\ell + 1)}$$

called the spin-orbit integral. From Eq. (2-1) and (2-10) and the definitions of n^* and T_n one finds,

$$2\Delta n^* = -n^* \frac{\Delta T}{T} = \frac{\alpha^2 (Z_c + p')^2}{\ell(\ell + 1/2)(\ell + 1)}$$

showing that for a fixed orbital angular momentum, the difference Δn^* for the two components of a doublet term is constant to the same extent as $Z_c + p'$. This near constancy of Δn^* is of practical use as a guide in predicting fine-structure intervals of unobserved levels in an unperturbed level series. When only one level of a series is known or when perturbations are suspected, a plot of $(\Delta E_{n\ell})^{1/4}$ versus Z_c immediately shows a wrong identification or a perturbation as a deviation from a smooth curve.

2-3. EXPERIMENTAL DETAILS

To excite and separate the spectra of scandium and vanadium a vacuum sliding spark light source was used connected in a series LCR electrical circuit (L = inductance, C = capacitance, R = resistance). The vacuum sliding spark light source, its mode of operation, behaviour, and ability to excite and separate higher ionized atomic states as the circuit parameters L, C, R, and the voltage V_o across the capacitor are varied have been described in Chapter 1. Lines belonging to a given stage of ionization were identified by observing their common intensity behaviour with current. In the sliding-spark spectrum lines of oxygen, silicon, and carbon spectra are also present due to the excitation of the spacer material, especially at peak currents greater than 400 amperes. Several different spectrographs were employed to observe the spectra from 500 to 9500Å. They are listed in Table 2.1, along with their figures of merit. Kodak spectroscopic plates were used: short wavelength radiation (SWR) plates in the vacuum region, and 1-O, 1-F, 1-N, and 1-Z plates in the air region.

The scandium spectra were first surveyed at 20Å/mm in air which confirmed the strong Sc III lines predicted by Russell and Lang.[23] More careful separation of the spectra was then obtained at 5Å/mm in air and 2.78Å/mm in vacuum. A peak current of 250 amperes, at which the final spectrum was taken, was selected as the minimum excitation with which a good number of Sc III lines

TABLE 2.1. Spectrograph Characteristics.

Mounting	Focal Length (m)	Grooves/mm	mλ(at blaze) (order × Å)	$m\frac{d\lambda}{dx}$ (order × Å/mm)
Ebert,air	3.4	79	225900	17.5
Ebert,air	3.4	600	5000	5.2
Czerny-Turner,air	0.75	600	7000	20
Eagle,vacuum (NBS)	10.7	1200	1200	0.78
Eagle,vacuum	3.0	1200	1380	2.78

could be photographed at reasonable exposure times. The Sc III spectrum was then photographed, at a peak current of 250 amperes, from 550 to 2675Å with the 10.7-m vuv normal-incidence spectrograph at the National Bureau of Standards (NBS) in Washington; from 2680 to 7900Å with the $m\lambda = 225900$-Å grating, which recorded the stronger lines (intensity ≥ 9) in this region; and from 2400 to 9500Å with the 5Å/mm grating in order to obtain the remaining weaker lines (at exposures up to $1\frac{1}{2}$ hours). Most of the shorter-wavelength lines in the vuv were photographed in the first, second, and third order on the NBS spectrograph. Some of the lines photographed with and 5Å/mm grating were also obtained in several different orders. The weak 9371Å line could be obtained only with the 20Å/mm grating. For the 250-amperes peak current the circuit parameters were $L = 133$ μh, $C = 24$ μf, $R_{added} \approx 4.5$ Ω, and $V_o = 800$ volts, giving a current-pulse full width at half-maximum of 130 μs. The spark was triggered every 65 msec.

The vanadium spectra were separated at 5Å/mm in air and 2.78Å/mm in vacuum. To obtain good excitation of V V a peak current of 1000 amperes was selected. The electrical circuit parameters were $L = 13$ μh, $C = 24$ μf, $R_{added} < 1\Omega$, and $V_o = 1160$ volts. The current-pulse full width at half maximum was 56 μsec and the spark was triggered 15 times per sec. The V V spectrum was photographed from 450Å to 2800Å with the 3-m normal-incidence vacuum spectrograph (2.78Å/mm dispersion), and from 2600Å to 8500Å with the 5.2Å/mm spectrograph in air. The triplet at 483Å was photographed in the

first four orders, and the lines at 962Å and 978Å were photographed in the first and second order. The lines at 285Å and 286Å appeared in the second and third order.

Calibration spectra below 2680Å were obtained from a water-cooled copper hollow cathode with Ge and Si in the cathode,[32-34] and above 2680Å from a ThI electrodeless lamp.[35-37] Plate measurements were made on a 25-cm Grant comparator; 25-40 calibration lines were used on every 25-cm plate. When fitted with a sixth-order polynomial, the wavelengths of the calibration lines deviated from their interferometric value by not more than ±1.5μ × (plate factor). For some of the scandium wavelengths the fourth decimal was retained because these lines were measured on several plates and agreed to better than the third decimal, e.g., the 730-Å and and 731-Å lines were each measured six times on different plates in the second and third orders with an rms deviation of 0.0004Å. The error limits in the scandium wavelengths are estimated to be a few units in the last decimal retained. The vanadium lines obtained in multiorders showed an rms deviation of 0.002Å (except the lines of 285Å and 286Å which agreed to ±0.01Å) when the wavelengths were reduced to the first order; the values listed are the average values. The error limits in the vanadium wavelengths are estimated to be 0.004Å in vacuum and 0.008Å in air.

Intensities were estimated visually from the plates on a scale 1-350.

2-4. DATA AND RESULTS

The analysis of the structure of Sc III and V V was started on the basis of the previously reported levels and a study of isoelectronic and quantum-defect regularities. The lowest unknown levels were predicted from known isoelectronic data with a possible error of the order of $\pm (100 + \Delta E_{ion})$ cm^{-1} where ΔE_{ion} is the possible error in the ionization energy. Fine-structure intervals were predicted from the near constancy of the difference Δn^* for the two components of a doublet term in a Rydberg series. The calculations are straight forward and were made using the computer program ISOEL, included in the appendix. The observed V V lines were then classified to establish the first three members of a series. At this point the higher levels of a series could be predicted and the ionization energy calculated by use of the program IENEXT. Remaining observed lines were then classified to establish these higher levels.

A. Wavelengths and Energy Levels

i. Doubly Ionized Scandium

The list of 93 classified lines of Sc III is presented in Table 2.2. The line at 1742Å appeared hazy at 2.78Å/mm and has been interpreted as two lines of the multiplet associated with the 7p-4d transition. The fine-structure separations of the 7p and 4d terms differ by 2.6 cm^{-1}. This weak line did not appear on the NBS plates. The weak line at 4642Å ($7p\,^2P^o_{3/2} - 5d\,^2D_{5/2}$) blends with an OII line

and could not be completely resolved at 5Å/mm. The 4740.954Å line was resolved from the neutral scandium line at 4741.030Å on the $m\lambda = 225900$-Å grating.

Investigation of the structure of Sc III was started on the basis of the analysis by Smith and the seven levels predicted by Russell and Lang. There was however a 3 cm^{-1} discrepancy in the key combination cycle 3d-4p-4d-4f (see Fig. 2.1) as given by Smith; it is attributed to the 1600-Å and 2000-Å triplets being about 0.06Å too large. The cycle now closes to within a few hundredths of a wave number with the improved wavelengths obtained. Because this discrepancy involved the key vacuum lines 3d-4p-4d, the levels given in Moore's[38] Atomic Energy Levels tables are all too low by about 2-3 cm^{-1}, with the exception of the 5s which is 1.3 cm^{-1} too high, owing to another discrepancy in the 1895-1912-Å doublet as reported by Russell and Lang. The 23 newly found levels and the corrected values for the previously known levels are presented in Table 2.3. The combination cycles close to within a few units in the second decimal place of the wave numbers, i.e., to within the experimental error, indicating that it was possible to maintain sufficient control over excitation to achieve internal consistency.

TABLE 2.2. Classified Lines of Sc III.

Level combination	Wave number (cm^{-1})	Wavelength (Å)	Intensity
$6p\ ^2P^o_{1/2} - 7s\ ^2S_{1/2}$	10667.45	9371.74	1
$4f\ ^2F^o_{5/2} - 5d\ ^2D_{3/2}$	11256.16	8881.585	15
$4f\ ^2F^o_{7/2} - 5d\ ^2D_{5/2}$	11276.08	8865.891	30
$5d\ ^2D_{5/2} - 5f\ ^2F^o_{7/2}$	11322.19	8829.785	50
$5d\ ^2D_{3/2} - 5f\ ^2F^o_{5/2}$	11342.09	8814.293	35
$5g\ ^2G - 6f\ ^2F^o$	11715.46	8533.383	2
$6f\ ^2F^o - 8g\ ^2G$	12426.97	8044.799	1
$5f\ ^2F^o - 6g\ ^2G$	12705.17	7868.648	70
$5s\ ^2S_{1/2} - 5p\ ^2P^o_{1/2}$	13244.64	7548.148	70
$5s\ ^2S_{1/2} - 5p\ ^2P^o_{3/2}$	13420.65	7449.155	90
$6d\ ^2D_{5/2} - 7f\ ^2F^o_{7/2}$	13611.43	7344.746	1
$6d\ ^2D_{3/2} - 7f\ ^2F^o_{5/2}$	13622.02	7339.033	1
$4d\ ^2D_{3/2} - 5p\ ^2P^o_{1/2}$	15849.52	6307.595	60
$4d\ ^2D_{5/2} - 5p\ ^2P^o_{3/2}$	15980.21	6256.010	80
$5f\ ^2F^o_{5/2} - 7d\ ^2D_{3/2}$	15984.67	6254.264	1
$5f\ ^2F^o_{7/2} - 7d\ ^2D_{5/2}$	15991.23	6251.698	1
$4d\ ^2D_{3/2} - 5p\ ^2P^o_{3/2}$	16025.54	6238.314	10
$5p\ ^2P^o_{3/2} - 5d\ ^2D_{3/2}$	19846.86	5037.176	9
$5p\ ^2P^o_{3/2} - 5d\ ^2D_{5/2}$	19866.93	5032.087	60
$6p\ ^2P^o_{3/2} - 7d\ ^2D_{5/2}$	19888.36	5026.665	2
$6p\ ^2P^o_{1/2} - 7d\ ^2D_{3/2}$	19967.25	5006.804	1
$5f\ ^2F^o - 7g\ ^2G$	20004.97	4997.365	6

(continued)

TABLE 2.2 (continued)

Level combination	Wave number (cm^{-1})	Wavelength (Å)	Intensity
$5p\,^2P^o_{1/2} - 5d\,^2D_{3/2}$	20022.91	4992.886	50
$6p\,^2P^o_{3/2} - 8s\,^2S_{1/2}$	20220.60	4944.072	1
$5p\,^2P^o_{3/2} - 6s\,^2S_{1/2}$	20910.86	4780.868	15
$5p\,^2P^o_{1/2} - 6s\,^2S_{1/2}$	21086.90	4740.954	10
$7p\,^2P^o_{1/2} - 5d\,^2D_{3/2}$	21507.93	4648.148	1
$7p\,^2P^o_{3/2} - 5d\,^2D_{5/2}$	21536.0	4642.08	2b
$4f\,^2F^o - 5g\,^2G$	23198.18	4309.471	40
$5d\,^2D_{5/2} - 6f\,^2F^o_{7/2}$	23637.52	4229.371	6
$5d\,^2D_{3/2} - 6f\,^2F^o_{5/2}$	23657.61	4225.779	6
$4d\,^2D_{5/2} - 4f\,^2F^o_{7/2}$	24571.17	4068.661	100
$4d\,^2D_{3/2} - 4f\,^2F^o_{5/2}$	24616.25	4061.209	80
$5f\,^2F^o - 8g\,^2G$	24742.36	4040.510	6
$4f\,^2F^o_{5/2} - 6d\,^2D_{3/2}$	28718.63	3481.064	5
$4f\,^2F^o_{7/2} - 6d\,^2D_{5/2}$	28729.19	3479.785	6
$4f\,^2F^o - 6g\,^2G$	35303.42	2831.754	10
$4s\,^2S_{1/2} - 4p\,^2P^o_{1/2}$	36564.98	2734.048	230
$4s\,^2S_{1/2} - 4p\,^2P^o_{3/2}$	37038.85	2699.067	350
$5p\,^2P^o_{3/2} - 6d\,^2D_{3/2}$	37309.41	2679.493	1
$5p\,^2P^o_{3/2} - 6d\,^2D_{5/2}$	37320.10	2678.725	8
$5p\,^2P^o_{1/2} - 6d\,^2D_{3/2}$	37485.47	2666.907	6
$5p\,^2P^o_{3/2} - 7s\,^2S_{1/2}$	37874.02	2639.546	2
$5p\,^2P^o_{1/2} - 7s\,^2S_{1/2}$	38050.05	2627.334	1

(continued)

TABLE 2.2. (continued)

Level combination	Wave number (cm^{-1})	Wavelength (Å)	Intensity
$5s^2S_{1/2} - 6p^2P^o_{3/2}$	40712.3	2455.52	1
$4f^2F^o - 7g^2G$	42603.27	2347.238*	6
$4d^2D_{3/2} - 6p^2P^o_{1/2}$	43232.16	2313.093*	6
$4d^2D_{5/2} - 6p^2P^o_{3/2}$	43272.25	2310.950*	7
$4d^2D_{3/2} - 6p^2P^o_{3/2}$	43317.58	2308.532*	5
$5p^2P^o_{3/2} - 7d^2D_{3/2}$	47173.64	2119.828*	1
$5p^2P^o_{3/2} - 7d^2D_{5/2}$	47180.41	2119.524*	5
$4f^2F^o - 8g^2G$	47340.62	2112.351*	1
$5p^2P^o_{1/2} - 7d^2D_{3/2}$	47349.89	2111.937*	2
$5p^2P^o_{3/2} - 8s^2S_{1/2}$	47512.51	2104.709*	2
$5p^2P^o_{1/2} - 8s^2S_{1/2}$	47688.6	2096.94 *	1
$4p^2P^o_{3/2} - 4d^2D_{3/2}$	49679.42	2012.906*	50
$4p^2P^o_{3/2} - 4d^2D_{5/2}$	49724.77	2011.070*	160
$4p^2P^o_{1/2} - 4d^2D_{3/2}$	50153.31	1993.886	90
$4p^2P^o_{3/2} - 5s^2S_{1/2}$	52284.29	1912.620	60
$4p^2P^o_{1/2} - 5s^2S_{1/2}$	52758.18	1895.441	40
$7p^2P^o - 4d^2D$	57382.7	1742.69	2h
$4d^2D_{5/2} - 6f^2F^o_{7/2}$	59484.69	1681.105	7
$4d^2D_{3/2} - 6f^2F^o_{5/2}$	59530.03	1679.824	5
$3d^2D_{3/2} - 4p^2P^o_{1/2}$	62104.30	1610.1945	150
$3d^2D_{5/2} - 4p^2P^o_{3/2}$	62380.55	1603.0637	180
$3d^2D_{3/2} - 4p^2P^o_{3/2}$	62578.16	1598.002	80

(continued)

TABLE 2.2. (continued)

Level combination	Wave number (cm^{-1})	Wavelength (Å)	Intensity
$4d^2D_{5/2} - 7f^2F^o_{7/2}$	66911.73	1494.506	1
$4d^2D_{3/2} - 7f^2F^o_{5/2}$	66956.75	1493.502	1
$4p^2P^o_{3/2} - 5d^2D_{3/2}$	85551.78	1168.883	10
$4p^2P^o_{3/2} - 5d^2D_{5/2}$	85571.92	1168.6077	25
$4p^2P^o_{1/2} - 5d^2D_{3/2}$	86025.72	1162.4431	20
$4p^2P^o_{3/2} - 6s^2S_{1/2}$	86615.87	1154.523	20
$4p^2P^o_{1/2} - 6s^2S_{1/2}$	87089.75	1148.241	15
$4s^2S_{1/2} - 5p^2P^o_{1/2}$	102567.8	974.965	6
$4s^2S_{1/2} - 5p^2P^o_{3/2}$	102743.8	973.295	8
$4p^2P^o_{3/2} - 6d^2D_{5/2}$	103025.1	970.638	4
$4p^2P^o_{1/2} - 6d^2D_{3/2}$	103488.3	966.293	3
$4p^2P^o_{3/2} - 7s^2S_{1/2}$	103578.81	965.4484	4
$4p^2P^o_{1/2} - 7s^2S_{1/2}$	104052.7	961.052	2
$3d^2D_{5/2} - 5p^2P^o_{3/2}$	128085.5	780.729	8
$3d^2D_{3/2} - 5p^2P^o_{1/2}$	128107.14	780.5966	6
$4s^2S_{1/2} - 6p^2P^o_{1/2}$	129950.4	769.524	1
$4s^2S_{1/2} - 6p^2P^o_{3/2}$	130035.9	769.019	1
$3d^2D_{5/2} - 4f^2F^o_{7/2}$	136676.45	731.6549	15
$3d^2D_{3/2} - 4f^2F^o_{5/2}$	136873.86	730.5997	10
$3d^2D_{5/2} - 6p^2P^o_{3/2}$	155376.7	643.597	2
$3d^2D_{3/2} - 6p^2P^o_{1/2}$	155488.8	643.133	2
$3d^2D_{5/2} - 5f^2F^o_{7/2}$	159274.60	627.8465	8

(continued)

TABLE 2.2. (continued)

Level combination	Wave number (cm^{-1})	Wavelength (Å)	Intensity
$3d^2D_{3/2} - 5f^2F^o_{5/2}$	159472.00	627.0693	7
$3d^2D_{5/2} - 6f^2F^o_{7/2}$	171589.99	582.7846	3
$3d^2D_{3/2} - 6f^2F^o_{5/2}$	171787.52	582.1144	2
$3d^2D_{5/2} - 7f^2F^o_{7/2}$	179016.6	558.608	1
$3d^2D_{3/2} - 7f^2F^o_{5/2}$	179213.2	557.995	1

b - Blends with an OII line.

h - Hazy.

* - Wavelength in vacuum as measured.

TABLE 2.3. Energy Levels of Sc III.

Symbol	Energy (cm^{-1})	Interval (cm^{-1})	Term Value (cm^{-1})	n^*	Δn^*
$4s\,^2S_{1/2}$	25539.32		174138.05	2.381491	
$5s\,^2S_{1/2}$	114862.48		84814.89	3.412398	
$6s\,^2S_{1/2}$	149194.03		50483.34	4.423049	
$7s\,^2S_{1/2}$	166157.17		33520.20	5.428033	
$8s\,^2S_{1/2}$	175795.73		23881.64	6.430781	
$9s\,^2S_{1/2}$	(181799)[a]		(17878)		
$4p\,^2P^\circ_{1/2}$	62104.30	473.88	137573.07	2.679348	0.004626
$^2P^\circ_{3/2}$	62578.18		137099.19	2.683974	
$5p\,^2P^\circ_{1/2}$	128107.12	176.03	71570.25	3.714749	0.004577
$^2P^\circ_{3/2}$	128283.15		71394.22	3.719326	
$6p\,^2P^\circ_{1/2}$	155489.78	85.42	44187.59	4.727653	0.004576
$^2P^\circ_{3/2}$	155575.20		44102.17	4.732229	
$7p\,^2P^\circ_{1/2}$	169637.96	47.9	30039.41	5.733899	0.00458
$^2P^\circ_{3/2}$	169685.9		29991.5	5.73848	
$8p\,^2P^\circ_{1/2}$	(177920)	(29.6)	(21757)		
$^2P^\circ_{3/2}$	(177950)		(21728)		
$3d\,^2D_{3/2}$	0.00	197.64	199677.37	2.223982	0.001102
$^2D_{5/2}$	197.64		199479.73	2.225084	
$4d\,^2D_{3/2}$	112257.62	45.33	87419.75	3.361174	0.000872
$^2D_{5/2}$	112302.95		87374.42	3.362046	

(continued)

TABLE 2.3. (Continued)

Symbol	Energy (cm^{-1})	Interval (cm^{-1})	Term Value (cm^{-1})	n^*	Δn^*
$5d\,^2D_{3/2}$	148130.03	20.11	51547.34	4.377162	0.000854
$^2D_{5/2}$	148150.14		51527.23	4.378016	
$6d\,^2D_{3/2}$	165592.55	10.74	34084.82	5.382887	0.000848
$^2D_{5/2}$	165603.29		34074.08	5.383735	
$7d\,^2D_{3/2}$	175457.03	6.53	24220.34	6.385658	0.000860
$^2D_{5/2}$	175463.56		24213.81	6.386518	
$8d\,^2D_{3/2}$	(181579)	(4.3)	(18098)		
$^2D_{5/2}$	(181584)		(18094)		
$4f\,^2F^\circ_{5/2}$	136873.87	.25	62803.50	3.965554	0.000008
$^2F^\circ_{7/2}$	136874.12		62803.25	3.965562	
$5f\,^2F^\circ$	159472.24		40205.13	4.956271	
$6f\,^2F^\circ$	171787.64		27889.73	5.950776	
$7f\,^2F^\circ$	179214.70		20462.67	6.947277	
$8f\,^2F^\circ$	(184031)		(15646)		
$5g\,^2G$	160072.18		39605.19	4.993668	
$6g\,^2G$	172177.41		27499.96	5.992799	
$7g\,^2G$	179477.24		20200.13	6.992278	
$8g\,^2G$	184214.61		15462.76	7.991941	
$9g\,^2G$	(187462)		(12215)		

[a]Predicted levels.

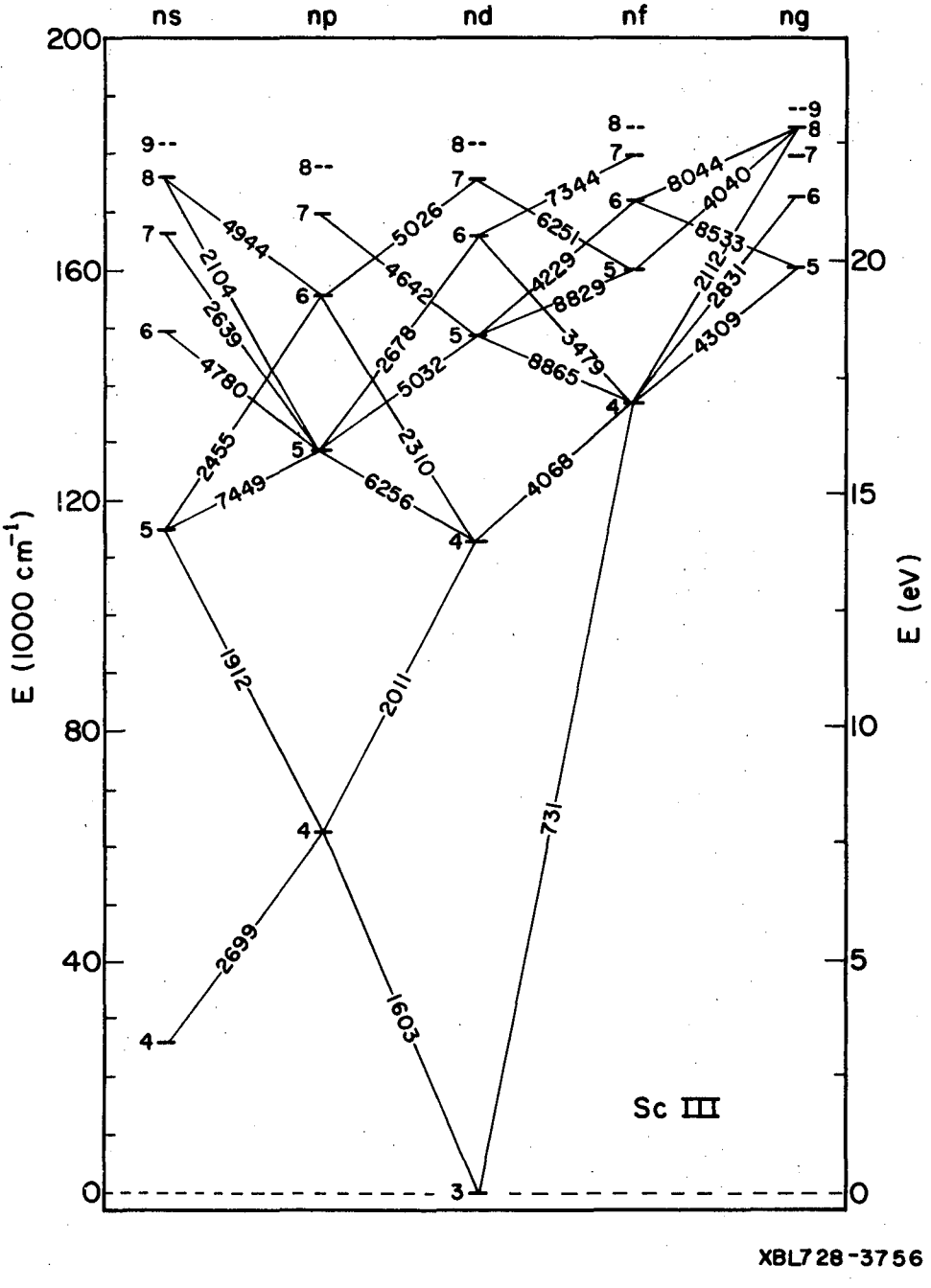

FIG. 2.1. Energy-level diagram for Sc III. The figures give the approximate wavelength of the leading line in each multiplet. Dotted lines are the next predicted terms.

ii. Quadruple Ionized Vanadium

Table 2.4 lists 59 classified lines of V VI, 46 of which are newly classified. The lines marked h appeared hazy, apparently caused by blending with impurity lines or with lines from lower ionization stages of vanadium. The line at 4293.74Å blends with a V III line at 4293.47Å.

The level analysis was begun on the basis of the levels reported by Gibbs and White. The wavelengths reported by them for the 483Å triplet and 590Å doublet are about 0.1Å too large and 0.3Å too small, respectively, and the lines at 285Å and 286Å (3d-4f) were wrongly classified - the 4f levels are inverted in V VI. Four lines between the $3p^6$ and $3p^5 3d^2$ configurations were observed. The triplet at 962Å has been classified as the $3p^6 4d\ ^2D - 3p^5 3d^2\ ^2F^o$ combination and places the latter term about 80 cm^{-1} below the value reported by Gabriel, Fawcett and Jordan.[39] The line at 5442Å has been tentatively assigned to the $3p^6 5g\ ^2G_{9/2} - 3p^5 3d^2\ ^2F^o_{7/2}$ transition which constitutes a double electron jump. The 18 newly found levels and the corrected values for the previously reported levels are presented in Table 2.5. The combination cycles close to within a few units in the first decimal place of the wave number. The uncertainty in the levels relative to the ground state is estimated to be about 3 cm^{-1} resulting from the uncertainty in the 4p-3d triplet. Figure 2.2 shows the energy level diagram for quadruple ionized vanadium. Table 2.6 lists several unclassified lines the intensity behaviour of which is similar to that of V VI lines.

TABLE 2.4. Classified Lines of V V.

Level Combination odd - even	Wave number (cm^{-1})	Wavelength (Å)	Intensity
$4f\,^2F_{5/2}$ - $3d\,^2D_{3/2}$	349675	285.98	1
$4f\,^2F_{7/2}$ - $3d\,^2D_{5/2}$	348628	286.84	2
$4p\,^2P_{3/2}$ - $3d\,^2D_{3/2}$	207660.2	481.556	3
$4p\,^2P_{3/2}$ - $3d\,^2D_{5/2}$	207035.9	483.008	30
$4p\,^2P_{1/2}$ - $3d\,^2D_{3/2}$	206393.7	484.511	20
$5p\,^2P_{3/2}$ - $4s\,^2S_{1/2}$	203874.6	490.498	4
$5p\,^2P_{1/2}$ - $4s\,^2S_{1/2}$	203356.6	491.747	2
$4p\,^2P_{1/2}$ - $6s\,^2S_{1/2}$	197461.0	506.429	1
$4p\,^2P_{3/2}$ - $6s\,^2S_{1/2}$	196196	509.694	2
$4p\,^2P_{1/2}$ - $5s\,^2S_{1/2}$	121822.9	820.864	20
$6p\,^2P_{3/2}$ - $4d\,^2D_{3/2}$	121773.0	821.200	1
$6p\,^2P_{3/2}$ - $4d\,^2D_{5/2}$	121628	822.18	6h
$6p\,^2P_{1/2}$ - $4d\,^2D_{3/2}$	121516.7	822.932	3
$4f\,^2F_{7/2}$ - $7g\,^2G$	121080.7	825.895	2
$4f\,^2F_{5/2}$ - $7g\,^2G_{7/2}$	120656.7	828.798	1
$4p\,^2P_{3/2}$ - $5s\,^2S_{1/2}$	120556.6	829.486	30
$3p^5 3d^2\,^2F_{7/2}$ - $4d\,^2D_{5/2}$	103946.2	962.036	15
$3p^5 3d^2\,^2F_{5/2}$ - $4d\,^2D_{3/2}$	102232.0	978.168	10
$3p^5 3d^2\,^2F_{5/2}$ - $4d\,^2D_{5/2}$	102087.6	979.551	1
$4f\,^2F_{7/2}$ - $6g\,^2G$	100771.5	992.344	10
$4f\,^2F_{5/2}$ - $6g\,^2G_{7/2}$	100348.0	996.532	5
$5p\,^2P_{1/2}$ - $7s\,^2S_{1/2}$	91575	1092.00	1h

(Continued)

TABLE 2.4. (Continued)

Level Combination odd – even	Wave number (cm^{-1})	Wavelength (Å)	Intensity
$5p\,^2P_{3/2} - 7s\,^2S_{1/2}$	91056.3	1098.222	2
$4p\,^2P_{1/2} - 4d\,^2D_{3/2}$	87508.7	1142.744	15
$4p\,^2P_{3/2} - 4d\,^2D_{5/2}$	86387.0	1157.581	25
$4p\,^2P_{3/2} - 4d\,^2D_{3/2}$	86242.5	1159.522	6
$4f\,^2F_{7/2} - 5g\,^2G$	67108.8	1490.118	20
$4f\,^2F_{5/2} - 5g\,^2G_{7/2}$	66684.2	1499.605	10
$4p\,^2P_{3/2} - 4s\,^2S_{1/2}$	59516.6	1680.204	100
$4p\,^2P_{1/2} - 4s\,^2S_{1/2}$	58250.4	1716.725	50
$5p\,^2P_{3/2} - 4d\,^2D_{3/2}$	58115.5	1720.710	4
$5p\,^2P_{3/2} - 4d\,^2D_{5/2}$	57971.2	1724.995	15
$5p\,^2P_{1/2} - 4d\,^2D_{3/2}$	57597.6	1736.183	10
$4f\,^2F_{5/2} - 4d\,^2D_{3/2}$	55772.9	1792.984	25
$4f\,^2F_{5/2} - 4d\,^2D_{5/2}$	55628.5	1797.639	6h
$4f\,^2F_{7/2} - 4d\,^2D_{5/2}$	55205.4	1811.418	30
$5p\,^2P_{1/2} - 6s\,^2S_{1/2}$	52355.0	1910.038	4
$5p\,^2P_{3/2} - 6s\,^2S_{1/2}$	51836.9	1929.126	9
$4f\,^2F_{7/2} - 5d\,^2D_{5/2}$	38791.2	2577.130	20
$4f\,^2F_{5/2} - 5d\,^2D_{5/2}$	38368.6	2605.523	4h
$4f\,^2F_{5/2} - 5d\,^2D_{3/2}$	38301.3	2610.098	10
$5p\,^2P_{1/2} - 5d\,^2D_{3/2}$	36476.7	2740.666	10
$5p\,^2P_{3/2} - 5d\,^2D_{5/2}$	36025.4	2774.998	15

(Continued)

TABLE 2.4. (Continued)

Level Combination odd - even	Wave number (cm^{-1})	Wavelength (Å)	Intensity
$5p\,^2P_{3/2}$ - $5d\,^2D_{3/2}$	35958.8	2780.144	3
$6h\,^2H$ - $5g\,^2G$	33886.8	2950.13	8w
$6p\,^2P_{3/2}$ - $5d\,^2D_{3/2}$	27698.54	3609.269	2
$6p\,^2P_{1/2}$ - $7s\,^2S_{1/2}$	27654.33	3615.039	2h
$6p\,^2P_{3/2}$ - $5d\,^2D_{5/2}$	27631.96	3617.966	15h
$6p\,^2P_{1/2}$ - $5d\,^2D_{3/2}$	27442.94	3642.887	8
$6p\,^2P_{3/2}$ - $7s\,^2S_{1/2}$	27399.03	3648.724	4
$5p\,^2P_{3/2}$ - $5s\,^2S_{1/2}$	23800.99	4200.322	20
$5p\,^2P_{1/2}$ - $5s\,^2S_{1/2}$	23283.2	4293.74	20b
$7h\,^2H$ - $6g\,^2G$	20463.86	4885.299	7w
$6h\,^2H$ - $7i\,^2I$	20276.12	4930.533	15w
$6p\,^2P_{1/2}$ - $6d\,^2D_{3/2}$	18883.64	5294.115	4
$6p\,^2P_{3/2}$ - $6d\,^2D_{5/2}$	18665.21	5356.070	8
$6p\,^2P_{3/2}$ - $6d\,^2D_{3/2}$	18628.07	5366.750	1
$3p^5 3d^2\ ^2F_{7/2}$ - $5g\,^2G_{9/2}$?	18368.12	5442.704	3
$6p\,^2P_{3/2}$ - $6s\,^2S_{1/2}$	11820.50	8457.555	1

h-hazy; b-blend; w-wide.

TABLE 2.5. Energy Levels of V V.

Symbol	Energy (cm^{-1})	Interval (cm^{-1})	Term Value (cm^{-1})	n^*	Δn^*
$4s\,^2S_{1/2}$	148143.3		378380.7	2.692652	
$5s\,^2S_{1/2}$	328216.9		198307.1	3.719424	
$6s\,^2S_{1/2}$	403854.8		122669.2	4.729084	
$7s\,^2S_{1/2}$	443074.2		83449.8	5.733663	
$8s\,^2S_{1/2}$	(466065)[a]		(60459)		
$4p\,^2P^\circ_{1/2}$	206393.7	1266.2	320130.3	2.927395	0.005807
$4p\,^2P^\circ_{3/2}$	207659.9		318864.1	2.933202	
$5p\,^2P^\circ_{1/2}$	351499.9	518.0	175024.1	3.959095	0.005871
$5p\,^2P^\circ_{3/2}$	352017.9		174506.1	3.964966	
$6p\,^2P^\circ_{1/2}$	415419.6	255.6	111104.4	4.969117	0.005725
$6p\,^2P^\circ_{3/2}$	415675.2		110848.8	4.974842	
$3d\,^2D_{3/2}$	0.0	623.6	526524.0	2.282631	0.001353
$3d\,^2D_{5/2}$	623.6		525900.4	2.283984	
$4d\,^2D_{3/2}$	293902.4	144.4	232621.6	3.434154	0.001066
$4d\,^2D_{5/2}$	294046.8		232477.2	3.435220	
$5d\,^2D_{3/2}$	387976.7	66.6	138547.3	4.449854	0.001070
$5d\,^2D_{5/2}$	388043.3		138480.7	4.450924	
$6d\,^2D_{3/2}$	434303.2	37.2	92220.8	5.454191	0.001100
$6d\,^2D_{5/2}$	434340.4		92183.6	5.455291	
$7d\,^2D_{3/2}$	(460702)	(22.7)	(65822)		
$7d\,^2D_{5/2}$	(460725)		(65799)		

(continued)

TABLE 2.5. (continued)

Symbol	Energy (cm^{-1})	Interval (cm^{-1})	Term Value (cm^{-1})	n^*	Δn^*
$4f^2F^\circ_{5/2}$	349675.3	-423.2	176848.7	3.938618	-0.004704
$4f^2F^\circ_{7/2}$	349252.1		177271.9	3.933914	
$5g^2G_{7/2}$	416359.5	1.4	110164.5	4.990269	0.000032
$5g^2G_{9/2}$	416360.9		110163.1	4.990301	
$6g^2G$	450023.5		76500.5	5.988426	
$7g^2G$	470332.5		56191.5	6.987302	
$8g^2G$	(483514)		(43010)		
$6h^2H^\circ$	450247.2		76276.8	5.997201	
$7h^2H^\circ$	470487.3		56036.7	6.996946	
$3p^5 3d^2\ ^2F^\circ_{5/2}$	396134.4	1858.6	130389.6	4.586943	0.033045
$3p^5 3d^2\ ^2F^\circ_{7/2}$	397993.0		128531.0	4.619988	

[a]Predicted levels.

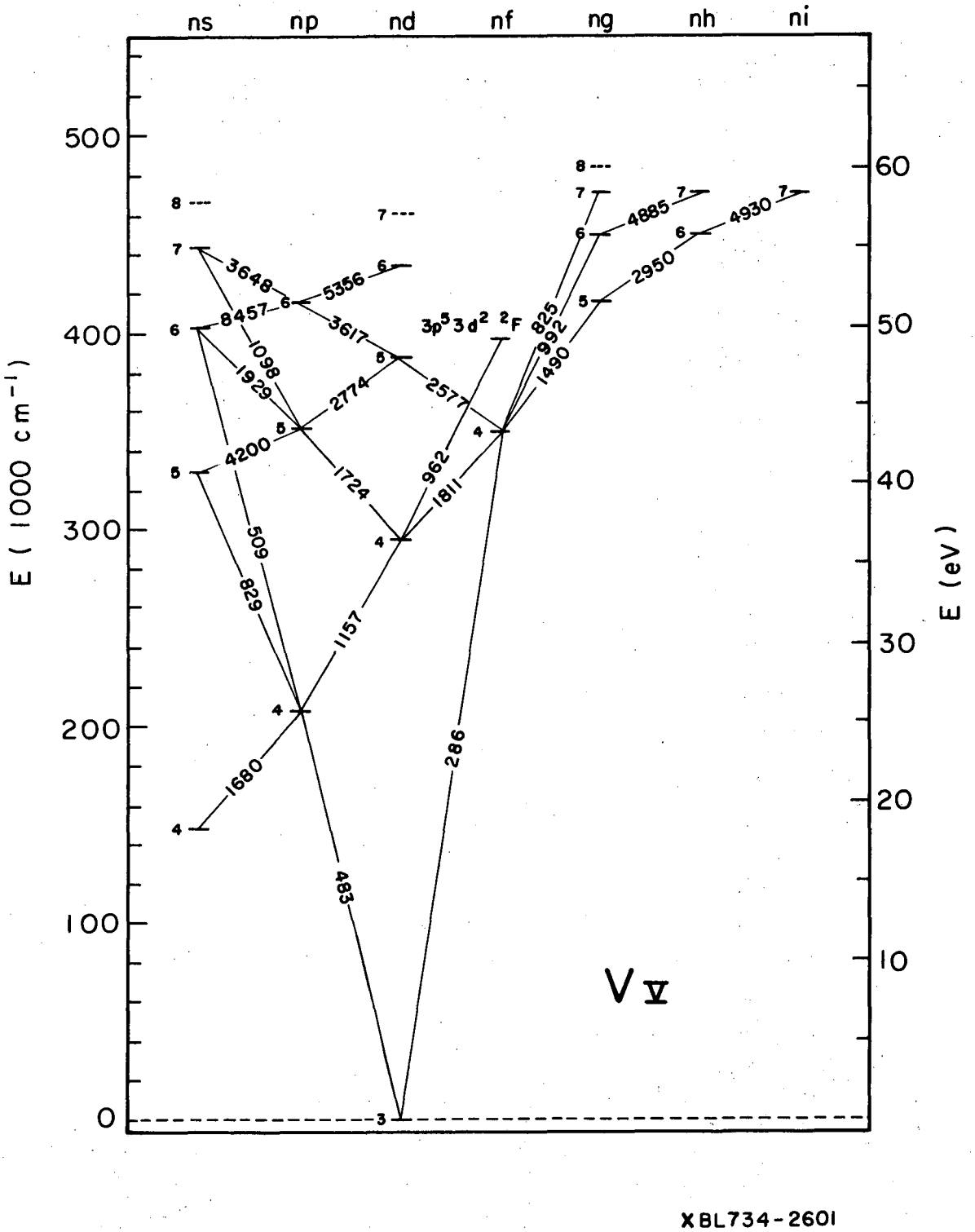

XBL734-2601

FIG. 2.2. Energy-level diagram for V V. The figures give the approximate wavelength of the leading line in each multiplet. Dotted lines are the next predicted terms.

TABLE 2.6. Unclassified Lines.

Wavelength (Å)	Wave number (cm^{-1})	Intensity
3316.470	30143.86	10
3363.517	29722.24	6
3966.598	25203.39	5
4106.318	24345.84	3

B. Ionization Energies and Series Formulae

The deduced energy levels of doubly ionized scandium present an opportunity to calculate ionization energies using more than four levels and the possibility of presenting unperturbed series by series formulae. In Tables 2.7 and 2.8 are listed the quantities calculated from the observed energy levels using the program IENEXT. The ionization energy of each level series was calculated using simultaneously all of the observed levels in the series. The ng series that reaches closest to the ionization energy and is representable by the least number of quantum-defect constants is assumed to give the best value of the ionization energy. The agreement between the ionization energies calculated from the different series improves as (1) more observed levels are included in the calculation, (2) the levels used in the calculation reach closer to the ionization limit, and (3) the number of constants necessary to represent a series decreases. Four quantum-defect constants were inadequate to represent the nd series within the experimental error, due to the irregularity of δ_n presumably caused by the core effects on these level series especially on the 3d ground term.

For Sc III the ionization energy obtained from the ns series agrees with that obtained from the ng series by 0.05 cm^{-1}. Until more levels are found the ionization energy of the Sc^{2+} ion may be given as

$$E_{ion} = 199677.37 \pm 0.1 \text{ cm}^{-1} \qquad \text{Sc III.}$$

TABLE 2.7. Ionization Energies and Quantum-Defect Formula Constants for Sc III.

n	Δ[a] or T_c	Constants[b]	Δ or T_c	Constants	Δ or T_c	Constants	Δ or T_c	Constants
	$^2S_{1/2}$		$^2P_{1/2}$		$^2P_{3/2}$			
4	0.00	1.562691	0.00	1.253729	0.00	1.249129		
5	0.00	2.908494^{-2}	0.00	4.285448^{-2}	0.00	4.298965^{-2}		
6	0.00	4.290675^{-3}	0.00	8.397243^{-3}	0.00	8.448915^{-3}		
7	0.00	-2.854532^{-4}	-0.12		-0.11			
8	0.01		21757.11		21727.53			
9	17878.31		16487.31		16467.78			
E_{ion}	199677.42		199676.88		199676.91			
	$^2D_{3/2}$		$^2D_{5/2}$		$^2F_{c.g.}$		^2G	
3	0.00	6.088486^{-1}	0.00	6.078507^{-1}				
4	0.00	2.062338^{-2}	0.00	2.173113^{-2}	0.00	6.322432^{-2}		
5	0.00	2.008575^{-2}	0.00	1.739745^{-2}	0.00	-6.008089^{-2}	0.01	9.168469^{-3}
6	0.00	-5.342621^{-3}	0.00	-2.848258^{-3}	0.00	2.168658^{-2}	-0.02	-7.858949^{-3}
7	0.00	8.695480^{-3}	0.00	7.984169^{-3}	0.00	-8.005183^{-3}	0.00	
8	18097.95		18093.64		15646.31		0.01	
9	14036.36		14033.37		12348.05		12215.44	
E_{ion}	199669.42		199670.09		199675.93		199677.37	

[a] $\Delta \equiv T_c - T_o$. [b] Constants a_i in ascending order for $\delta_n = \sum_{i=0} a_i \left(\frac{T_n}{R}\right)^i$, calculated using the value $E_{ion} = 199677.37\ cm^{-1}$. Superscripts indicate powers of 10.

Quantum-defect constants were calculated using the derived ionization energy (199677.37 cm^{-1}), and the minimum number of constants necessary to represent each series within the experimental error are presented in Table 2.7. The listed constants were used to calculate remaining observed levels and the differences $\Delta \equiv T_{calc} - T_{obs}$ are also listed in Table 2.7 together with the calculated values of new levels above the last observed levels. The calculations were carried out by means of an iterative procedure on the predicted value of T until

$$|T(I + 1) - T(I)| \leq 10^{-2} \text{ cm}^{-1} \quad ,$$

usually satisfied in one or two steps.

A similar procedure was followed for V V and the pertinent information is presented in Table 2.8. The ionization energy derived from the np $^2P^o_{3/2}$ series is 22 cm^{-1} less than the value derived from the np $^2P^o_{1/2}$ series and both are about 500 cm^{-1} less than the values obtained from the ng and ns series. This is probably due to a depression of these series caused by a perturbing level(s) located above the 6p $^2P^o$ term which is further indicated by the gradual decrease in Δn^* for this term series (Table 2.5). The perturbation is most likely caused by the $3p^5\ 3d^2(^2P^o, ^4P^o)$ terms. The ionization energies derived from the 3d-6d terms are about 300 cm^{-1} too large as compared to 130 cm^{-1} in the case of Sc III; in scandium with an additionally observed term included in the calculation the nd ionization energies agree with the values

TABLE 2.8. Ionization Energies and Quantum-Defect Formula Constants for V V.

	Δ[a] or T_c	Constants[b]	Δ or T_c	Constants	Δ or T_c	Constants	Δ or T_c	Constants
	$^2S_{1/2}$		$^2P_{1/2}$		$^2P_{3/2}$			
4	0.0	1.25766	0.0	1.01920	0.0	1.01400		
5	0.0	1.03935^{-2}	0.0	7.94246^{-3}	0.0	7.25557^{-3}		
6	0.0	1.37402^{-3}	0.0	3.55254^{-3}	0.0	3.75681^{-3}		
7	0.0	-6.07831^{-5}	76883		76740			
8	60459							
E_{ion}	526517		526039		526017			
	$^2D_{3/2}$		$^2D_{5/2}$		$^2G_{c.g.}$		^2H	
3	0.0	5.41263^{-1}	0.0	5.40023^{-1}				
4	0.0	3.38675^{-3}	0.0	3.62756^{-3}				
5	0.0	1.44223^{-3}	0.0	1.34572^{-3}	0.0	1.58069^{-2}		
6	0.0	1.14660^{-3}	0.0	1.16020^{-3}	0.0	-6.07093^{-3}	0.0	3.75800^{-3}
7	65822		65799		0.0		0.0	-1.37933^{-3}
8	49338		49323		43010		42900	
E_{ion}	526832		526835		526524		526529[c]	

[a] $\Delta \equiv T_c - T_o$. [b] Constants a_i in ascending order for $\delta_n = \sum_{i=0} a_i \left(\frac{T_n}{R}\right)^i$, calculated using the value $E_{ion} = 526524\ cm^{-1}$. [c] Calculated using $\delta_{6h} - \delta_{7h} = -0.00037 \pm 5\%$ as determined from the isoelectronic sequence.

obtained from the ng and ns series to within 8 cm^{-1}. The possible error in the ionization energy derived from the ng series is estimated to be a few wave numbers which is mainly due to the uncertainty in the wave numbers derived from the 4p-3d and 4f-ng lines. From the present investigation the ionization energy of the V^{4+} ion may be corrected from the previously reported value of 526100 cm^{-1} to

$$E_{ion} = 526524 \pm 5 \text{ cm}^{-1} \qquad \text{V V.}$$

In Table 2.8 is also presented the ionization energy calculated from the two observed nh levels (n = 6,7) with the quantum defect change -0.00037 ± 5% as determined from the isoelectronic sequence. The ionization energy thus obtained is 5 cm^{-1} larger than the value obtained from the ng series.

C. Isoelectronic Sequence

With the spectra of K I, Ca II and Ti IV well analyzed,[38,40,41] it is possible to observe how the Sc III and V V energy levels fit into the neutral potassium isoelectronic sequence. Figure 2.3 shows the isoelectronic trends for selected levels. Levels belonging to two other configurations, $3p^5 3d^2$ and $3p^5 3d4s$ as reported in the literature[39,42,43] have also been ploteed. Evidently the depression and inversion of the $3p^6 4f\ ^2F^\circ$ levels in V V are due to the perturbing interaction of the $3p^5 3d^2\ ^2F^\circ$ levels. This mutual repulsion was first recognized in Cr VI by Gabriel, Fawcett, and Jordan.[39] The more sensitive plots of $T^H - T + aZ_c$ and $(\Delta E)^{1/4}$ versus Z_c in Fig. 2.4 further illustrate the point. Other members of the $3p^6 nf$ series are expected to be perturbed also. Because the core charge Z_c outside the closed shell is small, LC coupling is a good approximation and interactions between terms of the same L and S and the same parity need only be considered; no interaction with the $3p^5 3d^2\ ^2D^\circ$ term was detected in V V. Note from Fig. 2.3 that extrapolating the $3p^5 3d^2\ ^2F^\circ$ levels to Sc III, places them well above the $3p^6$ ionization limit, though conceivably they may slightly depress the $3p^6 nf$ series in doubly ionized scandium which explains the rather low value of the ionization energy obtained from this series.

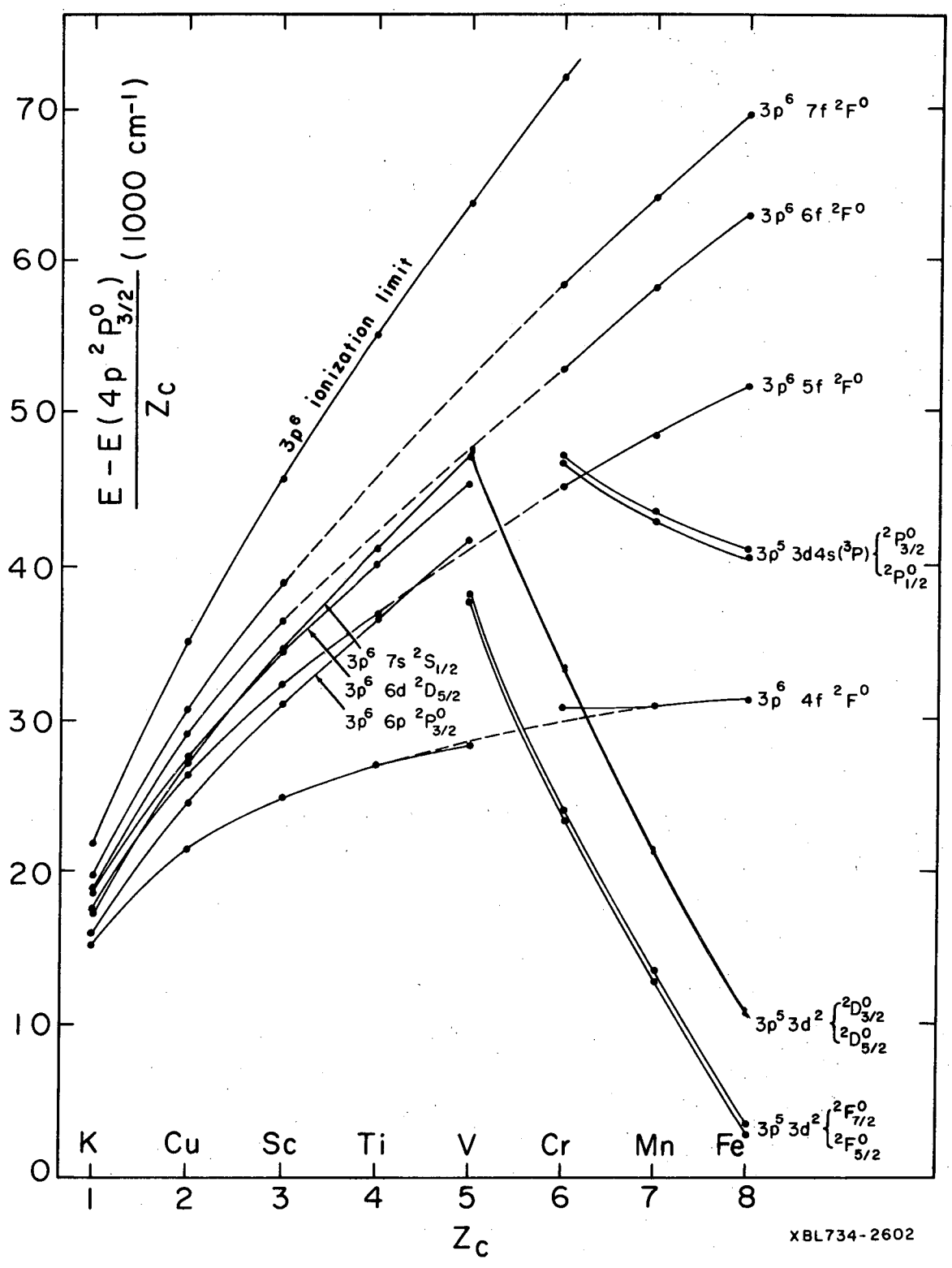

FIG. 2.3. K I isoelectronic sequence for selected levels.

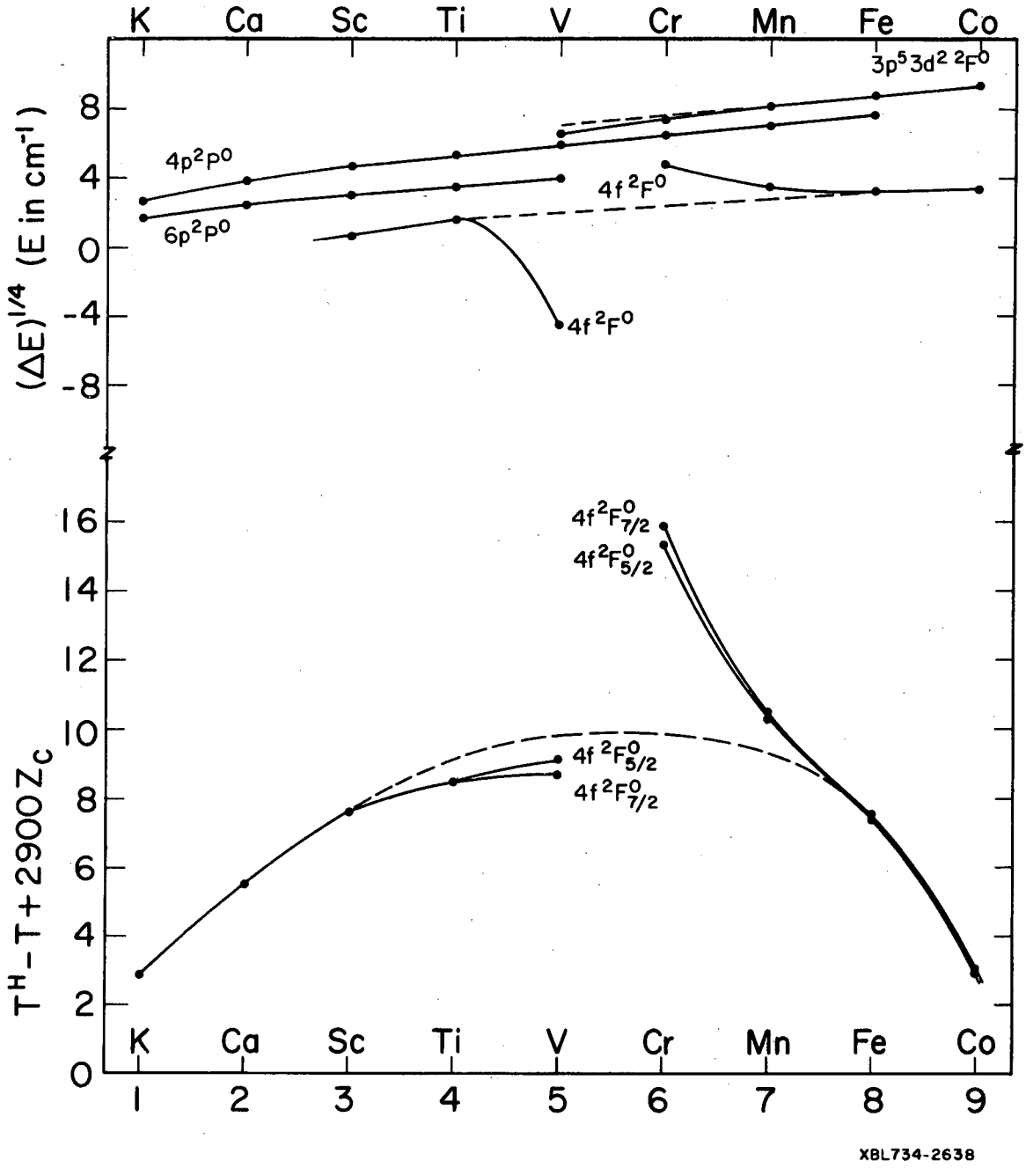

FIG. 2.4. Perturbing interactions and fine-structure intervals along the neutral potassium isoelectronic sequence.

2-5. CONCLUSION

This research has extended the knowledge of the doubly ionized state of scandium and the quadruple ionized state of vanadium; both ions are isoelectronic with neutral potassium. The $3p^6 4f$ levels in V V are inverted due to configuration interaction with the $3p^5 3d^2\ ^2F^o$ levels; the present classification is consistent with the isoelectronic data. It has been shown that the agreement between ionization energies calculated from different series of a configuration improves as (1) more levels are included in the calculation, (2) the levels used in the calculation reach closer to the ionization limit, and (3) the number of quantum-defect constants necessary to represent a series to within the experimental error decreases. Internal consistency was obtained in the level systems derived from the spectra, indicating that it is possible to maintain sufficient control over source excitation parameters. It would be of interest to study the line and level variation with varying source conditions. Investigation of the V V spectrum is continuing. In addition, many lines of the V II, V III, and V IV spectra, previously unreported, have been identified on the present spectrographic plates and remain to be measured.

ACKNOWLEDGMENTS

I thank Professor Sumner P. Davis for making this work possible. It is with pleasure that I express my sincere thanks to John G. Conway. His inspirational interest and excellent guidance, our discussions and his many suggestions were a well of encouragement. I also thank George V. Shalimoff for readily helping whenever it was needed.

I extend special thanks to Susan E. Whipple-Van Deurzen who understood.

REFERENCES

*Work performed under the auspices of the U. S. Atomic Energy Commission and a grant from the National Science Foundation.

1. M. F. Hasler and H. W. Dietert, J. Opt. Soc. Am. 33, 218 (1943).
2. B. Vodar and N. Astoin, Nature 166, 1029 (1950).
3. K. Bockasten, Ark. Fys. 9, 457 (1955).
4. G. H. Dieke, H. M. Crosswhite, and B. Dunn, J. Opt. Soc. Am. 51, 820 (1961).
5. C. H. Corliss, Spectrochimica Acta 5, 378 (1953).
6. B. O. Pierce and R. M. Foster, A Short Table of Integrals, 4th edition 78-102, Ginn and Company (1957).
7. Wm. R. Callahan, J. Opt. Soc. Am. 53, 695 (1963).
8. J. Sugar, J. Opt. Soc. Am. 53, 831 (1963).
9. J. Reader, G. L. Epstein, and J. O. Ekberg, J. Opt. Soc. Am. 62, 273 (1972).
10. A. Strasheim and F. Blum, Spectrochimica Acta 26, 694 (1971).
11. C. H. H. Van Deurzen, J. G. Conway, and S. P. Davis, J. Opt. Soc. Am. 63, 158 (1973).
12. Chapter 2, this dissertation.
13. C. E. Moore, An Ultraviolet Multiplet Table, Section 1, Natl. Bur. Std. (U.S.) circ. No. 488 (U. S. Government Printing Office, Washington, D. C. 1950).
14. C. E. Moore, A Multiplet Table of Astrophysical Interest, Nat. Stand. Ref. Data Ser., Nat. Bur. Stand. (U.S.) 40 (1972).
15. L. Iglesias, An. Real Soc. Esp. Fis. y Quim (Madrid) [A] 58, 191 (1962).

16. L. Iglesias y R. Velasco, An. Real Soc. Esp. Fis. y Quim (Madrid) [A] 54, 83 (1958).

17. L. Iglesias, J. Research Natl. Bur. Std. 72A, 295 (1968).

18. J. P. Walters, Applied Spectroscopy 26, 25 (1972).

19. A. E. Ruark and H. C. Urey, Atoms, Molecules and Quanta, pg. 457 (McGraw-Hill 1930).

20. T. P. Schreiber and D. L. Fry, Spectrochimica Acta 13, 104 (1958).

21. R. C. Gibbs and H. E. White, Proc. Nat. Acad. Sci. 12, 599 (1926).

22. S. Smith, Proc. Nat. Acad. Sci. 13, 66 (1927).

23. H. N. Russell and R. J. Lang, Astroph. J. 66, 19 (1927).

24. R. C. Gibbs and H. E. White, Phys. Rev. 33, 162 (1929).

25. B. Edlén, Handb. d. Phys. 27, 80-220 (Berlin: Springer-Verlag 1964).

26. W. Ritz, Phys. Z. 4, 406 (1903).

27. D. R. Hartree, Proc. Cambridge Phil. Soc. 24, 426 (1928).

28. D. R. Hartree, The Calculation of Atomic Structures (Wiley, N. Y. 1957).

29. A. G. Shenstone, Phil. Rrans. Roy. Soc. London A235, 195 (1936).

30. A. Landé, Zeits f. Phys. 25, 46 (1924).

31. E. U. Condon and G. H. Shortley, The Theory of Atomic Spectra, (Cambridge University Press 1935).

32. V. Kaufman, L. J. Radziemsky, Jr., and K. L. Andrew, J. Opt. Soc. Am. 56, 911 (1966).

33. L. J. Radziemsky, Jr., K. L. Andrew, V. Kaufman, and U. Litzén, J. Opt. Soc. Am. 57, 336 (1967).

34. V. Kaufman and J. F. Ward, J. Opt. Soc. Am. 56, 1591 (1966).

35. F. P. J. Valero, J. Opt. Soc. Am. 58, 484 (1968).

36. D. Goorvitch, F. P. J. Valero, and A. L. Clúa, J. Opt. Soc. Am. 59, 971 (1969).

37. A. Giacchetti, R. W. Stanley, and R. Zalubas, J. Opt. Soc. Am. 60, 474 (1970).

38. C. E. Moore, Atomic Energy Levels, Vol. I., Natl. Bur. Std. (U.S.) Circ. No. 467 (U. S. Government Printing Office, Washington, D. C., 1949).

39. A. H. Gabriel, B. C. Fawcett, and C. Jordan, Proc. Phys. Soc. 87, 825 (1966).

40. B. Edlén and P. Risberg, Ark. Fys. 10, 553 (1956).

41. The Ti IV analysis was kindly supplied by B. Edlén.

42. R. D. Cowan, Astroph. J. 147, 377 (1967).

43. E. Alexander, U. Feldman, and B. S. Fraenkel, J. Opt. Soc. Am. 55, 650 (1965)

```
      PROGRAM ISOEL(INPUT,OUTPUT,TAPE2=INPUT,TAPE3=OUTPUT)
C     ISOELECTRONIC CALCULATIONS FOR PREDICTING SINGLE-ELECTRON DOUBLETS
C
C                     ALL ENERGIES IN WAVENUMBERS
C     CARD  COLUMNS                                                FORMAT  SYMBOL
C       1     1- 4  +1.0 SIGNALS START OF ELEMENT                  F4.0    TEST
C       2     1-10  ELEMENT IDENTIFICATION                         A10     ELEM
C            11-20  ATOMIC WEIGHT - CHEMICAL SCALE                 F10.5   CM
C            21-30  CHARGE THAT THE ELECTRON SEES                  F10.2   Z1
C            31-40  IONIZATION ENERGY                              F10.2   EION
C            41-50  CONVENIENT REFERENCE LEVEL                     F10.2   EREF
C       3     1- 4  +2.0 SIGNALS START OF SERIES                   F4.0    TEST
C            11-20  BLANK OR CONFIGURATION IDENTIFICATION          A10     CFIG
C       4        1  ANGULAR MOMENTUM SYMBOL S,P,D,F,G,H ...       A1      P
C            11-12  NUMBER OF LEVELS WITH THIS ANGM               I2      NL
C       5     1-20  ENERGY OF FIRST LEVEL (LOWEST)               F20.9   E(1)
C            22-23  N VALUE OF FIRST LEVEL                        I2      N(1)
C       6           REPEAT CARD 5 FOR ALL LEVELS WITH THIS
C                   ANGULAR MOMENTUM,INCREASING WAVENUMBER.
C       X           REPEAT CARDS 3 TO 6 FOR ADDITIONAL SERIES
C                   REPEAT CARDS 1 TO X FOR ADDITIONAL ELEMENTS
C     LAST          AS CARD 1 WITH - IN COLUMN 1 (END OF DATA)
C
      DIMENSION E(20),N(21),T(20),TR(20),TH(20),QS(20),QD(20),QN(20)
     *,K(20),L(20),D1(20),D2(20),DE(20),G(20)
      DATA BLANK/10H          /
      READ (2,6) TEST,CFIG
  101 READ (2,1) ELEM,CM,Z1,EION,EREF
      RM=109737.31-60.22/CM
      RMZ=RM*(Z1**2)
      WRITE (3,2) ELEM,RM,RMZ,EION
      WRITE (3,3)
      READ (2,6) TEST,CFIG
  102 READ (2,4) P,NL
      READ(2,5) (E(I),N(I),I=1,NL)
      DO 50 I=1,NL
      PICK=0.
      G(I)=(E(I)-EREF)/(Z1+PICK)
      T(I)=EION-E(I)
      TH(I)=RMZ/(N(I)**2)
      D3=T(I)-TH(I)
      TR(I)=SQRT(T(I)/RM)
      QS(I)=SQRT(RMZ/T(I))
      QN(I)=N(I)
      QD(I)=QN(I)-QS(I)
      X=QS(I)
      IF(I.EQ.1) GO TO 30
      N(NL+1)=N(NL)+1
      K(I)=N(I)-N(I-1)
      L(I)=N(I+1)-N(I)
      IF(I.EQ.2) GO TO 24
      IF(K(I).EQ.L(I).AND.K(I-1).EQ.L(I-1)) GO TO 25
   22 D1(I)=(QS(I)-QS(I-1))*1.E+06
      I1=IFIX(D1(I))
      DE(I)=E(I)-E(I-1)
      FS=ABS(DE(I))**0.25
      IF(I.LT.3) GO TO 31
      D2(I)=(QD(I)-QD(I-2))*1.E+06
      I2=IFIX(D2(I))
      IF(K(I)-L(I)) 23,33,33
   23 IF(K(I).EQ.1) GO TO 33
```

```
      GO TO 32
   24 K(I)=N(I)-N(I-1)
      IF(K(I)-1) 22,25,100
   25 D2(I)=(QD(I)-QD(I-1))*1.E+06
      I2=IFIX(D2(I))
      GO TO 33
   30 WRITE (3,60) N(I),P,E(I),          T(I),X,   QD(I),   TR(I),G(I),D3
      GO TO 49
   31 WRITE (3,61) N(I),P,E(I),DE(I),FS,T(I),X,I1,QD(I),   TR(I),G(I),D3
      GO TO 49
   32 WRITE (3,62) N(I),P,E(I),DE(I),FS,T(I),X,I1,QD(I),I2,TR(I),G(I),D3
      GO TO 49
   33 WRITE (3,63) N(I),P,E(I),          T(I),X,   QD(I),I2,TR(I),G(I),D3
   49 CONTINUE
   50 CONTINUE
      READ (2,6) TEST,CFIG
      IF(TEST-1.) 100,101,110
  110 IF(CFIG.NE.BLANK) WRITE(3,112) CFIG
      GO TO 102
    1 FORMAT(A10,F10.5,3F10.2)
    2 FORMAT(1H1,     5X,8HELEMENT A10/5X,4HRM= F11.3/5X,4H*Z2 F11.3/5X,4
     *HIE= F10.2/)
    3 FORMAT(4X,3H NL,1X,10H     E      ,1X,8H DELTA E,1X,7H**(1/4),3X,10H
     *     T      ,1X,10H     N*     ,1X,8H DELTAN*,1X,10H   QDEF    ,1X,9H
     *DELTAQD,2X,9HSQRT(T/R),3X,14H(E-EREF)/(Z+C),2X,7H  T-TH )
    4 FORMAT(A1,9X,I2)
    5 FORMAT(F20.9,1X,I2)
    6 FORMAT(F4.0,6X,A10)
   60 FORMAT(/4X,I2,A1,    F11.2,1X,8X  ,1X,7X  ,2X,F11.2,1X,F10.7,1X,6X,
     *3X,F10.7,1X,9X,1X,F10.7,3X,F9.0,8X,F7.0)
   61 FORMAT( 4X,I2,A1,    F11.2,1X,F8.2,1X,F7.4,2X,F11.2,1X,F10.7,1X,I6,
     *3X,F10.7,1X,9X,1X,F10.7,3X,F9.0,8X,F7.0)
   62 FORMAT( 4X,I2,A1,    F11.2,1X,F8.2,1X,F7.4,2X,F11.2,1X,F10.7,1X,I6,
     *3X,F10.7,1X,I9,1X,F10.7,3X,F9.0,8X,F7.0)
   63 FORMAT( 4X,I2,A1,    F11.2,1X,8X  ,1X,7X  ,2X,F11.2,1X,F10.7,1X,6X,
     *3X,F10.7,1X,I9,1X,F10.7,3X,F9.0,8X,F7.0)
  112 FORMAT(/1X,A10)
  100 CALL EXIT
      END
```

```
      PROGRAM IENEXT(INPUT,OUTPUT,TAPE2=INPUT,TAPE3=OUTPUT)
C     CALCULATION OF A SERIES IONIZATION ENERGY AND PREDICTION OF NEW LEVELS
C     USING QDEF=N-N*=A(0)+A(1)*T+A(2)*(T**2)+A(3)*(T**3)+A(4)*(T**4)+ .....
C
C                  T(N)=EXPANSION PARAMETER=(EIGN-E(N))/S
C                  ALL ENERGIES IN WAVENUMBERS
C                  S=SCALING FACTOR= 1 , R , RZ**2
C     CARD  COLUMNS                                                FORMAT  SYMBOL
C       1     1-10  ELEMENT IDENTIFICATION                         A10     ELEM
C            11-20  ATOMIC WEIGHT - CHEMICAL SCALE                 F10.5   CM
C            21-30  CHARGE THAT THE ELECTRON SEES                  F10.2   Z1
C            31-40  0. OR TRUE IE FOR ALL SERIES                   F10.2   TIE
C       2       1   ANGULAR MOMENTUM SYMBOL S,P,D,F,G,H ...        A1      P
C            11-12  N VALUE OF THE FIRST LEVEL (LOWEST)           I2      NFIR
C            21-22  N VALUE OF THE LAST LEVEL                     I2      NLAR
C            31-40  TRIAL IONIZATION ENERGY FOR THIS SERIES        F10.2   TRYIEL
C            41-50  DELTA IONIZATION ENERGY FOR THIS SERIES        F10.4   DELTA
C            51-60  0. OR QDEF(N)-QDEF(N+1) FOR 2-LEVEL IE         F10.5   QDC2L
C            61-62  ASSIGNS WEIGHT IN AVERAGING CONSTANTS         I2      IA2
C                   LESS THAN 1 IF LOWER LEVELS MOST ACCURATE
C                   IF 1 ALL WEIGHTS ARE SET EQUAL TO 1.
C                   MORE THAN 1 IF UPPER LEVELS MOST ACCURATE
C            71-72  NUMBER OF NEW LEVELS DESIRED                  I2      NPRED
C       3     1-20  ENERGY VALUE OF FIRST LEVEL                   F20.9   E(NFIR)
C       4           REPEAT CARD 3 FOR ALL LEVELS TO E(NLAR)
C                   REPEAT CARDS 2-4 FOR ADDITIONAL SERIES
C     LAST          AS CARD 2 WITH - IN COLUMN 71 (END OF DATA).
C
      DIMENSION E(20),TO(20),Q(20),D(20),DD(20),T(20),Z(20,20),TRY(110)
     *,C(20,20),CNM(20),A(20),AS(20),W(20),S(20),ED(20),Y(20),TN(20,5)
     *,Y1(20),Y2(20),Y3(20),SUM1(20),SUM2(20),SUM3(20)
      EQUIVALENCE (Y1(2),A(1)),(Y2(2),AS(1)),(Y3(2),S(1))
    1 FORMAT(A10,F10.5,F10.2,F10.2)
    2 FORMAT(A1,9X,,I2,8X,I2,8X,F10.2,F10.4,F10.5,I2,8X,I2)
    3 FORMAT(F20.9)
   11 FORMAT(1H1,58X,8HELEMENT A10/59X,12HR(M)*(Z**2)=F12.3
     */59X,7HLEVELS I1,1H-I2,A1)
   12 FORMAT(8X,44H     EL          LHS         RHS        DIFF  )
      READ(2,1) ELEM,CM,Z1,TIE
      RM=109737.31-60.22/CM
      RMZ=RM*(Z1**2)
      SC=RM
    4 READ(2,2) P,NFIR,NLAR,TRYIEL,DELTA,QDC2L,IA2,NPRED
      IF(NPRED.LT.0) 500,6
    6 NFI=NFIR
      NLR=NLAR-NFIR+1
      NU1=NLAR+1
      NUL=NLAR+NPRED
      READ(2,3) (E(N),N=NFIR,NLAR)
      NLMIN=MINO(NLR,3)
      DO 200 NL=NLMIN,NLR
   10 DELTAL=DELTA
      NLA=NFI+NL-1
      NL1=NLA-NFI
      WRITE(3,11) ELEM,RMZ,NFI,NLA,P
      IF(NL.GT.1) WRITE(3,12)
      NO=1
      EL=TRYIEL
      IA3=1
   14 IFLAG=1
   15 DO 80 K=1,100
```

```
      IFLAG=IFLAG+1
      IF(IFLAG.GE.165) GO TO 200
      DO 20 N=NU1,NUL
      FN=N
      E(N)=EL-((FN-1.)/FN)**2*(EL-E(N-1))
   20 CONTINUE
      DO 25 N=NFIR,NUL
      TO(N)=EL-E(N)
      Q(N)=SQRT(RMZ/TO(N))
      D(N)=N-Q(N)
      IF(N.GT.NFIR) DD(N)=D(N)-D(N-1)
      T(N)=TO(N)/SC
      Z(N,N)=D(N)
   25 CONTINUE
      IF(NLR.EQ.1) 30,40
   30 WRITE(3,96) EL
      WRITE(3,97) NFI,P,E(NFI),TO(NFI),Q(NFI),D(NFI)
      WRITE(3,98) (N,P,E(N),TO(N),Q(N),D(N),DD(N),N=NU1,NUL)
      WRITE(3,31)
   31 FORMAT(/59X,25HFIRST LEVEL OBSERVED ONLY,
     */59X,48HCONSTANT SCREENING ASSUMED TO PREDICT NEW LEVELS)
      GO TO 4
   40 DO 50 J=1,NL1
      NLJ=NLA-J
      DO 50 N=NFI,NLJ
      Z(N,N+J)=(Z(N,N+J-1)-Z(N+1,N+J))/(T(N)-T(N+J))
   50 CONTINUE
      IF(IA3.EQ.2) GO TO 95
C-----TO 80 FIND CORRECT IONIZATION ENERGY
      IF(NLR.GT.2) GO TO 62
      IF(QDC2L.EQ.0.) GO TO 95
      XLHS=Z(NFIR,NLAR)*(E(NLAR)-E(NFIR))/SC
      XRHS=QDC2L
      GO TO 63
   62 XLHS=(Z(NFI,NLA-2)-Z(NFI+1,NLA-1))/(Z(NFI+1,NLA-1)-Z(NFI+2,NLA))
      XRHS=(E(NLA-1)-E(NFI))/(E(NLA)-E(NFI+1))
   63 TRY(K)=XLHS-XRHS
      WRITE(3,65) K,EL,XLHS,XRHS,TRY(K)
   65 FORMAT(4X,I3,1X,F11.3,1X,F11.7,1X,F10.7,1X,F11.7)
      IF(K.LT.3) GO TO 79
      F=TRY(K-2)
      G=TRY(K-1)
      H=TRY(K)
      IF(ABS(G).LE.1.0E-06) GO TO 70
      IF(ABS(G).LE.ABS(F).AND.ABS(G).LE.ABS(H)) 71,75
   70 IA3=2
   71 EL=EL-DELTAL
      DELTAL=DELTAL/10.
      IF(G.GT.0..AND.H.GT.0..OR.G.LT.0..AND.H.LT.0.) DELTAL=-DELTAL
      GO TO 15
   75 IF(ABS(H).GT.ABS(F)) DELTAL=-DELTAL
   79 EL=EL+DELTAL
   80 CONTINUE
      WRITE(3,85)
   85 FORMAT(/6X,49HTRIAL IE OR DELTA INCORRECT TO ITERATE IN N STEPS)
      GO TO 200
   95 WRITE(3,96) EL
   96 FORMAT(/85X,3HEL=F11.2//59X,2HNL,6X,4HE(O),20X,4HT(O),8X,2HN*,8X,
     *4HQDEF,6X,6HCHANGE)
      WRITE(3,97) (N,P,E(N),TO(N),Q(N),D(N),N=NFIR,NFIR)
      N2=NFIR+1
      WRITE(3,98) (N,P,E(N),TO(N),Q(N),D(N),DD(N),N=N2,NLAR)
```

```
   97 FORMAT(58X,I2,A1,1X,F11.2,12X,1X,F11.2,2(1X,F10.7))
   98 FORMAT(58X,I2,A1,1X,F11.2,12X,1X,F11.2,3(1X,F10.7))
      WRITE(3,99) P
   99 FORMAT(/10X,5HQDEF(A1,11H) CONSTANTS,8X,3HAVE,8X,7HRMS DEV,6X,2HNL
     *,6X,4HE(C),6X,9HE(O)-E(C),5X,4HT(C),8X,2HN*,8X,4HQDEF,6X,6HCHANGE)
C-----TO 130 CALCULATE CONSTANTS
      DO 100 N=NFIR,NUL
      T(N)=TC(N)/SC
      TN(N,1)=E(N)
  100 CONTINUE
      DO 102 M=1,NL1
      SUM1(M)=0.
      SUM2(M)=0.
      SUM3(M)=0.
  102 CONTINUE
      DO 120 N=NFI,NLA
      NLN=NLA-N+1
      DO 110 MO=1,NLN
      M=NLN-MO
      A(M)=Z(N,N+M)
      AS(NL-1)=A(NL-1)
      IF(M.GE.NL1) GO TO 110
      CALL COEFT(T(N),M,NL1,CNM)
      M1=M+1
      DO 105 I=M1,NL1
      A(M)=A(M)-A(I)*CNM(I)
  105 CONTINUE
      IF(N.EQ.NFI) AS(M)=A(M)
      W(N)=1.
      IF(IA2.LT.1) W(N)=(1/Q(N))**3
      IF(IA2.GT.1) W(N)=Q(N)**3
      SUM1(M+1)=SUM1(M+1)+W(N)
      SUM2(M+1)=SUM2(M+1)+W(N)*A(M)
      SUM3(M+1)=SUM3(M+1)+W(N)*A(M)**2
  110 CONTINUE
  120 CONTINUE
      DO 130 M=1,NL1
      A(M-1)=SUM2(M)/SUM1(M)
      S(M-1)=SQRT(ABS(SUM3(M)/SUM1(M)-A(M-1)**2))
  130 CONTINUE
C-----TO 162 CALC T(OBS)-T(CALC) AND ITERATE
      NIT=NFI
      DO 162 IT=2,4
      DO 161 N=NIT,NUL
      D(N)=0.
      DO 140 I=1,NL
      D(N)=D(N)+A(I-1)*T(N)**(I-1)
  140 CONTINUE
      Q(N)=N-D(N)
      T(N)=RMZ/Q(N)**2
      ED(N)=EL-T(N)
  141 M=N-NFI
      IF(N.NE.NFIR) DD(N)=D(N)-D(N-1)
      TN(N,IT)=ED(N)
      Y(N)=TN(N,IT-1)-TN(N,IT)
      IF(IT.GT.2.OR.N.GT.NFIR) 145,142
C-----TO 155 REGULATING OUTPUT
  142 IF(NO.EQ.2.) WRITE(3,152)
      WRITE(3,144) M,AS(M),A(M),S(M),N,P,ED(N),Y(N),T(N),Q(N),D(N)
      GO TO 160
  145 IF(N-NLA) 146,148,150
  146 WRITE(3,147) M,AS(M),A(M),S(M),N,P,ED(N),Y(N),T(N),Q(N),D(N),DD(N)
```

```
      GO TO 160
  148 WRITE(3,149) M,A(M),N,P,ED(N),Y(N),T(N),Q(N),D(N),DD(N)
      GO TO 160
  150 IF(N.EQ.NLA+1) WRITE(3,152)
      WRITE(3,155) N,P,ED(N),Y(N),T(N),Q(N),D(N),DD(N)
  144 FORMAT(10X,2HA(I1,2H)=,2(1X,E13.6),2X,E7,I8,A1,3(F12.2),2(F11.7))
  147 FORMAT(10X,2HA(I1,2H)=,2(1X,E13.6),2X,E7,I8,A1,3(F12.2),3(F11.7))
  149 FORMAT(10X,2HA(I1,2H)=,1X,E13.6,23X,I8,A1,3(F12.2),3(F11.7))
  152 FORMAT(1X)
  155 FORMAT(52X,I8,A1,3(1X,F11.2),3(1X,F10.7))
  160 T(N)=T(N)/SC
  161 CONTINUE
      NIT=NLA+1
  162 CONTINUE
      IF(TIE.EQ.0..OR.NO.EQ.2) GO TO 200
C-----RETURN TO CALC NL NEW CONSTANTS WITH TRUE IE
      NO=2
      EL=TIE
      GO TO 14
C-----RETURN TO INCLUDE 1 MORE LEVEL
  200 CONTINUE
      GO TO 4
  500 CALL EXIT
      END
      SUBROUTINE COEFT(T,M,NL1,CNM)
      DIMENSION T(1),C(20,20),CNM(20)
      M1=M+1
      L1=M+1
      L2=L1+1
      NL=NL1+1
      DO 1 K=1,M1
      C(L1,K)=1.
    1 CONTINUE
      DO 2 I=L2,NL
      DO 2 K=1,M1
      C(I,K)=0.
      DO 2 J=K,M1
      C(I,K)=C(I,K)+T(J)*C(I-1,J)
      CNM(I-1)=C(I,1)
    2 CONTINUE
      RETURN
      END
```

TECHNICAL INFORMATION DIVISION
LAWRENCE BERKELEY LABORATORY
UNIVERSITY OF CALIFORNIA
BERKELEY, CALIFORNIA 94720